IMPROVING SIGNAL IDENTIFICATION FOR FAST-SCAN CYCLIC VOLTAMMETRY

Justin Allen Johnson

A dissertation submitted to the faculty at the University of North Carolina at Chapel Hill in partial fulfillment of the requirements for the degree of Doctor of Philosophy in the Department of Chemistry.

Chapel Hill
2017

Approved by:

R. Mark Wightman

James W. Jorgenson

Matthew R. Lockett

Regina M. Carelli

Paul B. Manis

ABSTRACT

Justin Allen Johnson: Improving Signal Identification for Fast-Scan Cyclic Voltammetry
(Under the direction of R. Mark Wightman)

Fast-scan cyclic voltammetry (FSCV) is a powerful analytical tool for monitoring the *in vivo*
concentration dynamics of electroactive neurotransmitters. Coupled with the use of microelectrodes, the
approach allows for unsurpassed spatiotemporal resolution and is readily amendable to studies in freely
moving animals. However, since its inception, the issue of selectivity has been of central concern. Correct
identification and isolation of neurotransmitters signals is critical to interpretation of FSCV data, and much
of the progress in the field has focused on methods of improving the ability to do this more robustly. Here,
this work is expanded upon to both improve the use of existing methods (i.e. principal component
analysis-inverse least squares regression, or PCA-ILS) and introduce new tools (i.e. multivariate curve
resolution, or MCR-ALS, and convolution-based removal of non-faradaic currents) for this purpose.
Chapter 1 presents the historical context of this work, highlighting the methods that have been
successfully developed and employed for isolating catecholamine signals. In Chapter 2, the evaluation of
the pitfalls of common methods of model training (i.e. the use of non-experimental training data) for PCA-
ILS is discussed, with focus on elucidating the source of errors that arise from this approach. To help
avoid these pitfalls, MCR-ALS, a method that does not require independent training data, characterized
for use with FSCV data as a possible alternative. Next, Chapters 4 and 5 focus on the introduction, and
exploration of the possibilities afforded by, the use of convolution to predict and remove non-faradaic
currents from FSCV data. Chapter 4 specifically focuses on optimization of this method and the removal
of ionic interferences from background-subtracted data collected with standard waveforms. Chapter 5
builds on this work to explore possible modifications to the experimental protocol (i.e. the use of high scan
rates and higher waveform holding potentials) that tailor to this convolution-based procedure, which
allows for the removal of the majority of the background current. The potential of this latter approach for
simultaneous monitoring of information about phasic and basal levels of dopamine is then evaluated.

ACKNOWLEDGEMENTS

I must start by thanking my advisor, Dr. R. Mark Wightman, for his mentorship throughout my time at graduate school. He has been an invaluable source of guidance, knowledge, and wisdom, and this work would not have been possible without his guiding hand and encouragement. I must also thank him for slogging through the (considerably longer) drafts of these chapters and for his continued patience while I (slowly) learn the art of 'less is more'.

I must also thank those that contributed to the work presented in these chapters. First, I must acknowledge the assistance of my lab mate Nathan Rodeberg, who contributed to the work presented in Chapters 2, 3, and 5. He has been an excellent partner in conducting research, and I thank him for all the hours he has put in to helping this work become a reality. Additionally, I must acknowledge my undergraduate, Josh Gray, who contributed to Chapter 3. He is an exceptional student, and I wish him the best of luck during his pursuit of a MD/PHD degree. Finally, I thank Caddy Hobbs, who contributed to Chapter 4, and who made my life as a TA considerably easier for a semester.

I also want to thank Dr. Elizabeth (Bucher) Schultze for showing me the ropes when I first joined the Wightman lab. Additionally, I must thank my partner, Sara Turner, who has kept me level-headed throughout the process of graduate school, and my parents, who have supported me in innumerous ways in my pursuit of a scientific career since I was young. Finally, I thank my friends – in particular, Wesley Storm, Chris Backlund, Douglas Kirkpatrick, Andrew Walden, and Javier Grajeda – who have made my time here at graduate school considerably easier by their presence.

TABLE OF CONTENTS

LIST OF TABLES

LIST OF FIGURES

x

LIST OF ABBREVIATIONS AND SYMBOLS

*	probability less than 0.05
**	probability less than 0.01
***	probability less than 0.001
[X]	concentration of analyte X
$^{\circ}C$	degrees Celsius
AA	ascorbic acid
Ag/AgCl	silver/silver chloride
C	concentration matrix
$CaCl_2$	calcium chloride
CV	cyclic voltammogram
D	experimental data matrix
DA	dopamine
DOPAC	3,4-dihydroxyphenylacetic acid
DV	dorsal-ventral
E	error matrix
E_{app}	applied potential
EFA	evolving factor analysis
FFT	fast Fourier transform
FSCV	fast-scan cyclic voltammetry
FSCAV	fast-scan controlled adsorption voltammetry
g	grams
HCl	hydrogen chloride
H_2O_2	hydrogen peroxide
HDCV	High-Definition Cyclic Voltammetry
Hz	Hertz
i.p.	intraperitoneal injection
KCl	potassium chloride

kg	kilograms
L	liters
μA	microamperes
μm	micrometer
μM	micromolar
mA	milliamperes
MCR-ALS	multivariate curve resolution-alternating least squares
mg	milligrams
$MgCl_2$	magnesium chloride
ML	medial-lateral
mL	milliliters
mm	millimeter
mM	millimolar
ms	millisecond
n	number of samples
N_2	molecular nitrogen
nA	nanoamperes
nM	nanomolar
NaCl	sodium chloride
NaH_2PO_4	monosodium phosphate
$NaHCO_3$	sodium bicarbonate
NaOH	sodium hydroxide
$NaSO_4$	sodium sulfate
NE	norepinephrine
O_2	molecular oxygen
OPA	orthogonal projection approach
P	probability
P-ALS	penalized alternating least squares

PC	principal component
PCA-ILS	principal component analysis-inverse least-squares regression
PCR	principal component regression
PLS	partial least squares
R^2	coefficient of determination
σ	standard deviation
s	second
S	spectral matrix
S.E.M.	standard error of the mean
t	time
TRIS	tris(hydroxymethyl)aminomethane
TTL	transistor-transistor logic
UEI	universal electrochemical instrument
UNC	University of North Carolina at Chapel Hill
V	volts

CHAPTER 1: UNRAVELING VOLTAMMETRIC NEUROTRANSMITTER MEASUREMENTS

INTRODUCTION

Neurotransmission is a multifaceted phenomenon, relying on both electrical and chemical impulses for information propagation and processing throughout the nervous system. In its most basic form, neurons act as the central units of this transmission. Control of their transmembrane voltage gradients allow these specialized cells to transform extracellular chemical information, sensed at the cell body and dendrites, into electrical signals called action potentials. These action potentials are conducted through axons to synapse, where the action potential translates into controlled chemical release to influence downstream cells. A complete picture of neurotransmission thus requires tools to probe these multiple aspects on the cellular level and to understand the interplay between them.

The study of neuronal electrical activity has a well-established history in the field of electrophysiology, beginning in the 1950s with the pioneering experiments of Hodgkin and Huxley. (Hodgkin & Huxley, 1952a, 1952b, 1952c) However, the real-time *in vivo* chemical analysis of neurotransmission, and more specifically neurotransmitters, is a less mature field and a formidable analytical challenge. The heterogeneous and complex nature of the neuronal environment demands high sensitivity, spatiotemporal resolution, and chemical selectivity to glean meaningful insight into the neurobiological phenomena studied. Consequently, electrochemistry, which can provide sub-second measurements of charge stemming from redox reactions of electroactive compounds, has found considerable, if not straightforward, success in this endeavor.(Bucher & Wightman, 2015) Appropriate choice of instrumentation, experimental design, and electrode materials (e.g. carbon-fiber microelectrodes) can readily deliver the nanomolar limits of detection needed for neurotransmitter tracking in micron-sized environments. However, the issue of selectivity has plagued *in vivo* electrochemical measurements throughout the development of the field.(Wightman et al., 1987) Indeed, in its first realization by Ralph Adams and colleagues in 1973, attempted cyclic voltammetric

1

measurements of a catecholamine neurotransmitter (i.e. dopamine, or DA) were prevented by interference by the neuroprotective antioxidant ascorbic acid, which is present in orders of magnitude larger concentrations within the extracellular environment.(Kissinger et al., 1973) Even with the advances in the field since this report, the topic of appropriate isolation, assignment, and quantitation of electrochemical signals remains a central concern for researchers.

Indeed, many of these advances have been focused on enhancing the selectivity of *in vivo* electrochemical measurements. While controlled-potential amperometry has exquisite time resolution and sensitivity, the poor selectivity of the method has hindered its widespread adoption. All redox active species that can undergo electron transfer at the electrode contribute to the single measurements taken at a time point, and there exists no mechanism for separation of these contributions using this data alone. As such, cyclic voltammetry has become the preferred approach. Stratification of the analyte responses along the potential axis generates unique voltammetric profiles that depend on the electrochemical properties of the analyte at the specific electrode surface, introducing another degree of separation into the measurements. However, traditional approaches to cyclic voltammetry, either in measurement or analysis, do not directly provide the selectivity or sensitivity desired to measure crucial neurotransmitters (i.e. catecholamines and indolamines), requiring further refinements to optimize the method for *in vivo* analysis.

Here, the development of cyclic voltammetry for *in vivo* neurotransmitter analysis will be briefly discussed. Focus will be placed on the experimental innovations permitting robust and selective dopamine measurements, as this has been the traditional system studied in *in vivo* cyclic voltammetric experiments. The discussion will then shift to the analysis of *in vivo* voltammetric data, specifically the evolution of the methods used and their interpretation. Finally, the sources of measurement error will be discussed.

EXPERIMENTAL APPROACHES TO DOPAMINE SIGNAL ISOLATION

It is a primary goal of *in vivo* electrochemistry to be able to convert the obtained measurements into meaningful statements on neurotransmitter temporal dynamics and concentrations with confidence. To accomplish this, several criteria must be met. First, the phenomena that contribute to the measured

electrochemical signal must be understood, and the experiment must be designed such that it will generate a measurable signal from a phenomenon relating to the neurotransmitter of interest. Second, a subsection of the signal that carries information solely about the specific neurotransmitter of interest must be isolated. Finally, a means of transforming the isolated information about the neurotransmitter into concentration estimates must be deployed. The first two criteria can be partially met through experimental means (e.g. the deployment of appropriate electrochemical methodologies), while complete fulfillment of the second and third criteria relies on the use of robust calibration methodologies. This discussion begins by tracing the development of the experimental methodologies that lead to the current state of *in vivo* voltammetry.

As mentioned before, it was realized early that the traditional voltammetric procedures would prove insufficient to gain clear insight into catecholamine dynamics due to the interferences provided by its metabolites and other ambient species, which are typically found in orders of magnitude higher concentrations than dopamine in extracellular fluid.(Wightman et al., 1988b) The first step towards interpreting the electrochemical data was then identifying the subset of electroactive species present in the extracellular environment capable of generating signals. For this, experiments carried out using electrochemistry with modified electrodes and perfusion methods coupled to offline liquid chromatography were used to identify homovanillic acid, uric acid, 3,4-dihydroxyphenylacetic acid, and ascorbic acid as the primary components of the electrochemical signals.(Kovach et al., 1984; Salamone et al., 1984). Of these, the primary species of concern are 3,4-dihydroxyphenylacetic acid (DOPAC), the oxidative catabolite produced by monoamine oxidase, and ascorbic acid (AA), a neuroprotective antioxidant, both of which have similar voltammetric peak positions as dopamine on unmodified carbon electrodes.

The first path towards improving selectivity focused on understanding of the carbon electrode surface and possible modifications to improve selectivity. Gonon and colleagues reported that brief application of a high-frequency triangular wave (0 to ~3 V vs. Ag/AgCl) resulted in the separation of a peak attributable to catecholamines (DA and DOPAC) from one attributable to ascorbic acid during subsequent differential pulse voltammetry experiments at that electrode.(F. Gonon et al., 1980; F. G. Gonon et al., 1981) This result was attributed to surface-oxide groups formed during pretreatment that served to catalyze the redox reactions of these species, resulting in negative shifts in the peak potentials.
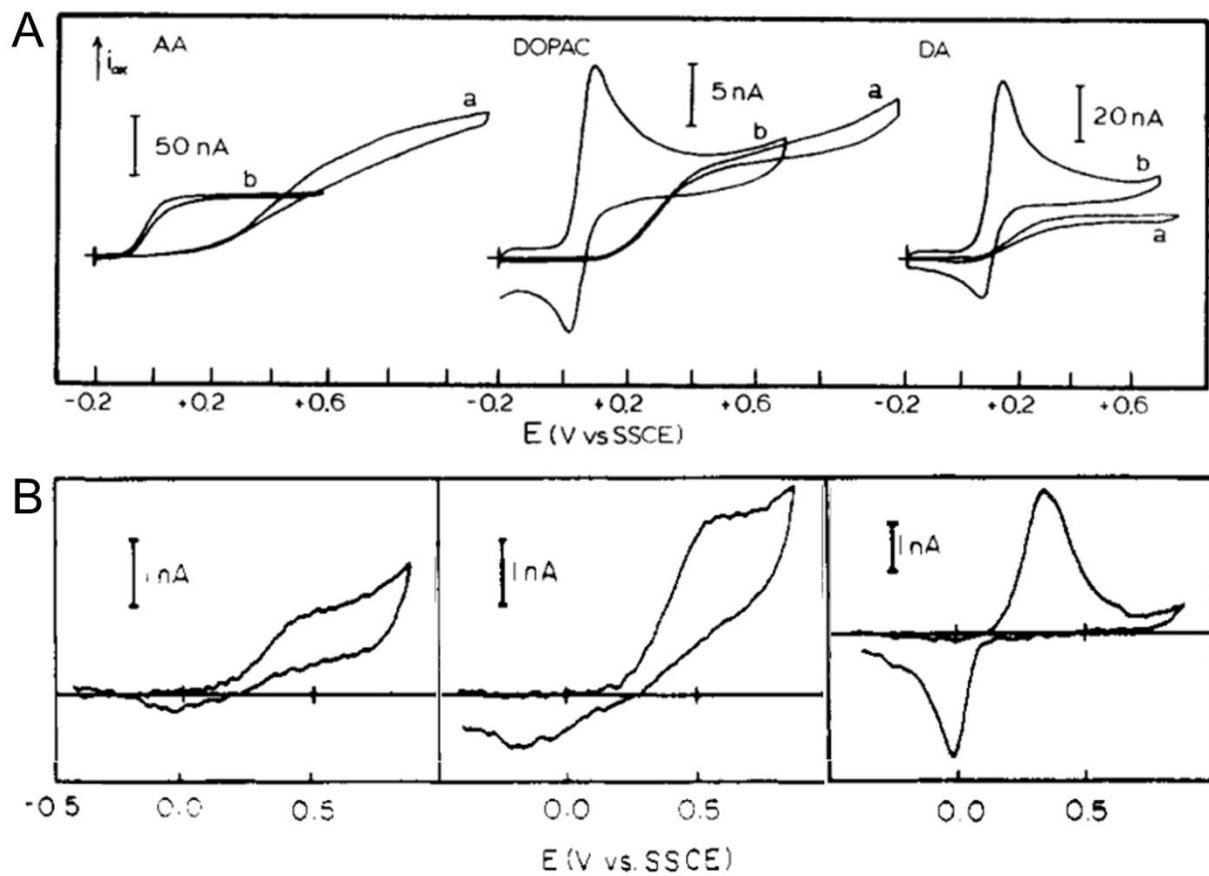
Figure 1.1. Comparison of voltammetric measurements of ascorbic acid (AA), 3,4-dihydroxyphenylacetic acid (DOPAC), and dopamine (DA) at carbon-fiber microelectrodes. (A) Slow-scan voltammograms (100 mV/s) for AA, DOPAC, and DA (left to right) taken at unmodified (a) and electrochemically pretreated (b) carbon-fiber microelectrodes. (Kovach, et al., 1984) (B) Fast-scan voltammograms (200 V/s) for AA, DOPAC, and DA (left to right) taken at bare carbon-fiber microelectrodes.(Baur et al., 1988)

Further, cyclic voltammetric characterization of these compounds using modified electrodes showed a change in their behavior (Figure 1.1A), namely the appearance of peaks in the voltammograms of DOPAC and DA, suggesting adsorptive pre-concentration at the electrode. (Kovach, et al., 1984) Consequently, there was a corresponding increase in sensitivity reported for use of these oxidized fibers towards the catecholamines.(Feng et al., 1987) However, these fibers exhibit a decrease in sensitivity in brain tissue with time, leading to high detection limits unsuitable for robust analysis of small dopamine changes. As such, later approaches focused on continued excursions to more moderate anodic potential limits (~1.4) during the measurement, which was demonstrated to help increase and maintain sensitivity throughout measurements, albeit at the cost of selectivity.(Hafizi et al., 1990; Heien et al., 2003; Takmakov et al., 2010b) A second electrode modification for the increase in selectivity was the use of a perflourinated ion-exchange membrane (i.e. Nafion) at the electrode surface. (Gerhardt et al., 1984; Nagy et al., 1985) The negatively charged polymer membrane acts to filter out anions (e.g. ascorbic acid and DOPAC at physiological pH), preventing their access to the electrode surface. This allows for the relative isolation of the dopamine signal, coupled to a slight increase in sensitivity.(Baur, et al., 1988)

The second breakthrough for selective electrochemical measurements was the introduction of fast-scan cyclic voltammetry (FSCV), in which the scan rate of the voltammetric sweep is hundreds of volts per second. This approach was introduced by Millar and colleagues for calibration of the amount of iontophoretically ejected dopamine.(Millar et al., 1981) However, its potential for direct measurement of naturally released dopamine was soon realized. Four years later, the technique was shown to be capable of selective *in vivo* measurement of dopamine evoked from electrical stimulation, a finding supported by iontophoretic evaluation of DOPAC and dopamine.(Millar et al., 1985) Subsequent characterization of the technique showed that this selectivity derives from the differing electron transfer rates between dopamine and its interferents. At high scan rates, the slow kinetics of ascorbic acid and DOPAC oxidation push their voltammetric peaks to potentials more positive than that of dopamine (Figure 1.1B), allowing resolution of the dopamine signal.(Baur, et al., 1988) Further, the shortening of the measurement window allows for the reduction wave, generated from the oxidized dopamine (i.e. dopamine-*o*-quinone), to be observed in the resulting voltammogram, as this species does not have sufficient time to leave the electrode surface.(Bath et al., 2000; Millar, et al., 1985) Beyond selectivity, the use of high scan rates has other

inherent advantages. Increasing scan rates results in increasing voltammetric signal intensities, and thus in sensitivity.(Bard & Faulkner, 2001) The shortening of the measurement window also enables access to sub-second information about the dynamics of neurotransmitter changes.

However, there are drawbacks to these approaches towards increasing selectivity. Modified electrodes distort the temporal response of the sensor beyond that attributable to diffusion from the release site to the electrode.(Feng, et al., 1987; Kovach, et al., 1984) These artifacts stem from the adsorptive characteristics of the electrode and, in the case of Nafion films, the time needed to diffuse through the film to the electrode surface.(Bath, et al., 2000; Kile et al., 2012) Subsequent treatment of the obtained data is then needed to obtain a correct picture of the dopamine response, which is typically done with convolution. (Engstrom et al., 1988; Kawagoe & Wightman, 1994; Wightman et al., 1988a) Another issue that arises is the presence of new types of interferences. The most prominent one is the large background current observed when using rapid scan rates for voltammetric measurements, which, at carbon electrodes, consists of non-faradaic and faradaic components. In many ways, the union of microelectrodes and FSCV is mutually advantageous, as the small exposed electrode surface permits the background current to be minimized. However, given the concentrations of neurotransmitters found *in vivo*, this background signal still dwarfs the analytical signal by order of magnitude, necessitating digital background subtraction for resolution.(Howell et al., 1986) Further, the measurements then become dependent on the background stability, resulting in a number of issues. First, even in stable environments, the background signal tends to drift with time, likely due to largely unavoidable changes at the electrode related to surface fouling and evolution driven by the applied waveform.(Hermans et al., 2008; Takmakov et al., 2010a; Wiedemann et al., 1990) This limits measurements to the time windows over which the background signal remains stable, restricting the information gained from the technique to that concerning phasic dopamine release as compared to long-term shifts in neurotransmitter concentrations. Second, FSCV measurements are open to interference by chemical species that can modulate the background current, either its non-faradaic or faradaic component. The non-faradaic current arising from charging of the electrical double layer is determined by the impedance characteristics of the electrochemical system. Thus, any species that alters this, such as ions that alter the effective double-layer capacitance, result in artifacts in the background-subtracted measurements.(Jones et al., 1994;

6

Takmakov, et al., 2010a) Additionally, for moderately oxidized carbon fibers, a voltammetric wave attributable to the two-electron, two-proton redox reaction of a surface quinone-like species appears in the background current.(Dengler et al., 2015; Karweik et al., 1985; Kawagoe et al., 1993a; Runnels et al., 1999; Takmakov, et al., 2010a) As the process is dependent on protons, this functionality is pH-sensitive. As dopamine terminal activity results in local pH shifts attributable to metabolic activity, this results in common contributions to FSCV measurements relating to this phenomena.(Venton et al., 2003) These, however, are preferable interferences, as their voltammetric behavior is drastically different from dopamine under species like DOPAC and ascorbic acid and readily dealt with through appropriate data analysis methods (as will be discussed below).

No method for increasing specificity is fool-proof. For instance, differentiation of dopamine from another catecholamine not discussed, norepinephrine, is not currently practically possible.(Heien, et al., 2003; Park et al., 2009) As such, criteria for appropriate signal attribution have been laid out in the literature, either in traditional use of FSCV or in the establishment of alterations to these procedures, and have been used with success in establishing the technique as a reliable method through which to monitor electroactive neurotransmitters.(Kawagoe et al., 1993b; Wightman, et al., 1987) Here, these criteria will be briefly reiterated. First, thorough *in vitro* characterization of the voltammetric behavior of the species of interest at the specific type of electrode used in a media containing all expected extracellular fluid components is needed to verify that the *in vivo* signal exhibits similar behavior. Second, the use of independent methods of analysis (e.g. dialysis techniques coupled to offline analytical techniques or post-mortem liquid chromatography) is recommended to corroborate the general electrochemical findings.(Buda et al., 1981; Church et al., 1987; Justice & Neill, 1986; Justice et al., 1983; Park, et al., 2009) Third, the electrochemical measurements should match up with the known chemical composition and physiology of the neural structure studied. This also requires confirmation of the positioning of the electrode, which is most often done through electrolytic lesioning of the carbon fiber electrode post-experiment and subsequent histological analysis.(Roberts et al., 2013) Finally, pharmacological manipulation with well-characterized agents should modulate the signal in a manner matching the known effect on the underlying neurotransmitter.

CALIBRATION METHODOLOGIES

As highlighted, the selectivity imparted by experimental modifications alone often proves insufficient for complete isolation of the voltammetric dopamine signal. Thus, the use of robust calibration methodologies is needed to extract the pure dopamine signal from the data. Most commonly, the current at the dopamine oxidation potential is used as the indicator of the dopamine concentration, as it has maximal sensitivity to the dopamine concentration. Thus, the goal of calibration has largely been estimation of the 'true' value of this parameter for use in quantitation.

Early methods focused on identifying and analyzing only voltammograms that had only contributions from dopamine and using traditional univariate analysis of the measured peak current. To reduce the subjective nature of this identification, a template method was introduced, where the correlation of an obtained *in vivo* signal was determined against a series of *in vitro* signals of expected components.(Phillips & Wightman, 2003; Rodeberg et al., 2017; Troyer et al., 2002; Venton & Wightman, 2003) Alternatively, the *in vivo* signal was compared to another *in vivo* signal evoked by a known method of eliciting the specific neurotransmitter response (e.g. electrical stimulation).(Phillips et al., 2003) There are, however, two issues with this approach. First, selection of a correlation threshold for selecting measurements with sufficiently pure dopamine signals was an arbitrary user-defined value rather than a statistically robust parameter. Second, this introduces an inherent bias into the pool of analyzed data.(Rodeberg, et al., 2017) Despite these drawbacks, this approach was a hint of things to come, as it utilized the power of the voltammogram, namely that there are multiple current measurements that relate to the dopamine concentration that can be used for identification of the underlying analyte. Indeed, in an extension of this approach, a bivariate analysis method was used, where current measurements at potentials dominated by known interferents were used to predict and subtract their contributions at the dopamine oxidation potential.(Cheer et al., 2004; Venton, et al., 2003)

However, full utilization of the power of the voltammogram was not realized until the introduction of chemometric multivariate analysis methods, which use the entire set of current measurements in the voltammogram. Heien and colleagues first reported the use of a technique called principal component analysis-inverse least squares regression (PCA-ILS), also referred to as principal component regression (PCR) for short, for the analysis of FSCV data.(Heien et al., 2004) This approach consists of two steps.

First, principal component analysis, a dimensionality reduction factor analysis technique, is used to produce noise-free estimates of the pure spectra of all expected components. These components are defined by the user by providing the model a set of training voltammograms (i.e. training set) measured at the electrode. The spectral estimates are provided by analyzing the training set data to determine the signal shapes (i.e. factors or principal components) that define the majority of the variance of the training set data, which are assumed to describe only the analytically relevant variance. These principal components are used to then estimate the noise-free spectra, which are then used to analyze the data using inverse least-squares regression to determine the linear combination of spectra that best fits it. From this, the oxidative peak current of the fitted spectra is then converted into an estimate of concentration using either average calibration factors for similar electrodes or *ex vivo* calibration. This final step is discussed more in the following section.

Since its introduction, the technique has been further refined to provide tools to help in model construction and validation. Techniques such as PCA-ILS can realize what is referred to in the chemometrics literature as the first-order advantage.(Booksh & Kowalski, 1994; Olivieri, 2008) Univariate methods (i.e. zero-order methods) have no means of detecting the presence of interferents contributing to the single measurement used for calibration. However, first-order methods like PCA-ILS can detect their presence through a validation technique called residual analysis.(Jackson & Mudholkar, 1979; Keithley et al., 2009; Lavine & Workman, 2013) This procedure relies on the unattributed current left in the data after spectral fitting, which has the advantage of having well-defined statistical properties that can be used for robust detection of the presence of interferents. This is important, as the presence of considerable residual current indicates that the model is poorly suited for analysis of the data and that the model predictions likely have error. Adaptation and rigorous implementation of a residual analysis procedure for FSCV was introduced by Keithley and colleagues.(Keithley, et al., 2009) Further, tools for the evaluation of model quality (i.e. Cook's distance plots for the detection of outliers and k vectors for visual inspection of estimated analyte spectra) have been introduced and implemented into a user-friendly analysis program, permitting the facile construction and evaluation of PCA-ILS models.(Bucher et al., 2013; Keithley & Wightman, 2011) These developments have helped establish PCA-ILS as the standard for FSCV data analysis, and its success for *in vivo* removal of interferents such as pH and background drift

has been successfully demonstrated.(Heien et al., 2005; Hermans, et al., 2008) However, the implementation of PCA-ILS has not been without controversy. The main point of contention has been the proper construction of training sets, which adds experimental complexity due to the need for additional data collection. This issue was first reported by Rodeberg et al. and is expanded on in Chapter 2. (Johnson et al., 2016a; Rodeberg et al., 2015)

It is worth noting that other analysis methods have been explored. First, a method called partial least squares regression (PLS) has been reported for FSCV analysis.(Yorgason et al., 2011) The method is highly similar to PCA-ILS, differing solely in how the pure spectra are determined from the training set prior to regression.(Kramer, 1998) For this step, PCA focuses solely on the major variance present in the voltammograms, while PLS considers both the voltammograms and corresponding concentration values to attempt to define factors that best explain the variance in both. The advantage of this approach typically relies on the independence of errors in the concentration values and the obtained spectra, which, if not accounted for, can reduce the effectiveness of noise removal.(Kramer, 1998) However, concentration values are typically estimated from the peak oxidative current of the training set voltammograms, as a method for independent verification of the corresponding concentrations has not been established, so it is unclear how much of an advantage this approach would provide. Additionally, no direct comparison of PLS and PCA-ILS has been reported in the literature to evaluate this. A second method recently reported is the use of a penalized linear regression approach called elastic net.(Kishida et al., 2016) The main reasons for use of factor analysis techniques, like PLS and PCA, prior to regression are to avoid 1) ill-defined regression equations and 2) issues that arise when a number of the predictive variables (e.g. the individual current measurements in the voltammograms) are highly correlated.(Haaland & Thomas, 1988; Kramer, 1998) This latter condition is called multicollinearity and is certainly present in the current measurements in a voltammetric wave. If these issues are not considered during model building, the resulting solutions can be non-unique and bias towards the disproportionate use of a subset of the current measurements for concentration measurement. Penalized linear regression techniques address this issue in an alternative manner by modifying the regression equations themselves with additional terms that 'penalize' solutions that bias towards unreasonably large weightings of a subset of measurements, providing boundaries to define the regression equation such that it provides unique

solutions.(Meloun et al., 1994) In the report by Kishida et al., this approach was used for analysis of the derivatives of the non-background-subtracted FSCV voltammograms, and it was claimed that the technique performed more reliably than PCA-ILS on the data analyzed and could be used to monitor tonic dopamine concentrations. However, a thorough characterization of this technique is needed to validate the results, as well as the development of tools like residual analysis for verification of the model results.

PRESENT LIMITATIONS IN QUANTITATING FSCV MEASUREMENTS

To close out this discussion, the final issue of converting the isolated dopamine signal into an estimate of concentration will be briefly discussed, particularly the limitations placed by *in vivo* measurements and the currently employed methodologies. As noted above, the true output of the calibration models is an estimate of the oxidative peak *current* expected for dopamine in the absence of interferents. Estimates of concentration are produced by use of a conversion, or calibration, factor. The source of this calibration factor is *ex vivo* analysis at the specific electrode after the experiment or an average *ex vivo* calibration factor from similarly treated electrodes. The latter is typically used, because, as noted before, the electrode is more often lesioned to provide a marking for histological verification of electrode placement.

These approaches open up the estimates to a certain degree of quantitation error. First, it is not guaranteed that the calibration factor obtained *ex vivo*, even at the same electrode, will be the effective calibration factor *in vivo*. Indeed, comparison of the results from FSCV and microdialysis studying the levels of acetyl-*p*-aminophenol after injection revealed that both precalibration and *ex vivo* postcalibration differed significantly from the microdialysis result and from each other.(Logman et al., 2000) While part of this discrepancy may lie in the different sampling properties of the techniques, there has been no definitive establishment of the accuracy of these approaches. Several factors could drive the introduction of error into these calibration factors. It is known that the sensitivity of the carbon electrodes is a function of the composition of the surrounding solution, so mismatches between the calibration solution and the extracellular environment could result in errors in the calibration factor estimate.(Kume-Kick & Rice, 1998) Further, fouling of the electrode has been shown to result in sensitivity changes upon implantation and
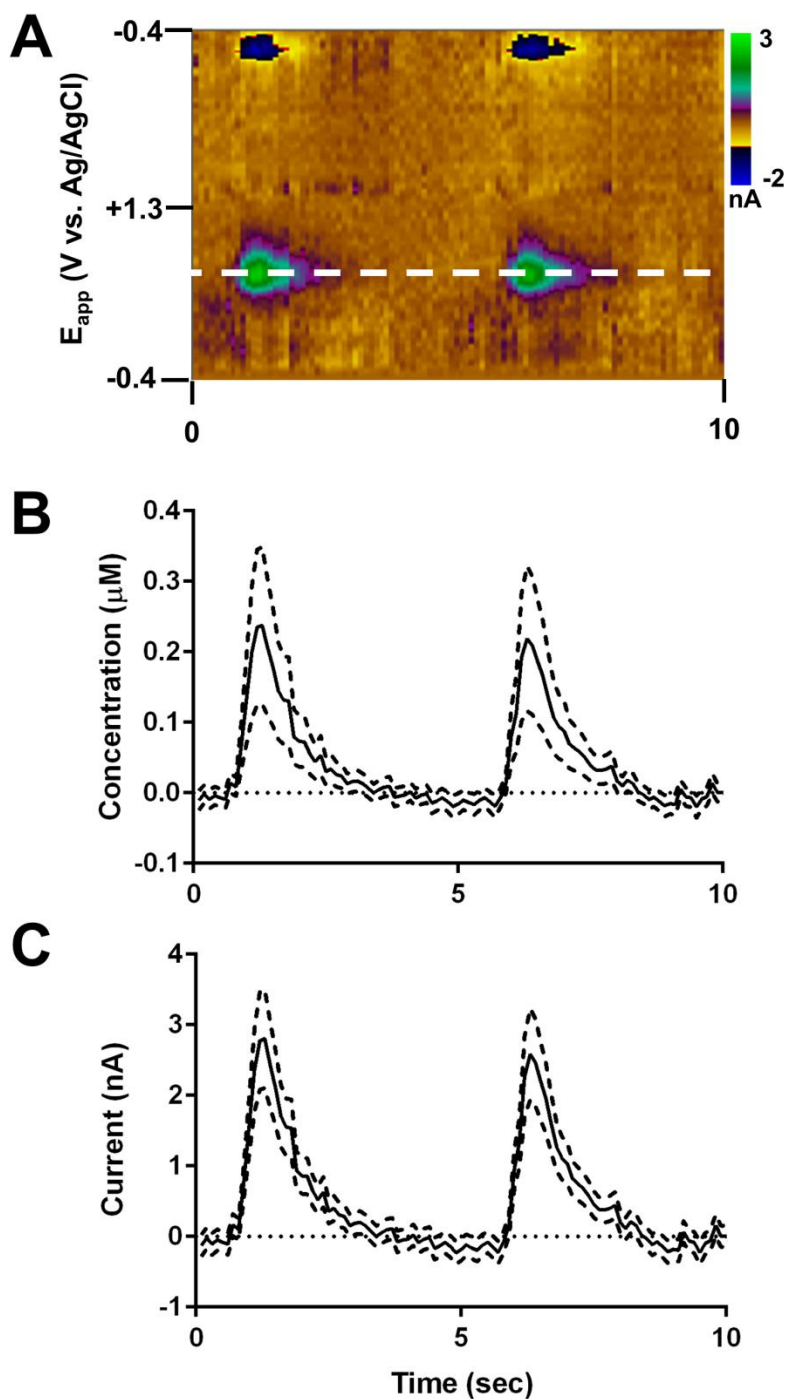
Figure 1.2. Concentration error estimation for PCA-ILS analysis of a representative FSCV recording. (A) Color plot showing two dopamine transients elicited by electrical stimulation during an intracranial self-stimulation session. (B) Chemometric concentration estimates and corresponding 95% confidence interval when considering calibration factor error. (C) Chemometric current concentration and corresponding 95% confidence interval when the calibration factor is ignored.

with time, while use of waveforms with extended anodic limits also drive surface evolution with time.(Johnson et al., 2016b; Singh et al., 2011; Takmakov, et al., 2010b) Changes driven by these factors over the time between a given experimental measurement and calibration, either during the rest of the experiment, during the removal procedure, or during equilibration with the calibration solution, would then introduce error into the calibration factor estimate. However, the experimental difficulty in determining the extent of this error has prevented any real understanding of its importance.

Additionally, even ignoring this error, the use of an average calibration factor introduces a deterministic error into the concentration estimates produced for a specific electrode based on the discrepancy between the actual calibration factor and this average calibration factor. This error can be treated more directly through theoretical considerations. The methodology for obtaining error estimates when using first-order methodologies like PCR has been the subject of research in the chemometrics literature. Here, an attempt is made to use the formulas provided by this work to illustrate the uncertainty in the estimation of the true concentrations measured during *in vivo* FSCV. The fundamental equation used for the calculation of the variance in the predicted concentration values for multivariate models is:

$$V(y_{pred}) = SEN^{-2} * \sigma_x^2 + h * SEN^{-2} * \sigma_x^2 + \mathbf{x}_u^T \mathbf{V_0}(\beta)\mathbf{x}_u \qquad \text{(Eq. 1-1)}$$

where $V(y_{pred})$ is the variance in the predicted y (concentration) values, h is the leverage, SEN is the multivariate sensitivity (defined as the inverse of the length of the vector of calibration coefficients), σ_x^2 is the variance in the x values, $\mathbf{x}_u$ is the unknown cyclic voltammogram, and $V_0(\beta)$ is the zeroth-order approximation of the covariance matrix associated with the calibration coefficients. It can be seen that there are three independent additive terms in this equation, which represent three main contributions to the uncertainty in the concentration estimate – the uncertainty in the experimental current measurements, the current measurements of the training data, and the concentration estimates for the training data, respectively.

The specifics of this presented analysis and assumptions made are presented in Appendix 1.1. This method was used to analyze a ten-second snippet taken from an *in vivo* FSCV during an intracranial self-stimulation session, during which two distinct electrically-evoked dopamine transients can be seen

(Figure 1.2). PCA-ILS was first used to generate concentration estimates through use of the calibration factor (mean and standard deviation: 11.8 ± 2.1, n = 6), and the error (shown as a 95% confidence interval) was determined through the error analysis procedure described (Figure 1.2B). Additionally, an analysis was done where no attempt was made to convert the signal into concentration values, but rather just produce chemometric estimates of the current at the dopamine oxidation potential, to show the degree to which the calibration uncertainty plays a role in decreasing confidence in the concentration estimates (Figure 1.2C). It can easily be seen that the concentration estimates have a relatively large uncertainty. For instance, at the peak of the first dopamine transient, the concentration estimate is 240 ± 110 nM. For this reason, current measurements are sometimes report in lieu of concentrations, as this can be estimated with greater confidence. However, it is important to note a few points. First, relative measurements at the same electrode have lower uncertainty given sensitivity stability. Second, this error can theoretically be averaged out through multiple measurements.

CONCLUSION

The search for selectivity has been one of the primary driving forces behind the evolution of the field of *in vivo* electrochemistry. The advances in this arena made in the past four decades have facilitated the maturation of the field to the point where it can be used to robustly track neurotransmitters in awake, freely moving animals and produced profound insights into the roles of release of these neurotransmitters in encoding information. Looking forward, many exciting new technologies have begun successful translation for *in vivo* use, including new electrode materials (e.g. carbon-nanotube coated electrodes), experimental configurations (e.g. microelectrode arrays and coupling of FSCV to iontophoresis and electrophysiology), and novel electrode coatings (e.g. PEDOT). Certainly, the issue of selectivity will continue to be a central concern for researchers as they explore the possibilities afforded by these breakthroughs and expand the uses of FSCV to the study of new neural phenomena and systems.

DISSERTATION OVERVIEW

In this vein, the focus of this dissertation is the critical analysis, development, and refinement of methods for isolation of neurotransmitter signals using FSCV. The first half of the dissertation (Chapters 2-3) deals with the use of multivariate calibration methods for FSCV data analysis. Chapter 2 addresses with a criticism of a widely used approach for training principal component regression models for FSCV data analysis. Chapter 3 presents an alternative multivariate analysis method, multivariate curve resolution, aimed at mitigating the demands placed on the researcher in collecting data for model development. The latter half of the dissertation (Chapters 4-5) focuses on a novel method for dealing with the background current at carbon-fiber microelectrodes to minimize its interference with analytical signals. Chapter 4 introduces this convolution-based method and characterizes its use with the standard FSCV waveform. Chapter 5 extends on this work by introducing a measurement protocol tailored to this method and explores the possibilities opened by largely removing the electrode background current.

REFERENCES

Bard, A. J., & Faulkner, L. R. (2001). *Electrochemical Methods: Fundamentals and Applications* (2nd ed.). New York, NY: John Wiley & Sons, Inc.

Bath, B. D., Michael, D. J., Trafton, B. J., Joseph, J. D., Runnels, P. L., & Wightman, R. M. (2000). Subsecond adsorption and desorption of dopamine at carbon-fiber microelectrodes. *Analytical Chemistry, 72*(24), 5994-6002.

Baur, J. E., Kristensen, E. W., May, L. J., Wiedemann, D. J., & Wightman, R. M. (1988). Fast-Scan Voltammetry of Biogenic-Amines. *Anal Chem, 60*(13), 1268-1272.

Booksh, K. S., & Kowalski, B. R. (1994). Theory of Analytical-Chemistry. *Anal Chem, 66*(15), A782-A791.

Bucher, E. S., Brooks, K., Verber, M. D., Keithley, R. B., Owesson-White, C., Carroll, S., et al. (2013). Flexible Software Platform for Fast-Scan Cyclic Voltammetry Data Acquisition and Analysis. *Anal Chem, 85*(21), 10344-10353.

Bucher, E. S., & Wightman, R. M. (2015). Electrochemical Analysis of Neurotransmitters. *Annu Rev Anal Chem, 8*, 239-261.

Buda, M., Gonon, F., Cespuglio, R., Jouvet, M., & Pujol, J. F. (1981). Invivo Electrochemical Detection of Catechols in Several Dopaminergic Brain-Regions of Anesthetized Rats. *Eur J Pharmacol, 73*(1), 61-68.

Cheer, J. F., Wassum, K. M., Heien, M. L. A. V., Phillips, P. E. M., & Wightman, R. M. (2004). Cannabinoids enhance subsecond dopamine release in the nucleus accumbens of awake rats. *J Neurosci, 24*(18), 4393-4400.

Church, W. H., Justice, J. B., & Byrd, L. D. (1987). Extracellular Dopamine in Rat Striatum Following Uptake Inhibition by Cocaine, Nomifensine and Benztropine. *Eur J Pharmacol, 139*(3), 345-348.

Dengler, A. K., Wightman, R. M., & McCarty, G. S. (2015). Microfabricated Collector-Generator Electrode Sensor for Measuring Absolute pH and Oxygen Concentrations. *Analytical Chemistry, 87*(20), 10556-10564.

Engstrom, R. C., Wightman, R. M., & Kristensen, E. W. (1988). Diffusional Distortion in the Monitoring of Dynamic Events. *Anal Chem, 60*(7), 652-656.

Feng, J. X., Brazell, M., Renner, K., Kasser, R., & Adams, R. N. (1987). Electrochemical Pretreatment of Carbon-Fibers for Invivo Electrochemistry - Effects on Sensitivity and Response-Time. *Anal Chem, 59*(14), 1863-1867.

Gerhardt, G. A., Oke, A. F., Nagy, G., Moghaddam, B., & Adams, R. N. (1984). Nafion-Coated Electrodes with High Selectivity for Cns Electrochemistry. *Brain Res, 290*(2), 390-395.

Gonon, F., Buda, M., Cespuglio, R., Jouvet, M., & Pujol, J. F. (1980). Invivo Electrochemical Detection of Catechols in the Neostriatum of Anesthetized Rats - Dopamine or Dopac. *Nature, 286*(5776), 902-904.

Gonon, F. G., Fombarlet, C. M., Buda, M. J., & Pujol, J. F. (1981). Electrochemical Treatment of Pyrolytic Carbon-Fiber Electrodes. *Anal Chem, 53*(9), 1386-1389.

Haaland, D. M., & Thomas, E. V. (1988). Partial Least-Squares Methods for Spectral Analyses .1. Relation to Other Quantitative Calibration Methods and the Extraction of Qualitative Information. *Anal Chem, 60*(11), 1193-1202.

Hafizi, S., Kruk, Z. L., & Stamford, J. A. (1990). Fast Cyclic Voltammetry - Improved Sensitivity to Dopamine with Extended Oxidation Scan Limits. *J Neurosci Meth, 33*(1), 41-49.

Heien, M. L. A. V., Johnson, M. A., & Wightman, R. M. (2004). Resolving neurotransmitters detected by fast-scan cyclic voltammetry. *Anal Chem, 76*(19), 5697-5704.

Heien, M. L. A. V., Khan, A. S., Ariansen, J. L., Cheer, J. F., Phillips, P. E. M., Wassum, K. M., et al. (2005). Real-time measurement of dopamine fluctuations after cocaine in the brain of behaving rats. *P Natl Acad Sci USA, 102*(29), 10023-10028.

Heien, M. L. A. V., Phillips, P. E. M., Stuber, G. D., Seipel, A. T., & Wightman, R. M. (2003). Overoxidation of carbon-fiber microelectrodes enhances dopamine adsorption and increases sensitivity. *Analyst, 128*(12), 1413-1419.

Hermans, A., Keithley, R. B., Kita, J. M., Sombers, L. A., & Wightman, R. M. (2008). Dopamine detection with fast-scan cyclic voltammetry used with analog background subtraction. *Anal Chem, 80*(11), 4040-4048.

Hodgkin, A. L., & Huxley, A. F. (1952a). Movement of Sodium and Potassium Ions during Nervous Activity. *Cold Spring Harb Sym, 17*, 43-52.

Hodgkin, A. L., & Huxley, A. F. (1952b). Propagation of Electrical Signals Along Giant Nerve Fibres. *Proc R Soc Ser B-Bio, 140*(899), 177-183.

Hodgkin, A. L., & Huxley, A. F. (1952c). A Quantitative Description of Membrane Current and Its Application to Conduction and Excitation in Nerve. *J Physiol-London, 117*(4), 500-544.

Howell, J. O., Kuhr, W. G., Ensman, R. E., & Wightman, R. M. (1986). Background Subtraction for Rapid Scan Voltammetry. *J Electroanal Chem, 209*(1), 77-90.

Jackson, J. E., & Mudholkar, G. S. (1979). Control Procedures for Residuals Associated with Principal Component Analysis. *Technometrics, 21*(3), 341-349.

Johnson, J. A., Rodeberg, N. T., & Wightman, R. M. (2016a). Failure of Standard Training Sets in the Analysis of Fast-Scan Cyclic Voltammetry Data. *Acs Chem Neurosci, 7*(3), 349-359.

Johnson, J. A., Rodeberg, N. T., & Wightman, R. M. (2016b). Failure of Standard Training Sets in the Analysis of Fast-Scan Cyclic Voltammetry Data. *ACS Chem Neurosci, 7*(3), 349-359.

Jones, S. R., Mickelson, G. E., Collins, L. B., Kawagoe, K. T., & Wightman, R. M. (1994). Interference by Ph and Ca2+ Ions during Measurements of Catecholamine Release in Slices of Rat Amygdala with Fast-Scan Cyclic Voltammetry. *J Neurosci Meth, 52*(1), 1-10.

Justice, J. B., & Neill, D. B. (1986). Interpretations of Voltammetry Invivo Using Dialyzed Perfusion. *Ann Ny Acad Sci, 473*, 170-187.

Justice, J. B., Wages, S. A., Michael, A. C., Blakely, R. D., & Neill, D. B. (1983). Interpretations of Voltammetry in the Striatum Based on Chromatography of Striatal Dialysate. *J Liq Chromatogr, 6*(10), 1873-1896.

Karweik, D. H., Hu, I. F., Weng, S., & Kuwana, T. (1985). Carbonaceous Surfaces - Modification, Characterization, and Uses for Electrocatalysis. *Acs Sym Ser, 288*, 582-595.

Kawagoe, K. T., Garris, P. A., & Wightman, R. M. (1993a). Ph-Dependent Processes at Nafion(R)-Coated Carbon-Fiber Microelectrodes. *J Electroanal Chem, 359*(1-2), 193-207.

Kawagoe, K. T., & Wightman, R. M. (1994). Characterization of Amperometry for in-Vivo Measurement of Dopamine Dynamics in the Rat-Brain. *Talanta, 41*(6), 865-874.

Kawagoe, K. T., Zimmerman, J. B., & Wightman, R. M. (1993b). Principles of Voltammetry and Microelectrode Surface-States. *J Neurosci Meth, 48*(3), 225-240.

Keithley, R. B., Heien, M. L., & Wightman, R. M. (2009). Multivariate concentration determination using principal component regression with residual analysis. *Trac-Trend Anal Chem, 28*(9), 1127-1136.

Keithley, R. B., & Wightman, R. M. (2011). Assessing Principal Component Regression Prediction of Neurochemicals Detected with Fast-Scan Cyclic Voltammetry. *Acs Chem Neurosci, 2*(9), 514-525.

Kile, B. M., Walsh, P. L., McElligott, Z. A., Bucher, E. S., Guillot, T. S., Salahpour, A., et al. (2012). Optimizing the Temporal Resolution of Fast-Scan Cyclic Voltammetry. *Acs Chem Neurosci, 3*(4), 285-292.

Kishida, K. T., Saez, I., Lohrenz, T., Witcher, M. R., Laxton, A. W., Tatter, S. B., et al. (2016). Subsecond dopamine fluctuations in human striatum encode superposed error signals about actual and counterfactual reward. *P Natl Acad Sci USA, 113*(1), 200-205.

Kissinger, P. T., Hart, J. B., & Adams, R. N. (1973). Voltammetry in Brain-Tissue - New Neurophysiological Measurement. *Brain Res, 55*(1), 209-213.

Kovach, P. M., Ewing, A. G., Wilson, R. L., & Wightman, R. M. (1984). Invitro Comparison of the Selectivity of Electrodes for Invivo Electrochemistry. *J Neurosci Meth, 10*(3), 215-227.

Kramer, R. (1998). *Chemometric Techniques for Quantitative Analysis*. New York, NY: Marcel Dekker, Inc.

Kume-Kick, J., & Rice, M. E. (1998). Dependence of dopamine calibration factors on media Ca2+ and Mg2+ at carbon-fiber microelectrodes used with fast-scan cyclic voltammetry. *J Neurosci Meth, 84*(1-2), 55-62.

Lavine, B. K., & Workman, J. (2013). Chemometrics. *Anal Chem, 85*(2), 705-714.

Logman, M. J., Budygin, E. A., Gainetdinov, R. R., & Wightman, R. M. (2000). Quantitation of in vivo measurements with carbon fiber microelectrodes. *J Neurosci Meth, 95*(2), 95-102.

Meloun, M., Militky, J., & Forina, M. (1994). *Chemometrics for Analytical Chemistry*. New York, NY: Ellis Horwood.

Millar, J., Armstrongjames, M., & Kruk, Z. L. (1981). Polarographic Assay of Iontophoretically Applied Dopamine and Low-Noise Unit Recording Using a Multibarrel Carbon-Fiber Microelectrode. *Brain Res, 205*(2), 419-424.

Millar, J., Stamford, J. A., Kruk, Z. L., & Wightman, R. M. (1985). Electrochemical, Pharmacological and Electrophysiological Evidence of Rapid Dopamine Release and Removal in the Rat Caudate-Nucleus Following Electrical-Stimulation of the Median Forebrain-Bundle. *Eur J Pharmacol, 109*(3), 341-348.

Nagy, G., Gerhardt, G. A., Oke, A. F., Rice, M. E., Adams, R. N., Moore, R. B., et al. (1985). Ion-Exchange and Transport of Neurotransmitters in Nafion Films on Conventional and Microelectrode Surfaces. *J Electroanal Chem, 188*(1-2), 85-94.

Olivieri, A. C. (2008). Analytical advantages of multivariate data processing. One, two, three, infinity? *Anal Chem, 80*(15), 5713-5720.

Park, J., Kile, B. M., & Wightman, R. M. (2009). In vivo voltammetric monitoring of norepinephrine release in the rat ventral bed nucleus of the stria terminalis and anteroventral thalamic nucleus. *Eur J Neurosci, 30*(11), 2121-2133.

Phillips, P. E. M., Stuber, G. D., Heien, M. L. A. V., Wightman, R. M., & Carelli, R. M. (2003). Subsecond dopamine release promotes cocaine seeking. *Nature, 422*(6932), 614-618.

Phillips, P. E. M., & Wightman, R. M. (2003). Critical guidelines for validation of the selectivity of in-vivo chemical microsensors. *Trac-Trend Anal Chem, 22*(9), 509-514.

Roberts, J. G., Lugo-Morales, L. Z., Loziuk, P. L., & Sombers, L. A. (2013). Real-time chemical measurements of dopamine release in the brain. *Methods Mol Biol, 964*, 275-294.

Rodeberg, N. T., Johnson, J. A., Cameron, C. M., Saddoris, M. P., Carelli, R. M., & Wightman, R. M. (2015). Construction of Training Sets for Valid Calibration of in Vivo Cyclic Voltammetric Data by Principal Component Analysis. *Anal Chem, 87*(22), 11484-11491.

Rodeberg, N. T., Sandberg, S. G., Johnson, J. A., Phillips, P. E. M., & Wightman, R. M. (2017). Hitchhiker's Guide to Voltammetry: Acute and Chronic Electrodes for in Vivo Fast-Scan Cyclic Voltammetry. *Acs Chem Neurosci, 8*(2), 221-234.

Runnels, P. L., Joseph, J. D., Logman, M. J., & Wightman, R. M. (1999). Effect of pH and surface functionalities on the cyclic voltammetric responses of carbon-fiber microelectrodes. *Anal Chem, 71*(14), 2782-2789.

Salamone, J. D., Hamby, L. S., Neill, D. B., & Justice, J. B. (1984). Extracellular Ascorbic-Acid Increases in Striatum Following Systemic Amphetamine. *Pharmacol Biochem Be, 20*(4), 609-612.

Singh, Y. S., Sawarynski, L. E., Dabiri, P. D., Choi, W. R., & Andrews, A. M. (2011). Head-to-Head Comparisons of Carbon Fiber Microelectrode Coatings for Sensitive and Selective Neurotransmitter Detection by Voltammetry. *Anal Chem, 83*(17), 6658-6666.

Takmakov, P., Zachek, M. K., Keithley, R. B., Bucher, E. S., McCarty, G. S., & Wightman, R. M. (2010a). Characterization of Local pH Changes in Brain Using Fast-Scan Cyclic Voltammetry with Carbon Microelectrodes. *Anal Chem, 82*(23), 9892-9900.

Takmakov, P., Zachek, M. K., Keithley, R. B., Walsh, P. L., Donley, C., McCarty, G. S., et al. (2010b). Carbon Microelectrodes with a Renewable Surface. *Anal Chem, 82*(5), 2020-2028.

Troyer, K. P., Heien, M. L. A. V., Venton, B. J., & Wightman, R. M. (2002). Neurochemistry and electroanalytical probes. *Curr Opin Chem Biol, 6*(5), 696-703.

Venton, B. J., Michael, D. J., & Wightman, R. M. (2003). Correlation of local changes in extracellular oxygen and pH that accompany dopaminergic terminal activity in the rat caudate-putamen. *J Neurochem, 84*(2), 373-381.

Venton, B. J., & Wightman, R. M. (2003). Psychoanalytical electrochemistry: Dopamine and behavior. *Anal Chem, 75*(19), 414a-421a.

Wiedemann, D. J., Bassetomusk, A., Wilson, R. L., Rebec, G. V., & Wightman, R. M. (1990). Interference by Dopac and Ascorbate during Attempts to Measure Drug-Induced Changes in Neostriatal Dopamine with Nafion-Coated, Carbon-Fiber Electrodes. *J Neurosci Meth, 35*(1), 9-18.

Wightman, R. M., Amatore, C., Engstrom, R. C., Hale, P. D., Kristensen, E. W., Kuhr, W. G., et al. (1988a). Real-Time Characterization of Dopamine Overflow and Uptake in the Rat Striatum. *Neuroscience, 25*(2), 513-523.

Wightman, R. M., Brown, D. S., Kuhr, W. G., & Wilson, R. L. (1987). Molecular Specificity of In Vivo Electrochemical Measurements. In J. B. Justice (Ed.), *Voltammetry in the Neurosciences* (pp. 103-138). Clifton, NJ: Humana Press.

Wightman, R. M., May, L. J., & Michael, A. C. (1988b). Detection of Dopamine Dynamics in the Brain. *Anal Chem, 60*(13), 769-779A.

Yorgason, J. T., Espana, R. A., & Jones, S. R. (2011). Demon voltammetry and analysis software: analysis of cocaine-induced alterations in dopamine signaling using multiple kinetic measures. *J Neurosci Methods, 202*(2), 158-164.

CHAPTER 2: FAILURE OF STANDARD TRAINING SETS IN THE ANALYSIS OF FAST-SCAN CYCLIC VOLTAMMETRY DATA[1]

INTRODUCTION

In the analysis of fast-scan cyclic voltammetry (FSCV) data, the use of standard training sets (i.e. sets of cyclic voltammograms obtained from electrodes, recording sessions, and/or subjects other than those used for experimental data collection) for conditioning principal component regression (PCR) calibration models has increased in popularity.(Clark et al., 2013; Flagel et al., 2011; Goertz et al., 2015; Hart et al., 2014; Hollon et al., 2014; Howe et al., 2013; Nasrallah et al., 2011; Parker et al., 2010; Wanat et al., 2013; Willuhn et al., 2012; Willuhn et al., 2014a; Willuhn et al., 2014b) However, theoreticians have long warned about the dangers associated with this approach, emphasizing the need for either consistency between the conditions for obtaining model training and experimental data, or the use of transfer methods when such consistency cannot be obtained.(Booksh, 2006; Feudale et al., 2002; Wang & Kowalski, 1992; Woody et al., 2004) Here, we aim to provide a clear theoretical explanation of PCR, with particular focus on using this discussion to evaluate the appropriateness of the use of standard training sets in analysis of FSCV data.

FSCV is an electroanalytical technique that allows for the real-time recording of the subsecond dynamics of electroactive neurotransmitters.(Bucher & Wightman, 2015) Cyclic voltammograms (CVs) obtained through its use can be used for analyte concentration change identification and subsequent quantification, both of which are critical to proper calibration. In practice, however, CVs obtained *in vivo* often have contributions from multiple analytes that require resolution before positive identification, much less quantification, can be made. As a multivariate calibration technique, PCR is equipped to handle this

---

[1] This chapter previously appeared as an article in ACS Chemical Neuroscience. The original citation is as follows: Johnson, J.A.; Rodeberg, N.T.; Wightman, R.M. "Failure of Standard Training Sets in the Analysis of Fast-Scan Cyclic Voltammetry Data," *ACS Chem. Neurosci.* Vol. 7, Issue 3. (March 2016): 349-359.

issue, as information across the scan-potential window can be used to separate these overlapping signals. As such, considerable work has gone into the development of PCR as a robust data analysis technique for FSCV.(Heien et al., 2004; Keithley et al., 2010; Keithley et al., 2009; Keithley & Wightman, 2011)

In using PCR, proper training set construction for model conditioning is a critical consideration.(Rodeberg et al., 2015) The current-concentration relationships at each potential for a given analyte, which are essential information for accurate signal resolution, are directly estimated from the CVs in the training set. As these relationships are known to vary between experimental sessions, it has been advised that training set data be collected under conditions resembling those of the experimental data collection as closely as possible (e.g. in the same animal and anatomical region, with the same equipment, and within the recording session).(Keithley, et al., 2009; Kramer, 1998; Lavine & Workman, 2013) However, procedural constraints have increased the use of standard training sets, which consist of data collected under circumstances significantly differing from those of experimental data collection. The questions then arise as to what degree these training sets can capture these experiment-specific relationships and whether their use leads to a detrimental effect on the ability of derived models to resolve analyte contributions. To this end, recent work from our laboratory demonstrated undesirable practical consequences stemming from their use, including systematic misestimation of analyte concentration changes and failure of model validation procedures.(Rodeberg, et al., 2015) However, the specific origin of these issues within the framework of PCR was not investigated.

The goal of this paper is multifold. First, we seek to increase the interpretability of PCR models by elucidating how principal component regression accomplishes the calibration goals of analyte resolution and quantification, particularly in the analysis of FSCV data. While there are many excellent resources for understanding the technique,(Keithley, et al., 2009; Kramer, 1998; Lavine & Workman, 2013) this discussion aims to avoid the heavy reliance on the language of vector calculus or linear algebra often found in these guides, instead substituting visual explanations where possible. Understanding of these calculations can be used to help guide training set construction, enabling proper PCR use. Second, this discussion is used to build on our previous work, focusing here on identification of the source of the previously demonstrated shortcomings of models built with standard training sets.(Rodeberg, et al., 2015)

Particularly, it is shown that the use of standard training sets indeed leads to improper assignment of the current-concentration relationships that define multivariate analysis, leading to poor analyte resolution. Ultimately, these results serve to highlight the need and practical utility of training set construction within a given experimental session.

THEORY

Calibration

Calibration Basics. The goal of analytical calibration is to determine the relationship between an instrumental response and the corresponding value of the sample property to be estimated (e.g. concentration of an analyte) under a given set of conditions for future prediction of the latter.(Booksh, 2006) This is done in two steps: calibration method selection and model training. Selection of a method is driven by the expected characteristics of the data (e.g. presence of interference and dimensionality), assumptions made about relationship between the instrumental response and sample property (e.g. linearity), and practical considerations (e.g. computation intensity and ease of use). Within that method's framework, estimated model parameters are determined by *training* the calibration model using data for which both the response and sample property value are known (i.e., *a training set*). This relationship can then be used to convert experimental measurements into estimations of the unknown value of the sample property. The accuracy of this procedure is limited by the underlying assumptions of the calibration method, and the validity of the relationship found in the training data to the experimental data.

Univariate Linear Regression. The univariate linear regression calibration method uses a single instrumental response value (e.g. a current measurement) and assumes a linear relationship between it and the value of the sample property. In the analysis of FSCV data, the peak faradaic current, the most sensitive measurement, is typically used for prediction. Additionally, due to the large charging current that arises at the high scan rates employed in FSCV, background subtraction, where currents are reported relative to a 'background' measurement, is performed to allow for reliable detection of the relatively small analytical signal, limiting quantitation to relative changes in analyte concentration.(Robinson et al., 2003)

Here, this is specified by the use of the symbols Δi and Δ[analyte], indicating the changes in current and analyte concentration, respectively, relative to their absolute values at the time of the 'background' measurement. The calibration equation of *classical* least-squares regression for background-subtracted FSCV dopamine quantitation can thus be written as:

$$\Delta i_{DA,peak} = Sen_{DA}\Delta[DA] + \Delta i_0 \qquad \text{(Eq. 2.1)}$$

where $\Delta i_{DA,peak}$ is the background-subtracted dopamine peak current, Sen_{DA} is the analytical sensitivity, $\Delta[DA]$ is the dopamine concentration change, and Δi_0 is the background-subtracted peak current in the absence of a relative dopamine concentration change (ideally, or possibly constrained to be, zero). Model training consists of estimation of the parameter values (i.e. the sensitivity and blank measurement) that minimize the sum of the squares of the residuals. A more useful formulation is the *inverse* model, Eq. 2 2:

$$\Delta[DA] = CF_{DA}\Delta i_{DA,peak} + \Delta[DA]_0 \qquad \text{(Eq. 2.2)}$$

where CF_{DA} is the calibration factor, $\Delta[DA]_0$ is the dopamine concentration change in the absence of a change in current (again, ideally, or constrained to, zero), and all other variables retaining their meaning from Eq. 2.1. Note that Eq. 2.2 can be converted into Eq. 2.1 (i.e. CF_{DA} and $\Delta[DA]_0$ are equal to $Sen_{analyte}^{-1}$ and $-\Delta i_0/Sen_{analyte}$, respectively); however, the estimated model parameters differ when regression is done in the two formulations.(Centner et al., 1998; Krutchkoff, 1967, 1969)

Multivariate Analysis. The simplicity and interpretability of the univariate linear regression model make it a powerful analytical tool. However, univariate models fail to make accurate predictions for signals containing multiple analyte contributions. For example, Figure 2.1 is a background-subtracted color plot of voltammograms obtained in a rodent brain with a carbon fiber microelectrode during an electrically stimulated dopamine release event, in which signals corresponding to dopamine and pH changes are present. A univariate model would interpret the basic pH shift as a decrease in DA. This error arises from the failure of the model to resolve the various analyte contributions prior to quantitation. Assuming linear superposition of analyte signals, a correction to this equation is:
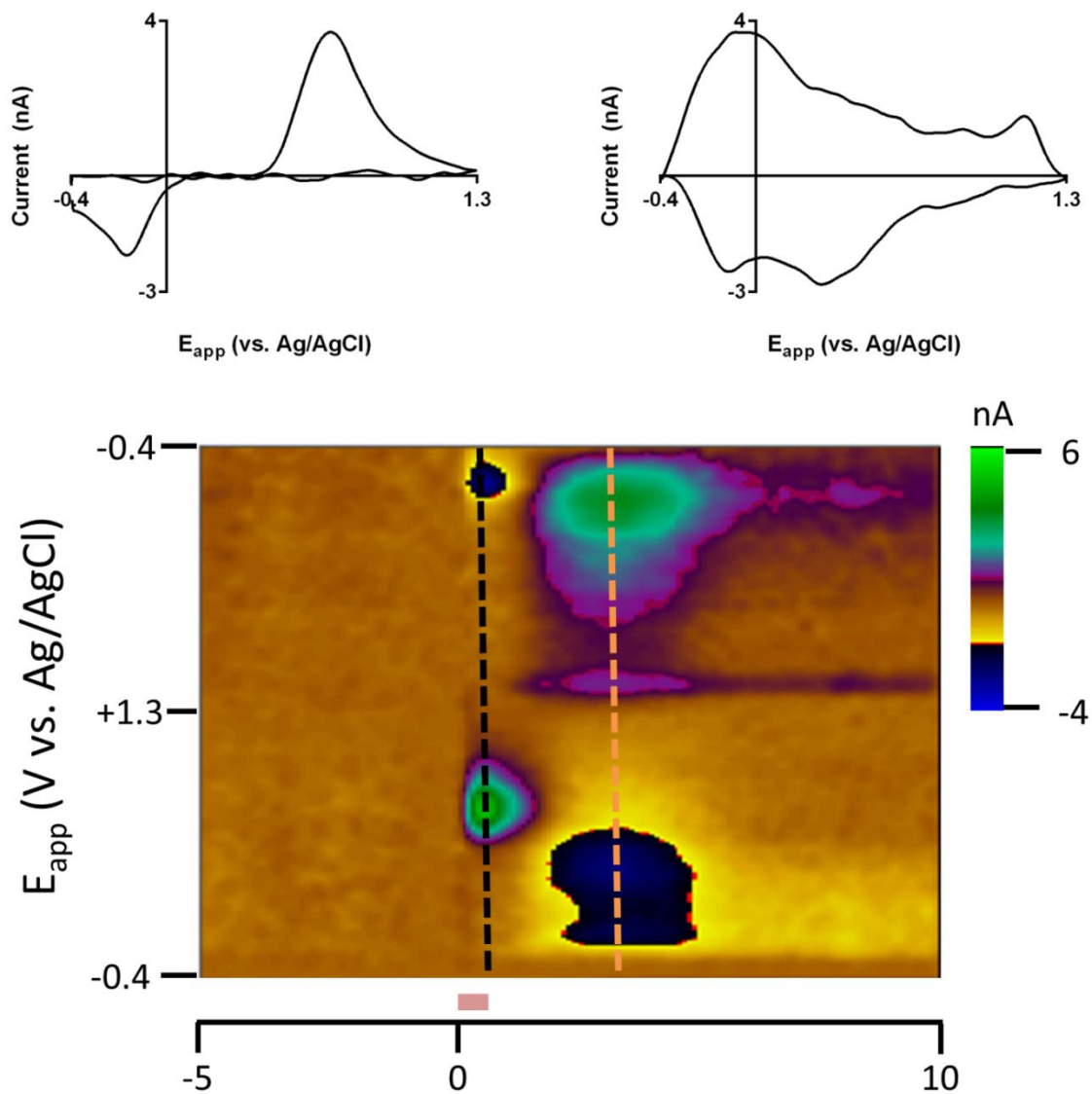
Figure 2.1. Representative *in vivo* electrochemical recording showing dopamine and pH changes. A color plot representation of background-subtracted voltammograms collected after electrical stimulation of dopamine neurons (bottom) in the brain of a freely-moving rat is constructed by plotting time as the abscissa, the applied potential as the ordinate, and the current in false color. The inset voltammograms represent dopamine and pH shifts collected at the black and orange dotted lines, respectively.

$$\Delta i_{DA,peak} = Sen_{DA}\Delta[DA] + Sen_{pH}\Delta pH + \Delta i_0 \qquad \text{(Eq. 2.3)}$$

However, for a given peak current, an infinite number of dopamine and pH concentration pairs satisfy this equation, as there are more unknown than known values. As this discussion shows, for multicomponent calibration, both component identification and its quantitation must be accomplished, and this requires use of multiple measurements to succeed.

The multivariate model, using the entire scan-potential window to provide more known values, can be stated in the classical formulation as a system of N equations, where N is the number of measurements taken into account in the model (850 in this paper, sampling frequency x waveform duration):

$$\Delta i_1 = Sen_{DA,1}\Delta[DA] + Sen_{pH,1} * \Delta pH$$

$$\Delta i_2 = Sen_{DA,2}\Delta[DA] + Sen_{pH,2} * \Delta pH \qquad \text{(Eq. 2.4)}$$

$$\dots$$

$$\Delta i_{850} = Sen_{DA,850}\Delta[DA] + Sen_{pH,850} * \Delta pH$$

The omission of an intercept term is intentional and standard in practice. Again, a more useful calibration equation is that of the inverse formulation:

$$\Delta[DA] = p_1\Delta i_1 + p_2\Delta i_2 + \dots + p_{850}\Delta i_{850}$$

$$\Delta pH = p_1\Delta i_1 + p_2\Delta i_2 + \dots + p_{850}\Delta i_{850} \qquad \text{(Eq. 2.5)}$$

where p is referred to as the calibration coefficient for the Nth data point (N = 1,2…850). Again, Eqs. 2.4 and 2.5 can be interconverted but differ in the estimated model parameters obtained from their use in regression. The assumption of this model is, "The value of the current measurements at each potential depends only, and linearly, on the concentration changes of dopamine and pH." If the data fail to meet this assumption, a prediction error will occur. Statistical techniques (i.e., residual analysis) allow for identification of data with significant additional signal contributions, which is referred to as the *first-order advantage*.(Olivieri, 2008) However, if there is any measurement contribution not included in the model, increased error should be expected in model predictions.
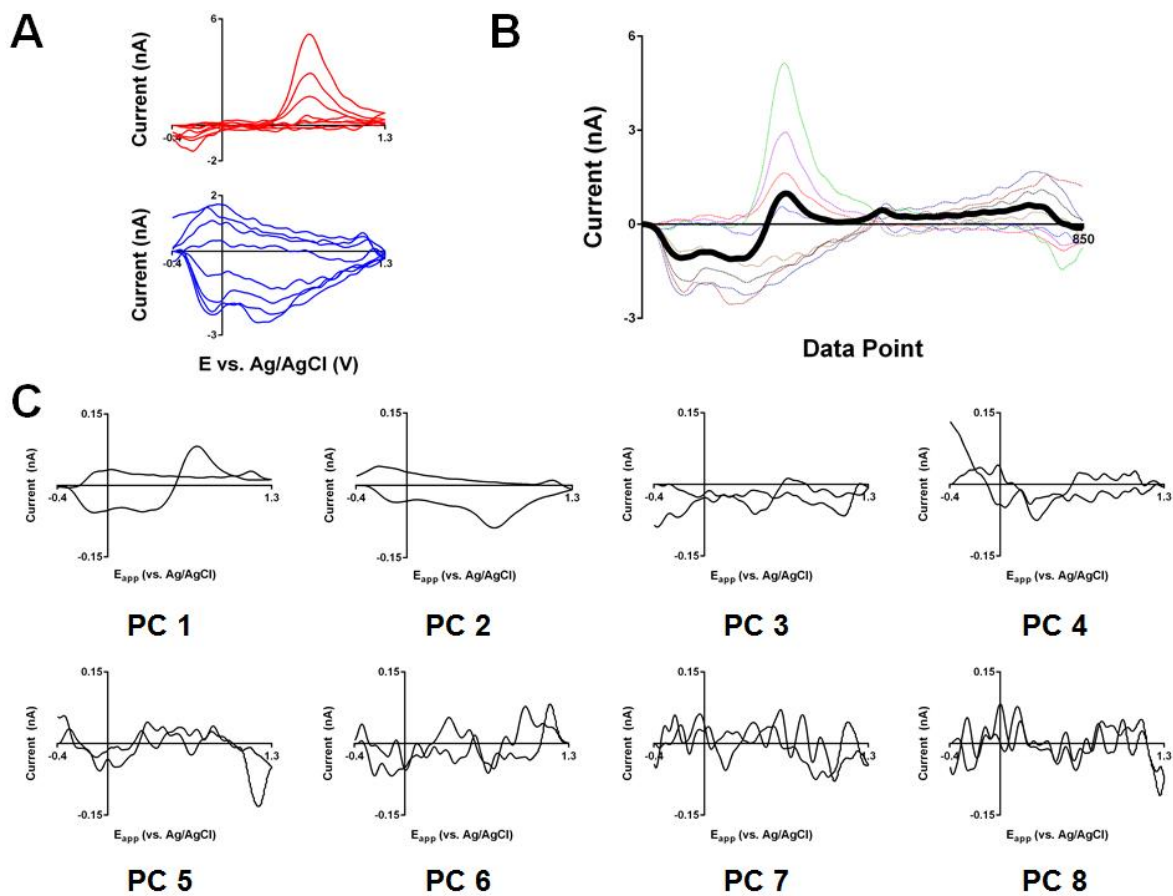
Figure 2.2. The generation of principal components. (A) Dopamine (top) and pH (bottom) training set voltammograms shown in the traditional electrochemical format (left, as function of potential) and in the 'unwrapped' format (right, as function of data point). (B) First principal component (dark black line) overlaid on the training set voltammograms in the 'unwrapped' format. (C) Eight principal components generated by the singular value decomposition algorithm for the training set shown in (B).

Principal Component Regression

The question now arises of how to train the model (i.e. optimize the p parameters of Eq. 2.5). The ideal solution would spread the burden of prediction across the scan-potential window and not be overly specific to the training data. Furthermore, the solution should minimize noise in the calibration data as it degrades the quality of the relationships in the training data, decreasing confidence in the model predictions.

Principal component analysis (PCA) addresses these issues. In PCA, each training CV is restated as the linear combination of a collection of scaled vectors called principal components (PCs). The advantage of this reformulation is that some PCs correspond to relevant deterministic variance (i.e. that carrying information about the analytes), while others correspond to non-deterministic noise. Exclusion of the latter ideally allows for the production of noise-free training set CVs, allowing for parameter estimation with greater confidence. This estimation is done in the inverse formulation (inverse least-squares regression, or ILS) with the data stated in the terms of PCs, simplifying the calculations. Collectively, the use of PCA and ILS is referred to as principal component regression (PCR). There are four major steps in the use of PCR:

1) Construction and selection of the relevant subset of principal components (PCA);
2) Scoring of standards on generated PCs (PCA);
3) Regression of PC scores against concentrations (ILS);
4) Application to experimental data.

Principal component construction. For generation of PCs, a training set must be constructed. We illustrate this with the training set shown in Figure 1A that contains both dopamine and pH background-subtracted CVs (n = 4/analyte). The PCR model is entirely defined by the relationships found in the training set. A good training set (ref 24) spans the concentration range of interest, contains mutually exclusive voltammograms of all expected analytes, and matches the characteristics of the experimental data (e.g. noise and peak positions).(Keithley, et al., 2009; Kramer, 1998) The limitations of *in vivo* training set construction make collection of single-analyte CVs preferable to allow for reliable estimation
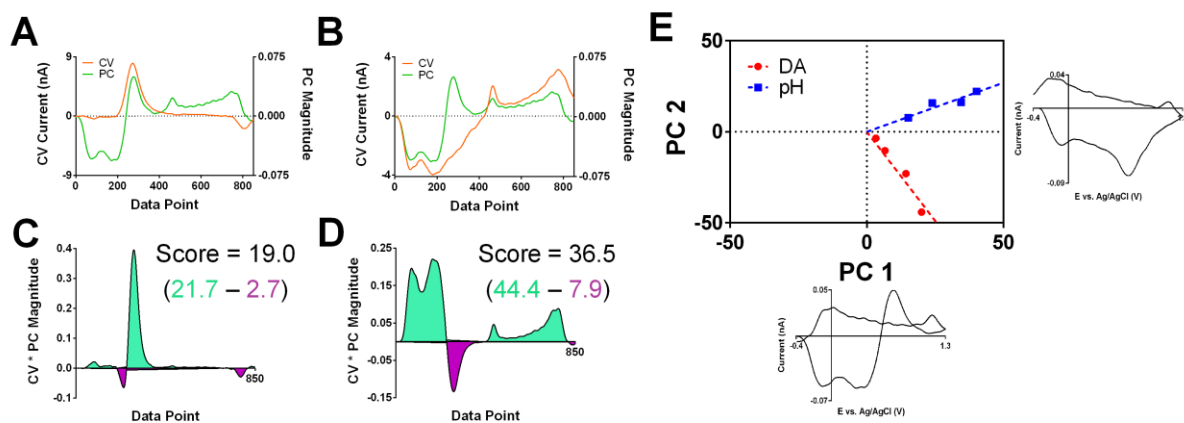
Figure 2.3. The scoring process of principal component analysis. (A) CV of dopamine standard (orange) and the first principal component (green) shown in the 'unwrapped' format. (B) As in (A) but with a pH standard. (C) Plot showing the value of product of the principal component and current amplitudes ($w_n\Delta i_n$ from Equation 6) from (A) for each data point. The regions beneath positive and negative values of this calculation are shown in green and purple, respectively, to assist with conceptualization of the score calculation, which is calculated from summation across the data window (see text). (D) As in (C) but using the PC and CV amplitudes from (B). (E) Cook's distance plot showing the scores for each CV on the first two principal components for the training set presented in Figure 1. Each axis corresponds to the adjacent principal component, and each training CV is shown as a point on the plot whose coordinates are defined by its scores on the corresponding principal component.

of the concentrations of the standards. This approach, however, mandates that the analyte voltammetric responses be independent of one another and the matrix, or model performance will suffer. This limits the use of models built in this way to conditions where these assumptions hold. Of note, as there is a known dependence of the dopamine voltammetric response on pH, use of PCR models built with pure DA and pH voltammogram standards should be limited to pH ranges around those used for training data collection.(Kawagoe et al., 1993) However, given the tight regulation of the neuronal environment, significant excursions of pH to extreme values are relatively rare.(Chesler, 2003) The goal of PC construction is to calculate a set of vectors that can describe the entirety of the training set (i.e. entirely reconstruct the training standards through combinations of scaled PCs). These PCs retain the dimensions of CVs (i.e. have a single value corresponding to each applied potential), allowing visualization using traditional electrochemical representation.(Keithley, et al., 2010) (To minimize confusion both the data and PCs are presented here 'unwrapped' (Figure 2.1B)). Construction is done with a linear algebra technique termed single value decomposition, or SVD (see Appendix 2.1 for more details). In brief, the first PC is calculated to span the maximum variance possible (Figure 2.1B and as 'PC 1' in 2.1C), without consideration of analyte identity or corresponding concentration change. The following PC then captures the most remaining variance and is constrained to being orthogonal (i.e. describe distinct information) to its successor. This process continues until all variance is described, resulting in a set of unique PCs equal to the number of the CVs in the training set (Figure 2.1C). Of note, without pre-treatment (e.g. mean-centering and scaling), CVs with the largest currents have a disproportionately greater influence on the shape of the PCs.(Keithley, et al., 2010; Kramer, 1998) Thus, the quality (e.g. how representative it is of the average data collected, how free it is from interferents, and the noise levels in the CV) of these CVs is critical.

Scoring of standards on PCs. After PC generation, the 'scores' of each of the training standards on each of the PCs can be calculated as the sum of the pointwise product of the principal component and background-subtracted current magnitudes using the following formula:

$$\text{Score} = \sum_{n=1}^{N} w_n \Delta i_n \qquad \text{(Eq. 2.6)}$$
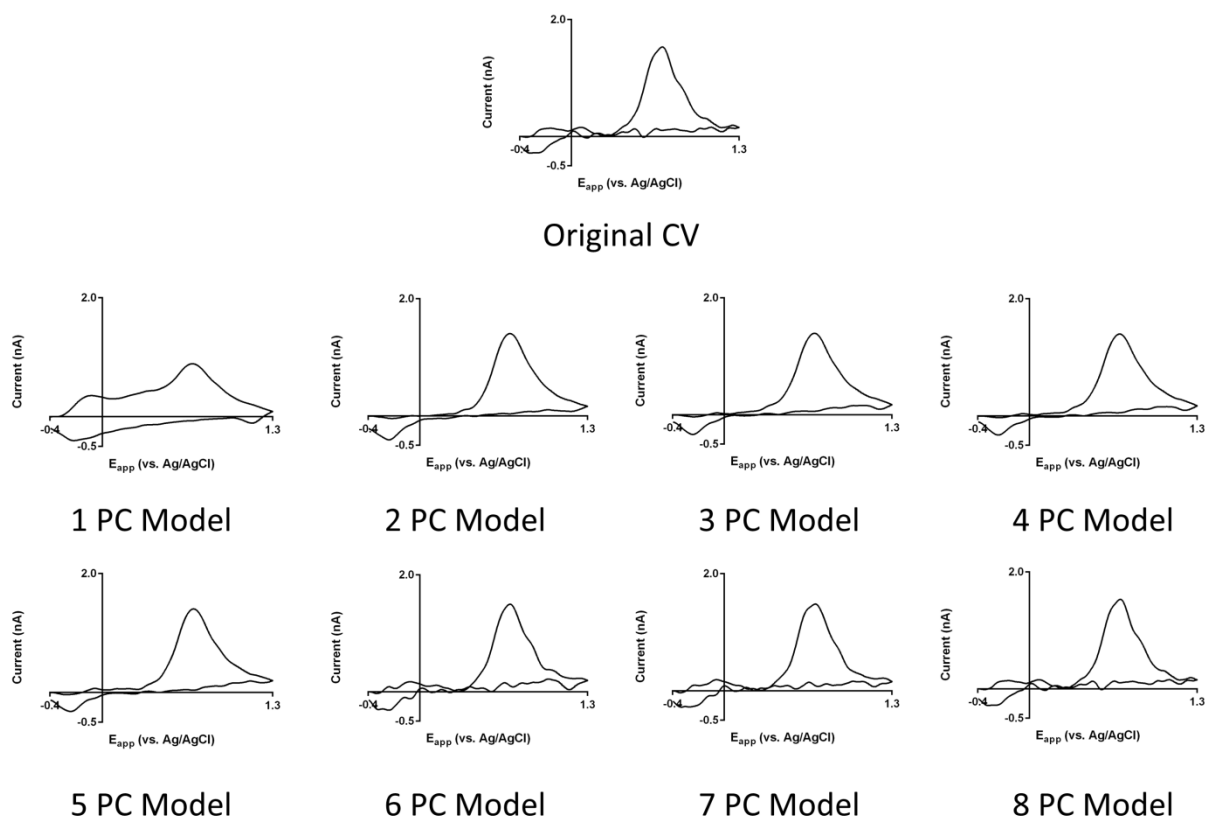
Figure 2.4. Construction of PCR model estimate for a dopamine cyclic voltammogram. The estimates are generated from successive addition of the PC loading vectors scaled by the corresponding score. The original CV is shown in the top row, while the PC model estimates, generated by consideration of increasing numbers of principal components, are shown in the bottom two rows. Note that the original CV is entirely reconstructed by consideration of all eight generated principal components.

where n is the data point, w_n is the magnitude of the principal component loading vector at a given data point, and Δi_n is the background-subtracted current magnitude at that data point. This calculation is referred to as the projection of CV onto the PC, or, more generally, the dot product of the CV and PC vectors.

This calculation can be decomposed into its constituent steps and illustrated graphically (Figure 2.2A-D). First, the product of the current and PC magnitudes is calculated at each point, as shown in Figure 2.2C and D. These products are then summed across the scan-potential window to obtain the score value. As the positive and negative contributions balance one another in this latter calculation, the areas beneath the product of the CV and PC magnitudes at each point are shaded different colors (green, positive; pink, negative) to assist in conceptualization of the regions contributing most to the score value.

When comparing CVs that differ in shape, higher score *magnitudes* indicate a higher degree of similarity in shape between the PC and CV. For instance, as seen in Figure 2.2C, both the PC and dopamine CV magnitudes are positive and large, leading to an area with a large positive contribution to the final score. For similarly shaped CVs, higher scores simply imply higher intensities within the regions heavily weighted by the PC. The polarity of the score is a secondary consideration. For a given PC polarity, regions in which the PC and CV are alike or differ in sign tend to make the score more positive or negative, respectively. However, if all PC magnitudes were reversed in sign (i.e. the PC polarity was flipped), the scores would be identical in magnitude but differ only in sign. One merely expects that similar CVs (e.g. the training CVs for a given analyte) are alike in sign.

Selection of PC subset for model. After scoring, a set of N scores, where N is equal to the number of principal components, is produced for each training CV (i.e. the dimensionality of the data is reduced). Indeed, if all scores for a training CV on all unique PCs are taken, the original CV can be entirely reconstructed by the linear combination of each PC scaled by its corresponding score (Fig. 2.4). However, we retain only the PCs that correspond to analytically relevant features of the training set voltammograms (i.e. primary PCs), while those composed primarily of noise are discarded (i.e. secondary PCs. PCs 3-8 in Figure 2.1). Thus, through use of only the primary PCs, the original CV can be reconstructed with the noise described by the secondary PCs excluded (2 PC model in Fig. 2.4).

The selection of primary PCs typically relies on statistical analysis of the proportion of information described by each PC (i.e. variance-based methods). Of note, for FSCV data, a previous study from our laboratory compared two such selection methods, concluding that use of the Malinowski's F-test was preferable for reliable identification and removal of PCs corresponding to noise.(Keithley, et al., 2010) Such variance-based tests rely on the assumption that the analytically relevant portion of the signal is considerably larger than that attributable to noise. However, if the noise levels become too high, too many PCs, including those describing noise, are likely to be retained. Estimates place this transition for the Malinowski's F-test between signal-to-noise ratios of 10-100.(Malinowski, 2004)

A useful tool to examine the model is the Cook's distance plot (Figure 2.2E), which has coordinates corresponding to a CV's score on a given PC (shown next to the corresponding axis). For simplicity, these are often two-dimensional plots where only coordinates corresponding to first two PCs (i.e. the two PCs that describe the most variance in the data) are shown. The utility of such plots is in the detection of outliers, which is discussed in detail elsewhere.(Cook, 1977; Keithley & Wightman, 2011) Generally, one expects to observe linear groups of data corresponding to a given analyte. These linear groups tend to spread more along one coordinate, indicating that the corresponding PC captures more of the variance in that analyte than the other PC. Additionally, these groups should be sufficiently separated from one another in the plot; otherwise, it is likely that some training set spectra are not sufficiently 'pure'.

Regression of PC scores against concentration. For a two-analyte, two-PC system, the calibration equations in terms of PCs are stated in the inverse formulation as:

$$\Delta[DA] = m_{DA,PC1}Score_{PC1} + m_{DA,PC2}Score_{PC2}$$

$$\Delta pH = m_{pH,PC1}Score_{PC1} + m_{pH,PC2}Score_{PC2}$$

(Eq. 2.7)

The values of *m* are estimated through least-squares regression, which is equivalent to estimating the *p* parameters in Eq. 2.5. This approach, however, limits the regression solutions to the subspace defined by the PCs and greatly simplifies the calculations. After this stage, the model, consisting of the retained PCs and the values of the *m* parameters, is completely defined, having only knowledge of the training set data.
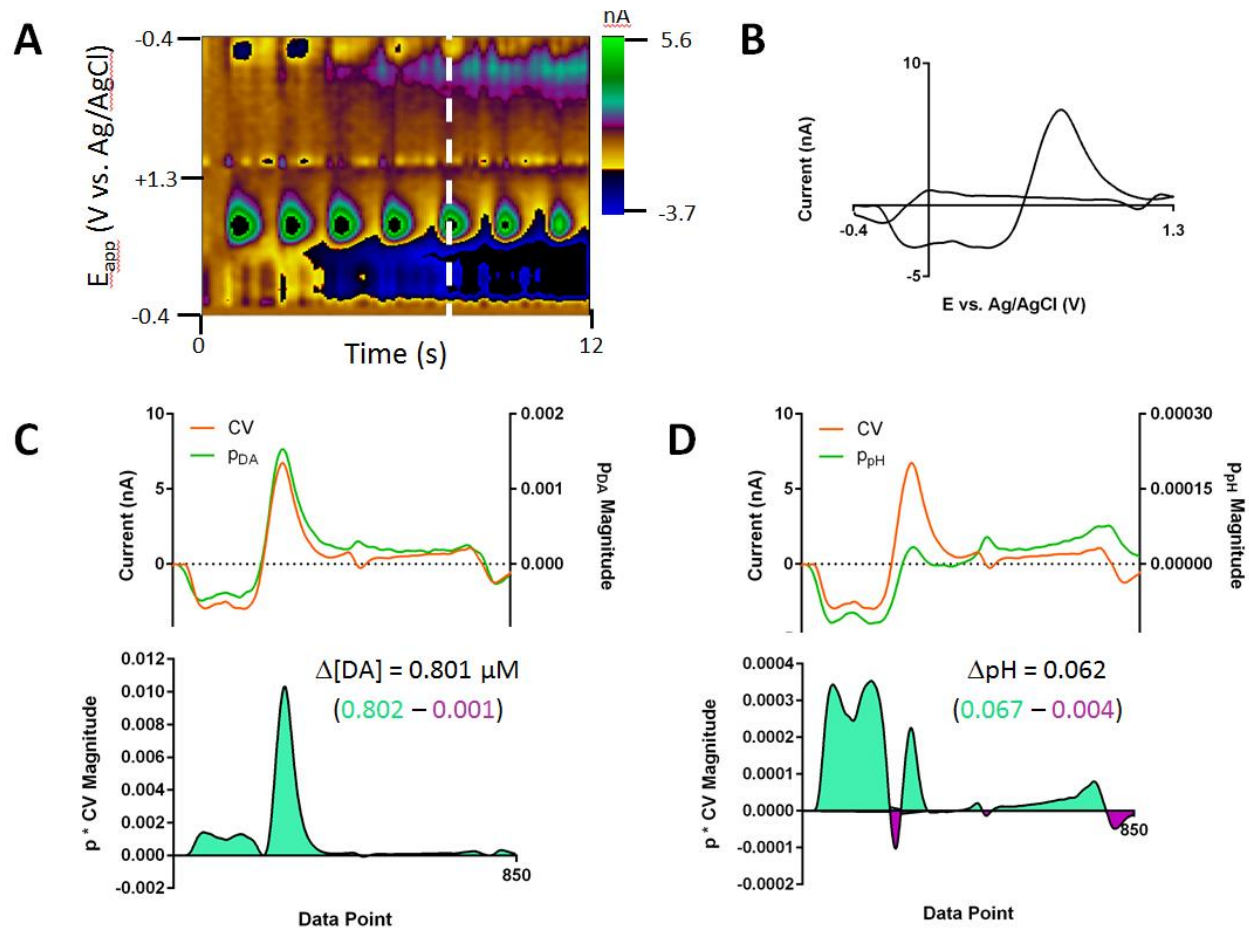
Figure 2.5. Use of the **p** vectors in the calculation of analyte concentrations. (A) Color plot showing dopamine and pH shifts from a lever press-induced electrical stimulation for an animal performing intracranial self-stimulation. (B) Cyclic voltammogram, showing contributions from pH and dopamine, collected at the white vertical line shown in (A). (C) Plots of the dopamine **p** vector and the CV from (B) (upper) and the value of the product of their amplitudes (lower) as a function of data point. Analogous to the scoring process show in Figure 2, the concentration is calculated from summation across the data window, and the regions below positive and negative values of the p and CV product are shown in green and purple, respectively. (D) As in (C) but with the $\mathbf{p_{pH}}$ matrix.

Application of experimental data. For concentration prediction, the scores of the experimental CVs on the retained PCs are simply calculated and used with Eq. 2 7. These scores can also be used construct the model estimate of the CVs for residual analysis. The difference of the current of the original CV and this PC-reconstructed estimate forms the residual value at each potential. Statistical methods exist for the evaluation of the sum of the squares of the residual values for each voltammogram (Q_t) to determine when there is sufficient residual current that the model-produced concentration estimate is significantly flawed. For FSCV data, the use of a Q_α residual threshold is recommended.(Jackson & Mudholkar, 1979; Keithley, et al., 2009) Q_α is a value estimated from the secondary PCs (i.e. those excluded from the model and considered to be noise) that can be compared to Q_t for each measurement, serving as a threshold of significance for the Q_t values at a given confidence level. If Q_t exceeds Q_α, significant residual current remains unaccounted for in the PCR model, and the model may be an inaccurate description of the data.

It is now useful to return to the calibration equations stated in either the classical or the inverse forms (Eqs. 2.4 and 5, respectively), either of which can be used to evaluate the now-defined calibration model. In examining the classical formulation (Eq. 2.4), it can be seen that the model, for each analyte, provides a fixed value for the sensitivity at each potential. The set of all these values across the scan-potential window corresponding to analyte *j* is referred to as the k_j vector. These vectors can be visually analyzed by plotting them either of our two visual conventions and thought of as the model estimates of the voltammetric response corresponding to single unit concentration change in analyte *j*.(Keithley & Wightman, 2011) Inspection of plots of each of a PCR model's k_j vectors allows the user to verify that the model predicts, for each analyte, the expected shape of the cyclic voltammogram.

The regression model also provides coefficients, *p* values, explaining the contribution of the current at each potential to the calculation of each analyte concentration. These *p* values, which may be negative, are the coefficients in the inverse formulation (Eq.2.5). The set of these coefficients across the scan-potential window corresponding to analyte *j* will be referred to as the p_j vector. Both the origin of the p_j vectors and its relationship to the k_j vectors are given in Appendix 3.1. With the knowledge of the p_j vector, the analyte concentration prediction for an unknown CV (Figure 2.3B) proceeds in a manner analogous to the determination of scores. The pointwise product of the p_j vector magnitude and the CV

amplitude is calculated at each potential (Figure 2.3C and D). The concentration of the analyte is then determined from the sum of these values.

Analysis of the values of the p_j vector and the pointwise product allows for the determination of the potentials weighted heavily for concentration calculation. Plots of the p_j vectors, like those of the PCs, have defined shapes and features (e.g. peaks and zero crossings) that are derived from features in the CVs of multiple analytes in the training sets. For example, the plot of the p_{DA} vector (Figure 2.3C, green) has an initial strong pH-like feature followed by a feature resembling the DA oxidation peak. In the analysis of a CV containing pH and DA contributions, which highly resembles the plot of the p_{DA} vector, these two regions also make the major contributions to the dopamine concentration calculation. The dopamine oxidative wave, which directly provides information about the dopamine concentration, creates a large positive contribution, as expected. The pH-like region additionally generates a positive contribution to the dopamine concentration estimation, which is accounting for the current decrease in the dopamine oxidative region caused by the presence of pH contributions. A similar pattern is seen in the analysis of the calculation of the pH concentration with the p_{pH} vector (Figure 2.3D). Within the early data region, where the signal contribution of pH is most pronounced, there is a large positive contribution to the concentration value. However, a positive contribution is also found in the region of the dopamine oxidation wave. This, in an analogous manner, is augmenting the pH concentration calculation to account for changes in the signal due to the presence of dopamine.

RESULTS AND DISCUSSION

Theoretical Failings of Standard Training Sets. Training sets that consist of CVs collected from different electrodes, recording sessions, and/or subjects (i.e. 'standard' training sets) have been increasingly used in the analysis of *in vivo* FSCV data. This trend is particularly popular for the analysis of data collected with chronically implanted microelectrodes due to difficulties for training set construction at the site of recording. While this approach eases the procedural burden, it violates a fundamental assumption of calibration – that the relationships in the training set are the same as in the experimental data. Correction for this error requires either knowledge of the differences between the experimental and calibration data, which is difficult to obtain, or the use of calibration transfer methods, which would require

additional data collection and reintroduce the experimental complexity which is aimed to be avoided by the use of standard training sets.(Feudale, et al., 2002) Indeed, recent work from our lab showed that the use of a training set collected in a different subject with a different electrode for PCR models resulted in significant underestimations of concentrations.(Rodeberg, et al., 2015) Additionally, standard training sets (i.e. those with CVs collected from multiple subjects) resulted in high numbers of retained PCs (i.e. high rank) with k_j vectors that no longer resembled the analyte voltammograms. Attempts to limit the rank of the models resulted in unreasonably high residual thresholds, removing the possibility of proper residual analysis and nullifying the first-order advantage. Here, this line of inquiry is furthered with focus on the origins of the shortcomings of standard training sets.

In the case of FSCV data, the primary differences in the data collected in different recording sessions can be seen in the voltammetric peak characteristics (e.g. peak width, position, and relative intensity), the electrode selectivity, and the noise levels.(Rodeberg, et al., 2015) There are several sources for this variability. Regarding the electrochemical aspects of the data, there is an inherent level of variability between electrodes, particularly with disorganized surfaces such as those found on carbon fibers, while implanted reference electrodes differ in quality and are known to drift with time.(Chand, 2000; Moussy & Harrison, 1994; Zhang et al., 1999) Between subjects, differences in mass transport kinetics within the biological matrix or at the electrode surface may increase this variability further. These considerations affect voltammetric peak characteristics, sensitivity, and selectivity for electrochemical reactions.(McCreery, 2008) It is also standard practice to use extended anodic limits to electrochemically introduce oxide functionalities to the surface of the carbon fiber microelectrodes prior to measurements, which results in favorable conditions for catecholamine detection.(Heien et al., 2003) However, the level of control over this process is limited, leading to varied electrochemical responses. This is particularly pronounced in the case of pH changes.(Takmakov et al., 2010) Finally, noise levels are expected to differ between instruments. Thus, there are unavoidable sources of variation in the collection of FSCV data.

To illustrate the importance of this, we used the p_{DA} vector to analyze the concentration prediction for the CV from Figure 2.3B with an artificial rightward shift introduced (Figure 2.4A), as might be introduced through reference electrode drift. In the case of DA and pH differentiation, the regions heavily weighted for the DA concentration feature sharp changes in the 'p' values, including a zero crossing and
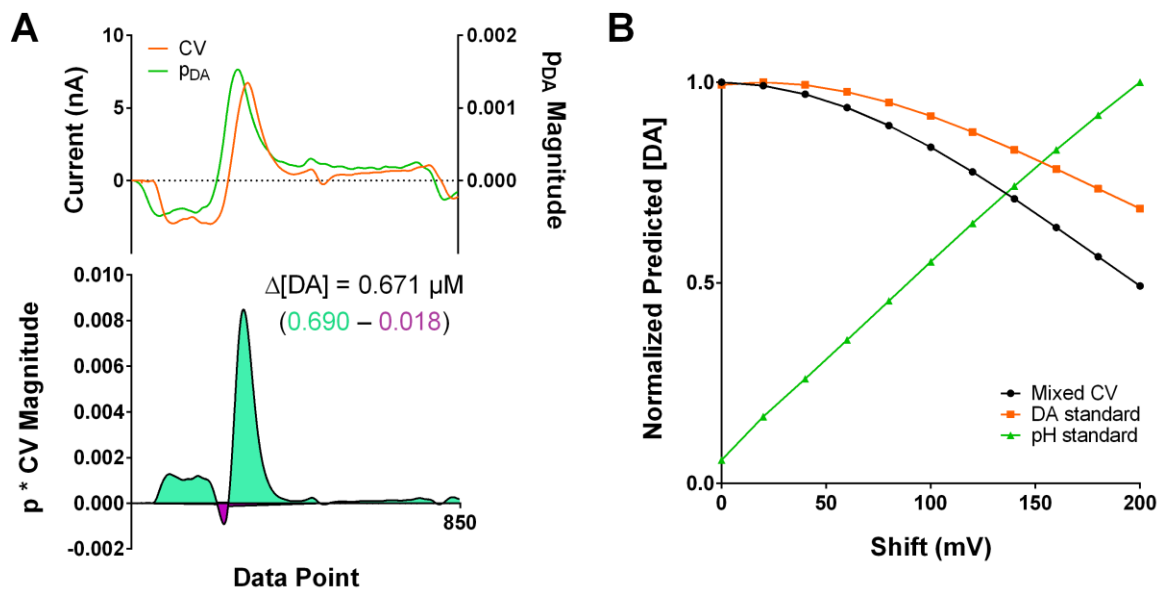
Figure 2.6. Errors in the use of non-experimental training sets. (A) Plots of the **p_DA** matrix and the CV from Figure 3B with an artificial rightward 100 mV shift (upper), and the value of the product of their amplitudes (lower) as a function of data point. (B) Plot of the predicted DA concentration, normalized to the maximum predicted value, as a function of the artificial shift magnitude introduced for the mixed CV from Figure 3B (black) and a DA (orange) and pH (green) standard from Figure 1A.

38
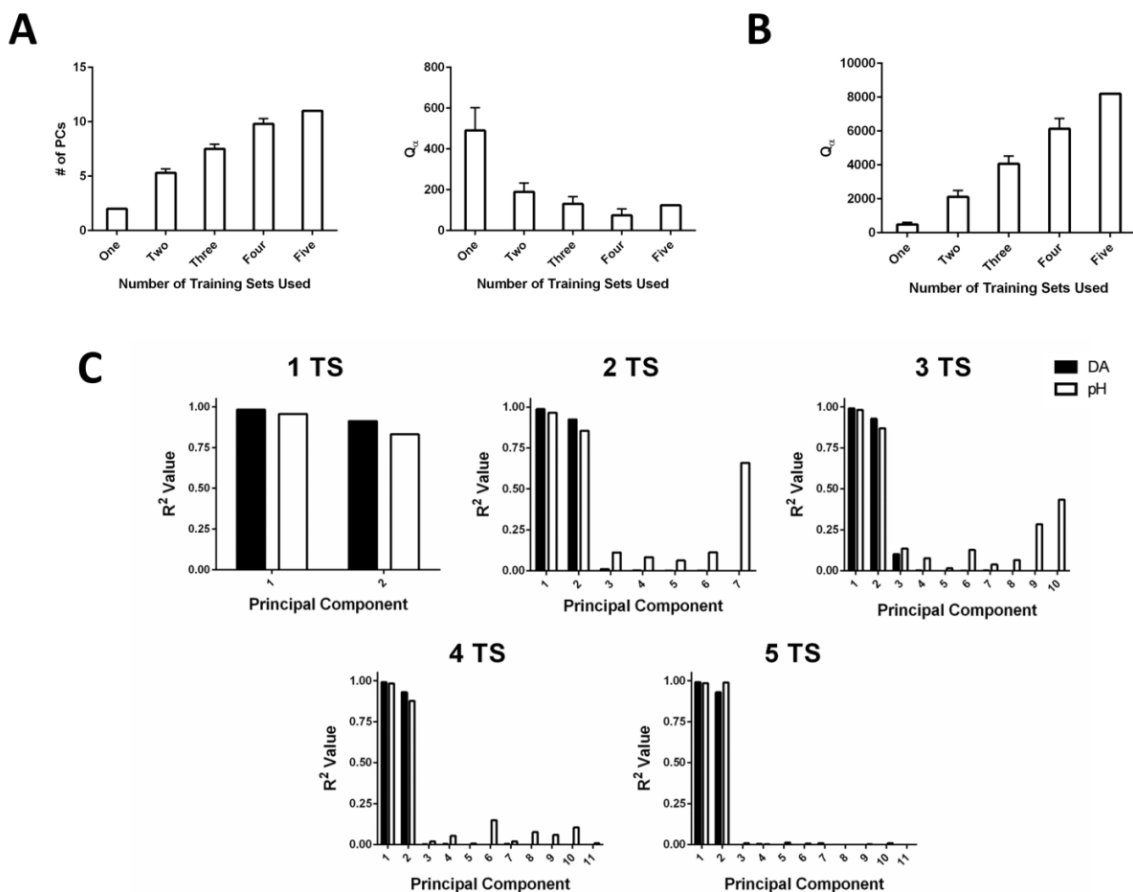
Figure 2.7. Model parameters of interest for concatenated training sets. (A) The number of PCs retained by the model (left) and the residual Q_α threshold (right) as a function of the total number of single-subject training sets included in the final training set used for PCR model generation. The one TS model corresponds to one training set used in all others. (B) The residual Q_α threshold for models forced to retain only two primary PCs. Values are shown as mean ± standard deviation. (C) Mean R^2 values for linear fits between the analyte concentration and the score on a given principal component for DA (black) and pH (white) training voltammograms for PCR models constructed by concatenating differing numbers of training sets (number given above graph).

polarity switch. A relatively minor shift leads to misalignment of these features, leading to significant changes in the predicted DA concentration. Such errors also arise in the analysis of DA and pH training standards (Figure 2.4B), leading to artificially low and high DA estimations, respectively. This illustrates that analyte resolution critically depends on correct assignment of the current-concentration relationships across the scan-potential window and, in particular, directly demonstrates the sensitivity of PCR to variations in the applied potential.

Concatenation of Training Sets from Multiple Animals. To demonstrate the incompatibility of data collected from different animals within a single model framework, training sets were constructed by the concatenation of entire training sets (TS, consisting of 10 CVs each) constructed in different animals (n = 5). One training set was selected as the primary TS (labeled A), while the number of training sets added was varied between one and four. (The data and labels used for these investigations are identical to those reported in Rodeberg et al., 2015). The number of PCs retained (i.e primary PCs by the Malinowski F-test) and the Q_α thresholds were calculated for the PCR models. The results (Fig. 2.7 A-B) agree with those described in Rodeberg et al., 2015. The number of primary PCs tended to increase with the inclusion of more training set CVs, while the Q_α thresholds tended to decrease, suggesting overfitting of the data. Limitation of the number of primary PCs to the first two (Fig. 2.7B) resulted in a drastic increase in the Q_α threshold, nullifying the first-order advantage.

To carry this analysis further, the assumptions that go into the regression step of PCR were tested. First, we examined whether there was a linear relationship, as measured by the R^2 values for the zero-intercept linear regression model, between the scores on all retained PCs and the concentration values (Eq. 2.7). It was found that only the first two components tended to have a linear relationship with the concentrations for both analytes (Fig. 2.7C). A Student's t-test of the significance of the estimated 'm' parameters revealed that 80% of the third or higher primary PCs were not significantly different from zero, suggesting that the use of these PCs in regression is inappropriate.(Krazanowski, 2007)

Next, we examined whether the proportionality constants ('m' values in Eq. 2.7) were shared between data collected from different animals. This was evaluated by an F-test comparing models in which the 'm' parameters were either global (shared between data from different subjects) or subject-
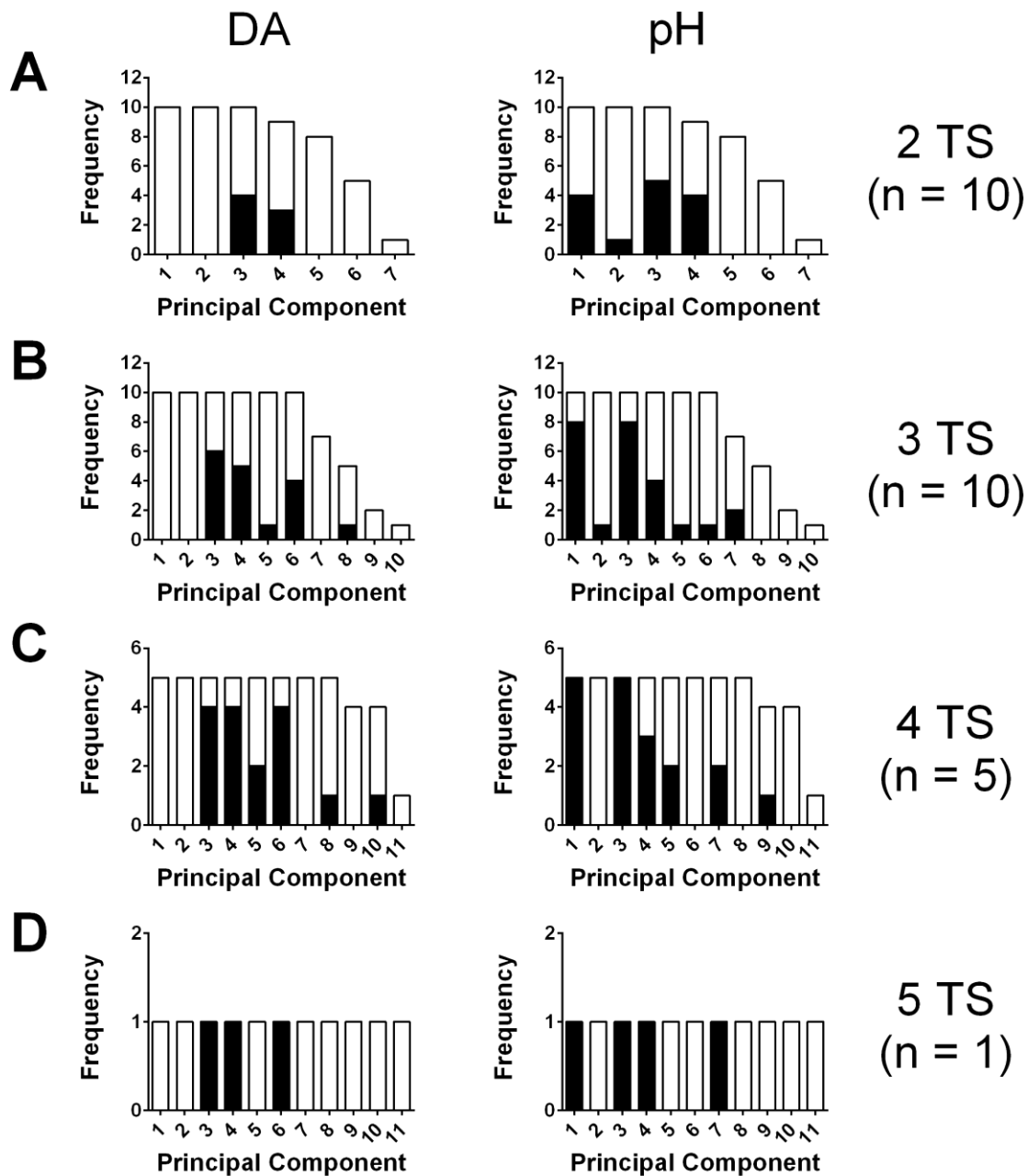
Figure 2.8. Results of F-test comparing models with subject-specific or global parameters for Equation 2.7 for concatenated training sets. (A) Cumulative histogram showing the number of PCR models, built from concatenated training sets of 2 single-subject training sets, containing a given number of principal components or greater (frequency). The black portion of the bars corresponds to the number of principal components that were found to have subject-specific parameters preferred over global parameters (F-test, $\alpha = 0.05$) for relating scores on that principal component and the dopamine (left) or pH (right) concentrations. (B) As in (A) but using concatenated training sets from three subjects. (C) As in (A) but using concatenated training sets from four subjects. (D) As in (A) but using concatenated training sets from five subjects.

specific (see Appendix 2.2).(Glatting et al., 2007) This regression was done using scores calculated from PCs defined using all training set voltammograms, leading to the expectation of some degree of generality. However, it was found that the subject-specific constants were preferred in a large number of cases (Figure 2.8). When considering both the dopamine and pH parameters, preference for group-specific parameters was found in a considerable number of the third and higher primary PCs, highlighting the fact that these are likely capturing variance specific to certain subjects. Additionally, in the case of the pH parameters (right column of Figure 2.8), there were a large number of models in which group-specific parameters were preferred for the first two primary PCs. Concatenation of just one additional training set resulted in four out of the ten models showing preference for subject-specific parameters in the first PC, the one that describing the largest amount of variance. All but two of models with higher number of training sets exhibited this preference as well. This result can likely be traced to the wide variability of the characteristics of the pH voltammograms between electrodes, highlighting that, even with global definition of the PCs, the uniqueness of data from a single animal would lead to poor estimates as compared with a training set derived from the experimental animal.

Evaluation of 'Library' Approach to Generalized Training Set Generation. To investigate the use of a library for the model generation, the construction of randomly generated CVs, derived from separate animals, was revisited. In this experiment, Animal B's experimental session was analyzed by a training set consisting of 10 CVs randomly selected from the other four animals (Animals A and C-D), resulting in 2.4×10^8 possible training sets. Of these, 19,704 were studied due to computational limitations, with the total analysis time being 10.1 days. These data were recorded during an intracranial self-stimulation trial and were binned into 75 five-second snippets.(Rodeberg, et al., 2015) As an initial measure of the appropriateness of the constructed model in the description of the data, the total sum of all residual values calculated at each analyzed time point was chosen, a measure of the amount of signal captured by the PCR model. Additionally, to gain insight into the models constructed, the number of primary PCs and the Q_α thresholds were again calculated.

The summary of the generated models is shown in Figure 2.9A as a function of the number of primary PCs retained for the model. Just under half of the models (45.8%) had more than two primary
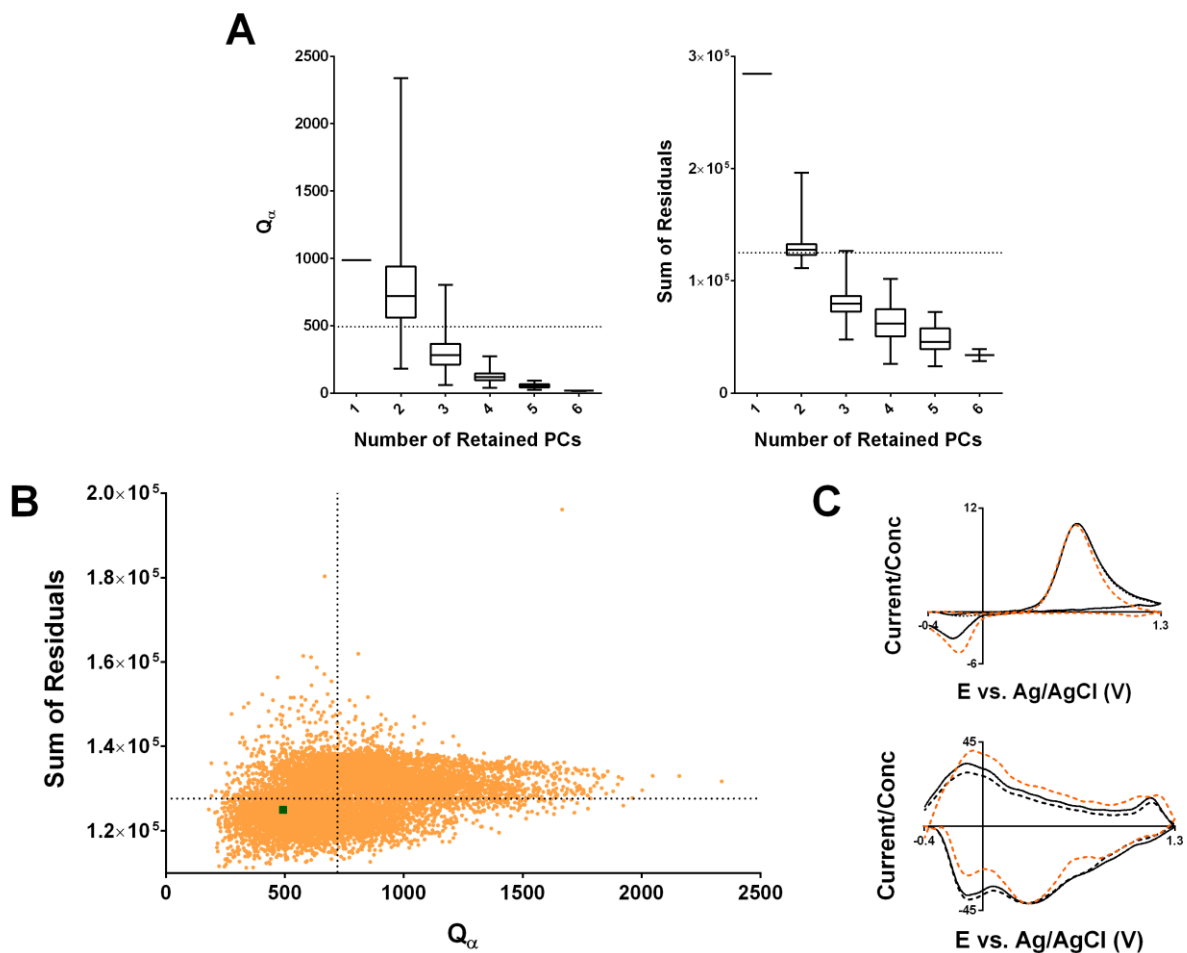
Figure 2.9. Summary of 'library' approach to generate randomized standard training sets. (A) Box plots showing the distribution of Q_α threshold values (left) and the residual sum for all snippets (right) shown as a function of the number of PCs retained in the constructed PCR model. The values for the training set constructed within the experimental subject (Subject B) are shown as a horizontal dashed lines. (B) Scatterplot showing the residual sums plotted against Q_α values for all 2 PC models. The dashed lines correspond to the medians of the distributions in each variable. The model constructed with Subject B's training set is shown as a green square in the lower left quadrant. (C) Average k_j vectors constructed from all 2 PC models (solid black line) and 2 PC models in falling in the lower half of the distributions for both the residual sum and Q_α values (lower left quadrant of (B), dashed black line), as well as Subject B's PC model (orange dashed line).
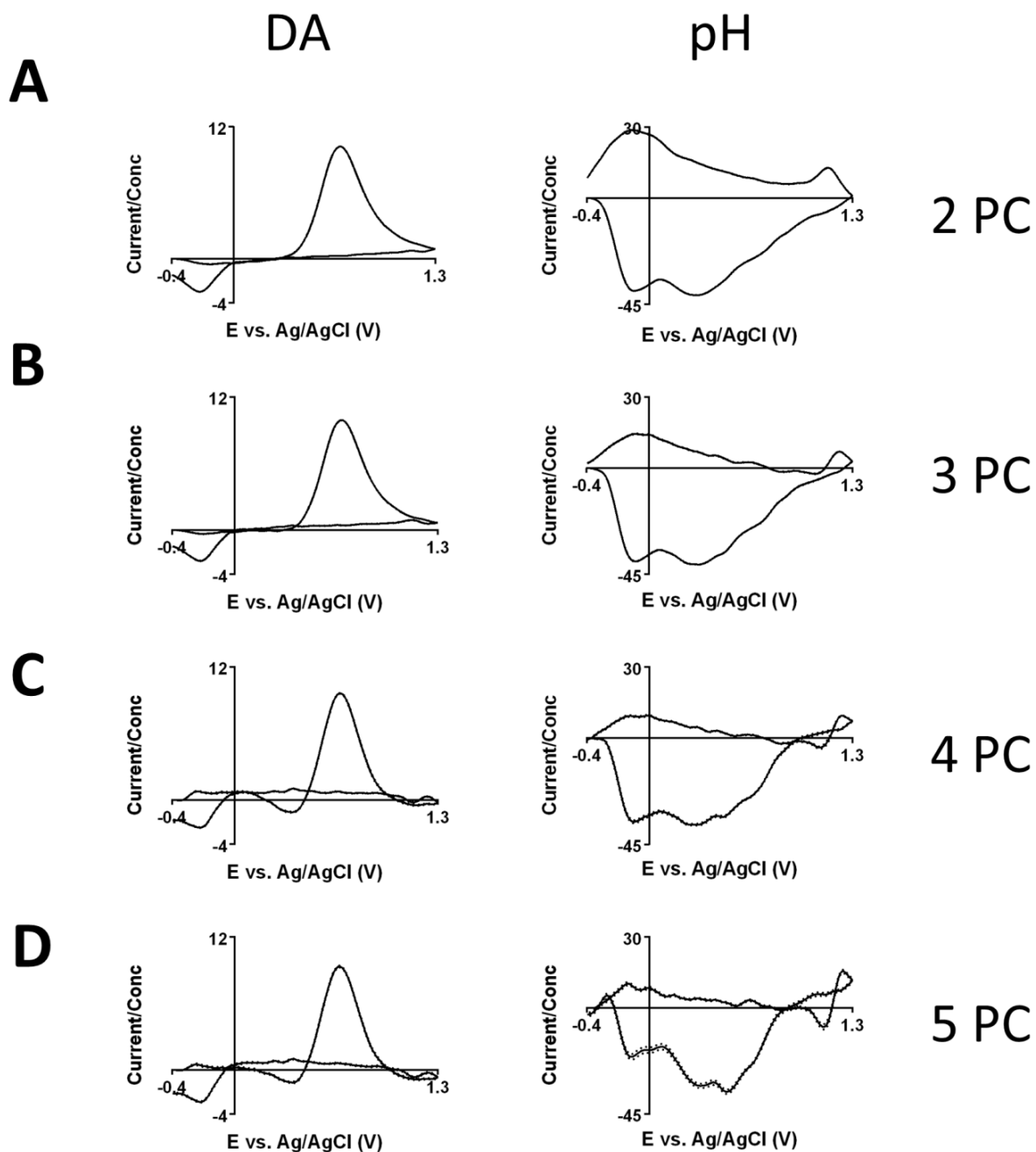
Figure 2.10. Average k_j vectors for models built using training sets (n = 10 CVs, 5 per analyte) generated by a randomized 'library' approach from training sets collected within different subjects and using different carbon electrodes. (A) Average k_j matrices (solid lines) for dopamine (left) and pH (right) and 95% confidence intervals (dashed lines) for models with two retained principal components (n = 10679 training sets). (B) As in (A) but for models with three retained principal components (n = 7727 training sets). (C) As in (A) but for models with four retained principal components (n = 1179 training sets). (D) As in (A) but for models with five retained principal components (n = 116 training sets).

components, with the remaining, with one exception, having two primary PCs. As expected, both the Q_α threshold and the sum of the residuals decreased as a function of the number of the PCs, suggesting overfitting. This is supported by evaluation of the average k_j vectors for the two analytes for a given number of PCs, which shows degradation in the quality of these model estimates with an increase in the number of components retained (Fig. 2.10). The inappropriateness of such high rank models in the analysis of Subject B's data is further illustrated by the majority of Q_α values and residual sums for 3+ PC models falling below those from Subject B's model (i.e. that trained with data from the experimental session, shown as the dashed line in the figure).

Given this, we limit the remaining discussion to the subset of models that retained two primary PCs (n = 10679 training sets). Within the distribution defined by this subset, Subject B's PCR model had a Q_α threshold (the green square in Figure 2.9B) falling in the lower 16th percentile. This suggests that most random models tended to overestimate this threshold, which would result in invalid data sets passing residual analysis undetected. Furthermore, the sum of residual values for training set B's model falls in the lower 38th percentile, suggesting that the majority of these models do not capture as much information from the data as the proper training set.

Further requirements for model selection could be implemented. In this experiment, the subset of models considered can be refined to those having both a low total residual sum and Q_α thresholds like Subject B's model (defined as those falling in the lower 50th percentile on both distributions – the lower left quadrant of Figure 2.9B). However, even this requirement fails to select models with current-concentration relationships like Subject B's PCR model. This can be seen by inspection of the plots of the k_j vectors shown in Figure 2.9C, which directly summarize these relationships. The k_j vectors for Subject B's PCR model (dashed orange line) differ noticeably in both absolute and relative peak amplitudes from the average k_j vectors of this low total residual sum, low Q_α threshold 2 PC subset (dashed black line). Instead, the latter closely resembles that obtained from all 2 PC models (solid black line).

Such a library approach also suffers from a number of theoretical drawbacks in its implementation. Here, even with knowledge of how the within-subject training set performed, criteria for selection of models that had similar performance were unable to be found. One could alternatively implement selection criteria on the CVs for model training. However, this would require the collection of

information about 'pure' analyte responses, minimizing the advantage of such an approach. Implementation would also require the generation of large library of spectra, as CVs could differ in a number of different characteristics (e.g. peak location, relative peak height, etc.) and multiple CVs are needed for each analyte. Finally, one of the principal advantages of using PCR is the ability to detect interferents through residual analysis. This process relies critically on estimation of the noise from the training set. Even if a combination of library analyte spectra matching the analytical characteristics of the data were found, these spectra will likely have unrepresentative noise within them, preventing proper residual analysis.

CONCLUSIONS

The strength of PCR in analysis of FSCV data comes from its ability to separate and quantitate analyte contributions, with the latter critically dependent on the former. Resolution of analyte signals relies on knowledge of the current-concentration relationships across the scan-potential window (the *k* and *p* values of Eqs. 2.4 and 5), which are improperly assigned when standard training sets are used. This error results in incorrect signal attribution, as illustrated by the predicted dopamine concentration changes for the shifted CVs in Figure 2.6B. This problem is not unique to PCR, but rather all of multivariate linear analysis, for which Eqs. 2.4 and 5 hold. Avoidance of this issue requires the collection and use of training set voltammograms that contain accurate information about the experimental current-concentration relationships for *all* expected analytes, as information about each analyte is used for the resolution of one (which was illustrated directly by the analysis of the p_j vectors in Figures 2.5C and D). The variability of these relationships between voltammetric data collected in different animals is such that unification within a single model framework results in easily detectable differences in model behavior (Figure 2.8), while their replication is not possible even with prior knowledge of derived model performance (Figure 2.9C). Thus, the only known reliable way to capture these relationships in a manner that allows for proper signal resolution is the collection of training set voltammograms under the experimental conditions. This can be most readily accomplished by including training set collection in the experimental protocol, minimizing the time between experimental and training data collection to avoid drift in experimental parameters (e.g. the state of the reference electrode), and collecting training data that satisfy the general recommendations

given in Keithley et al., 2009 (and repeated above). Other approaches for training set collection risk poor

analyte resolution, precluding accurate assessment of neurochemical dynamics.

METHODS

Data collection is described in Rodeberg, et. al., 2015. Animal procedures were approved by the

UNC-Chapel Hill Institutional Animal Care and Use Committee (IACUC). Data and statistical analyses

were performed in GraphPad Prism 6 (GraphPad Software Inc., La Jolla, CA), LabView (National

Instruments, Austin, TX), and MATLAB (Mathwork, Natick, MA) with and α value of 0.05.

REFERENCES

Booksh, K. S. (2006). Chemometric Methods in Process Analysis *Encyclopedia of Analytical Chemistry*: John Wiley & Sons, Ltd.

Bucher, E. S., & Wightman, R. M. (2015). Electrochemical Analysis of Neurotransmitters. *Annu Rev Anal Chem, 8*, 239-261.

Centner, V., Massart, D. L., & de Jong, S. (1998). Inverse calibration predicts better than classical calibration. *Fresen J Anal Chem, 361*(1), 2-9.

Chand, S. (2000). Carbon fibers for composites. *J Mater Sci, 35*(6), 1303-1313.

Chesler, M. (2003). Regulation and modulation of pH in the brain. *Physiol Rev, 83*(4), 1183-1221.

Clark, J. J., Collins, A. L., Sanford, C. A., & Phillips, P. E. (2013). Dopamine encoding of Pavlovian incentive stimuli diminishes with extended training. *J Neurosci, 33*(8), 3526-3532.

Cook, R. D. (1977). Detection of Influential Observation in Linear-Regression. *Technometrics, 19*(1), 15-18.

Feudale, R. N., Woody, N. A., Tan, H., Myles, A. J., Brown, S. D., & Ferre, J. (2002). Transfer of multivariate calibration models: a review. *Chemometrics and Intelligent Laboratory Systems, 64*, 181-192.

Flagel, S. B., Clark, J. J., Robinson, T. E., Mayo, L., Czuj, A., Willuhn, I., et al. (2011). A selective role for dopamine in stimulus-reward learning. *Nature, 469*(7328), 53-57.

Glatting, G., Kletting, P., Reske, S. N., Hohl, K., & Ring, C. (2007). Choosing the optimal fit function: Comparison of the Akaike information criterion and the F-test. *Med Phys, 34*(11), 4285-4292.

Goertz, R. B., Wanat, M. J., Gomez, J. A., Brown, Z. J., Phillips, P. E., & Paladini, C. A. (2015). Cocaine increases dopaminergic neuron and motor activity via midbrain alpha1 adrenergic signaling. *Neuropsychopharmacology, 40*(5), 1151-1162.

Hart, A. S., Rutledge, R. B., Glimcher, P. W., & Phillips, P. E. (2014). Phasic dopamine release in the rat nucleus accumbens symmetrically encodes a reward prediction error term. *J Neurosci, 34*(3), 698-704.

Heien, M. L. A. V., Johnson, M. A., & Wightman, R. M. (2004). Resolving neurotransmitters detected by fast-scan cyclic voltammetry. *Anal Chem, 76*(19), 5697-5704.

Heien, M. L. A. V., Phillips, P. E. M., Stuber, G. D., Seipel, A. T., & Wightman, R. M. (2003). Overoxidation of carbon-fiber microelectrodes enhances dopamine adsorption and increases sensitivity. *Analyst, 128*(12), 1413-1419.

Hollon, N. G., Arnold, M. M., Gan, J. O., Walton, M. E., & Phillips, P. E. (2014). Dopamine-associated cached values are not sufficient as the basis for action selection. *Proc Natl Acad Sci U S A, 111*(51), 18357-18362.

Howe, M. W., Tierney, P. L., Sandberg, S. G., Phillips, P. E., & Graybiel, A. M. (2013). Prolonged dopamine signalling in striatum signals proximity and value of distant rewards. *Nature, 500*(7464), 575-579.

Jackson, J. E., & Mudholkar, G. S. (1979). Control Procedures for Residuals Associated with Principal Component Analysis. *Technometrics, 21*(3), 341-349.

Kawagoe, K. T., Garris, P. A., & Wightman, R. M. (1993). Ph-Dependent Processes at Nafion(R)-Coated Carbon-Fiber Microelectrodes. *J Electroanal Chem, 359*(1-2), 193-207.

Keithley, R. B., Carelli, R. M., & Wightman, R. M. (2010). Rank estimation and the multivariate analysis of in vivo fast-scan cyclic voltammetric data. *Anal Chem, 82*(13), 5541-5551.

Keithley, R. B., Heien, M. L., & Wightman, R. M. (2009). Multivariate concentration determination using principal component regression with residual analysis. *Trends Analyt Chem, 28*(9), 1127-1136.

Keithley, R. B., & Wightman, R. M. (2011). Assessing principal component regression prediction of neurochemicals detected with fast-scan cyclic voltammetry. *ACS Chem Neurosci, 2*(9), 514-525.

Kramer, R. (1998). *Chemometric Techniques for Quantitative Analysis*. New York, NY: Marcel Dekker, Inc.

Krazanowski, W. (2007). *Statistical Principles and Techniques in Scientific and Social Investigations*. Cary, NC: Oxford University Press.

Krutchkoff, R. (1967). Classical and Inverse Regression Methods of Calibration. *Technometrics, 9*(3), 425-439.

Krutchkoff, R. (1969). Classical and Inverse Regression Methods of Calibration in Extrapolation. *Technometrics, 11*(3), 605-608.

Lavine, B. K., & Workman, J., Jr. (2013). Chemometrics. *Anal Chem, 85*(2), 705-714.

Malinowski, E. R. (2004). Adaptation of the Vogt-Mizaikoff F-test to determine the number of principal factors responsible for a data matrix and comparison with other popular methods. *J Chemometr, 18*(9), 387-392.

McCreery, R. L. (2008). Advanced carbon electrode materials for molecular electrochemistry. *Chem Rev, 108*(7), 2646-2687.

Moussy, F., & Harrison, D. J. (1994). Prevention of the Rapid Degradation of Subcutaneously Implanted Ag/Agcl Reference Electrodes Using Polymer-Coatings. *Anal Chem, 66*(5), 674-679.

Nasrallah, N. A., Clark, J. J., Collins, A. L., Akers, C. A., Phillips, P. E., & Bernstein, I. L. (2011). Risk preference following adolescent alcohol use is associated with corrupted encoding of costs but not rewards by mesolimbic dopamine. *Proc Natl Acad Sci U S A, 108*(13), 5466-5471.

Olivieri, A. C. (2008). Analytical advantages of multivariate data processing. One, two, three, infinity? *Anal Chem, 80*(15), 5713-5720.

Parker, J. G., Zweifel, L. S., Clark, J. J., Evans, S. B., Phillips, P. E., & Palmiter, R. D. (2010). Absence of NMDA receptors in dopamine neurons attenuates dopamine release but not conditioned approach during Pavlovian conditioning. *Proc Natl Acad Sci U S A, 107*(30), 13491-13496.

Robinson, D. L., Venton, B. J., Heien, M. L. A. V., & Wightman, R. M. (2003). Detecting subsecond dopamine release with fast-scan cyclic voltammetry in vivo. *Clin Chem, 49*(10), 1763-1773.

Rodeberg, N. T., Johnson, J. A., Cameron, C. M., Saddoris, M. P., Carelli, R. M., & Wightman, R. M. (2015). Construction of Training Sets for Valid Calibration of in Vivo Cyclic Voltammetric Data by Principal Component Analysis. *Anal Chem, 87*(22), 11484-11491.

Takmakov, P., Zachek, M. K., Keithley, R. B., Bucher, E. S., McCarty, G. S., & Wightman, R. M. (2010). Characterization of Local pH Changes in Brain Using Fast-Scan Cyclic Voltammetry with Carbon Microelectrodes. *Anal Chem, 82*(23), 9892-9900.

Wanat, M. J., Bonci, A., & Phillips, P. E. (2013). CRF acts in the midbrain to attenuate accumbens dopamine release to rewards but not their predictors. *Nat Neurosci, 16*(4), 383-385.

Wang, Y. D., & Kowalski, B. R. (1992). Calibration Transfer and Measurement Stability of near-Infrared Spectrometers. *Appl Spectrosc, 46*(5), 764-771.

Willuhn, I., Burgeno, L. M., Everitt, B. J., & Phillips, P. E. (2012). Hierarchical recruitment of phasic dopamine signaling in the striatum during the progression of cocaine use. *Proc Natl Acad Sci U S A, 109*(50), 20703-20708.

Willuhn, I., Burgeno, L. M., Groblewski, P. A., & Phillips, P. E. (2014a). Excessive cocaine use results from decreased phasic dopamine signaling in the striatum. *Nat Neurosci, 17*(5), 704-709.

Willuhn, I., Tose, A., Wanat, M. J., Hart, A. S., Hollon, N. G., Phillips, P. E., et al. (2014b). Phasic dopamine release in the nucleus accumbens in response to pro-social 50 kHz ultrasonic vocalizations in rats. *J Neurosci, 34*(32), 10616-10623.

Woody, N. A., Feudale, R. N., Myles, A. J., & Brown, S. D. (2004). Transfer of multivariate calibrations between four near-infrared spectrometers using orthogonal signal correction. *Anal Chem, 76*(9), 2595-2600.

Zhang, X. J., Wang, J., Ogorevc, B., & Spichiger, U. E. (1999). Glucose nanosensor based on Prussian-blue modified carbon-fiber cone nanoelectrode and an integrated reference electrode. *Electroanal, 11*(13), 945-949.

CHAPTER 3: MULTIVARIATE CURVE RESOLUTION FOR SIGNAL ISOLATION FROM FAST-SCAN CYCLIC VOLTAMMETRIC DATA

INTRODUCTION

Fast-scan cyclic voltammetry (FSCV) has several advantages over other electrochemical techniques when used to study *in vivo* extracellular neurotransmitter dynamics, particularly the selectivity afforded by the analyte voltammetric profiles. Full realization of this selectivity, however, demands multivariate data analysis.(Booksh & Kowalski, 1994; Lavine & Workman, 2013; Olivieri, 2008) Principal component analysis-inverse least squares (PCA-ILS, also referred to as principal component regression or PCR), a multivariate approach relying on factor analysis, has been shown to be a reliable approach for analyte signal isolation from FSCV data collected on multicomponent systems, both *in vitro* and *in vivo*.(Heien et al., 2004; Heien et al., 2005; Kramer, 1998) Further, work on the development of PCA-ILS for FSCV analysis has resulted in implementation of procedures that provide model validation, giving confidence in model-generated estimates.(Keithley et al., 2009; Keithley & Wightman, 2011)

However, the main drawback of its deployment for *in vivo* FSCV analysis has been the necessity of training set construction to generate the data analysis models. Chemometrics and previous research suggest training sets must be generated under the experimental conditions to properly validate the model and have confidence in model-generated concentration estimates without further analysis.(Booksh, 2006; Feundale et al., 2002; Wang & Kowalski, 1992; Woody et al., 2004) This requirement adds to experimental complexity, and its importance has been the subject of recent debate.(Johnson et al., 2016b; Rodeberg et al., 2015; Rodeberg et al., 2017) Thus, a method that relaxes this requirement should be of interest to the field.

Here, we explore the potential of an alternative method, self-modeling multivariate curve resolution by alternating least squares (MCR-ALS), to resolve overlapping FSCV signals. The technique shares much with PCA-ILS, namely the modeling of the data as a linear combination of appropriately scaled signals of the components. However, whereas training data is used with PCA to define spectral

51

shapes before fitting the data for concentration determination, MCR-ALS allows both the spectral shapes and concentrations to vary during the fitting procedure, using only the experimental data itself in defining the model. The algorithm is simply provided with an initial estimate of either the spectral shapes or the concentration traces, from which the data is iteratively fitted until convergence is achieved. This technique has been successfully used in the analysis of data derived from a number of analytical techniques, including mass spectrometry (Dantas et al., 2013; Pere-Trepat et al., 2005; Sinanian et al., 2016), spectroscopic techniques (Bortolato & Olivieri, 2014; Gargallo et al., 1996; Pere-Trepat et al., 2004), and slow-scan voltammetry (Diaz-Cruz et al., 1999; Esteban et al., 2000; Grabaric et al., 1997; Torres et al., 1998). Thus, this opens the possibility of circumventing the need for explicit training set construction.

However, due to increased freedom in model definition, there exist important concerns that must be addressed before proper use of MCR-ALS, particularly for *in vivo* FSCV data. First, all of above applications relied on the generation of second-order data (e.g. data separated along two variables, producing data in the form of a matrix).(Olivieri, 2014) This is most often achieved through separation techniques such as liquid chromatography or controlled manipulation of an independent variable (e.g. concentration). For FSCV, second-order data (i.e. current as a function of potential and time) is typically collected, most often visualized by a color plot. However, separation of signals in time must then rely on naturally occurring processes, leaving the success of the technique dependent on how naturally resolved these events are. Thus, the technique is expected to have limited potential for analysis of signals whose time courses significantly overlap.

Second, as the number of expected components and spectral shapes are not defined prior to fitting (as in PCR-ILS), solutions provided by MCR-ALS are more susceptible to a number of ambiguities, resulting in mathematical solutions that may or may not have actual correspondence to meaningful chemical information.(Malik & Tauler, 2016; Smilde et al., 2001) The most relevant of these are intensity and rotational ambiguities. Intensity ambiguity refers to the fact that MCR-ALS can only provide the shapes of the spectral and concentration profiles, rather than any information about their absolute scales. However, in the analysis of FSCV data, PCR-ILS suffers from similar ambiguities, and this problem can be addressed through normalization of the obtained spectral profiles and subsequent scaling by previously determined calibration factors. Rotational ambiguity is a more serious issue, which refers to the

fact that the data can be fit by an infinite number of combinations of spectral and concentration profiles. This problem is requires the imposition of constraints on the possible solutions derived from prior knowledge of characteristics of meaningful solution. Commonly employed constraints include non-negativity of values in the spectral or concentration profiles, concentration or spectral peak unimodality, and hard modeling approaches using known equations that govern the experimental system.(Malik & Tauler, 2016; R. Tauler et al., 1993a) For instance, in the previous study of electrochemical data, parametric equations and closure constraints (i.e. constant total concentrations of the various forms of a chemical species) to model the expected peak shape were used to define the solutions, in addition to non-negativity and unimodality constraints.(Esteban, et al., 2000) Background-subtracted FSCV data, however, is more limited in the types of parameters that can be used to identify the subset of meaningful fits. For instance, negative values can be found in both the spectra and concentration profiles due to the relative nature of measurements, while the equations governing the observed voltammetric behavior are not well-defined enough to use as strict constraints. Thus, a characterization of the subset of reported constraints that may be used (i.e. equality and selectivity constraints) and other techniques (i.e. simultaneous analysis of multiple experimental runs) is needed to ensure these are sufficient for robust deployment of MCR-ALS for FSCV data analysis.(Gemperline & Cash, 2003; Manne, 1995; R. Tauler, et al., 1993a; R. Tauler et al., 1995a; R. Tauler et al., 1993b; R. Tauler et al., 1995b)

In this study, the potential of MCR-ALS for the analysis of FSCV data is explored and compared to the performance of PCA-ILS. First, the basic implementation of the method is described, with comparisons to PCA-ILS when possible. Next, the method is characterized *in vitro* to determine the conditions under which the method is successful at separating signals. This is followed by *in vivo* comparison of PCA-ILS and PCR in a group of experiments. It is shown that the method is capable of producing highly similar results to PCA-ILS without the need for training data when given appropriate constraints. Further, methods to extend the utility of the technique and for validation (i.e. residual analysis) are explored.

EXPERIMENTAL SECTION

Instrumentation and Software. T-650 type, cylindrical carbon-fiber microelectrodes (Thornel, Amoco Corporation, Greenville, SC; pulled in glass capillaries and cut to 75-125 μm exposed lengths) were used in experimentation. After pulling, the seals of electrodes were dipped in epoxy (EPON Resin 828, Miller-Stephenson, Danbury, Connecticut) mixed with 14% w/w *m*-phenylenediamine (Sigma-Aldrich, St. Louis, MO) at 80°C, briefly washed with acetone, and heated at 100°C (5 hours) then 150°C (at least 12 hours).

Data was acquired with a commercial interface (PCI-6052, 16 bit, National instruments, Austin TX) with a personal home computer and analyzed using locally constructed hardware and software written in LabVIEW (HDCV, National Instruments, Austin, TX).(Bucher et al., 2013) Unless otherwise noted, triangular excursions of the working electrode potential were made at a scan rate of 400 V/s and repeated at a frequency of 10 Hz. Measurements were conducted inside a grounded Faraday cage to minimize electrical noise.

Electrochemical Experiments. Flow-injection analysis experiments were performed using a syringe pump (Harvard Apparatus, Holliston, MA) operated at 0.8 mL/min using PEEK tubing (Sigma-Aldrich) connected to a pneumatically controlled six-port injection valve (Rheodyne, Rohnert Park, CA). All solutions were prepared in TRIS (2.0 mM Na_2SO_4, 1.25 mM $NaH_2PO_4 \cdot H_2O$, 140 mM NaCl, 3.25 KCl, 1.2 mM $CaCl_2 \cdot 2H_2O$, 1.2 mM $MgCl_2 \cdot 6H_2O$, and 15 mM Trizma HCl) and adjusted to pH 7.4 with NaOH as necessary.

In Vivo Measurements. Male Sprague-Dawley rats from Charles River (Wilmington, MA, USA) were housed individually on a 12/12 h light/dark cycle. Animal procedures were approved by the UNC-Chapel Hill Institutional Animal Care and Use Committee (IACUC). The animals were surgerized in the manner described previously for intracranial self-stimulation (ICSS) experiments and given a minimum of 3 days of recovery prior to training.(Johnson et al., 2016a) Rats were trained in ICSS using previously described protocols on a fixed-ratio 1 or fixed-interval 5 schedule.(Garris et al., 1999)

Data Analysis. Data and statistical analyses were performed in GraphPad Prism 6 (GraphPad Software

Inc., La Jolla, CA), LabView (National Instruments, Austin, TX), and MATLAB (Mathwork, Natick, MA).

THEORY

Multivariate Curve Resolution-Alternating Least Squares. The theory of PCA-ILS and calibration has

been previously discussed.(Johnson, et al., 2016b) Here, we address the general theory behind the use

of MCR-ALS. As in PCR-ALS, data is modeled according to the 'bilinear' model.(Gemperline & Cash,

2003; Olivieri, 2014; R. Tauler, et al., 1995b) That is, each of the measurements (i.e. individual current

measurements and entire voltammograms) can be assumed a linear combination of the independent

contributions of analytes and noise. This leads to the following model equation in matrix form:

$$\mathbf{D} = \mathbf{CS}^{\mathrm{T}} + \mathbf{E} \qquad \text{(Eq. 3.1)}$$

where $\mathbf{D}$ is the (r x c) data matrix containing c spectra consisting of r individual measurements (e.g.

current measurements in a voltammogram), $\mathbf{C}$ and $\mathbf{S}$ are (r x l) and (c x l) matrices containing the l pure

concentration profiles and spectra, respectively, and $\mathbf{E}$ is the (r x c) error matrix. This equation is visually

shown in Figure 3.1. The goal is to find the solution to this equation that fits the data and provides

meaningful and interpretable information.

The next step requires definition of the model parameters and inputs, namely the number of

expected components and the initial estimates of the either the spectra or concentrations.(de Juan &

Tauler, 2016; R. Tauler, et al., 1995b) There exist many ways to achieve the former, and a comparison of

a large number of them effectiveness for analysis of LC-NMR data has been reported.(Wasim & Brereton,

2004) One class of techniques relies on factor analysis-based analysis of the experimental data, including

analysis of singular values produced by PCA (e.g. Malinowski's F-test and factor indicator function, or

IND) or PCA-based methods (e.g. evolving factor analysis and target factor analysis).(Borgen et al., 1986;

Gampp et al., 1987; Gemperline, 1984, 1986; Keithley et al., 2010; Maeder, 1987; Edmund R.

Malinowski, 1989) Additionally, orthogonalization methods such as orthogonal projection approach

(OPA), which selects the most dissimiliar spectra from the experimental data that have considerable

signal intensity, may be used to generate estimates of the relevant spectral shapes.(Sanchez et al., 1996)
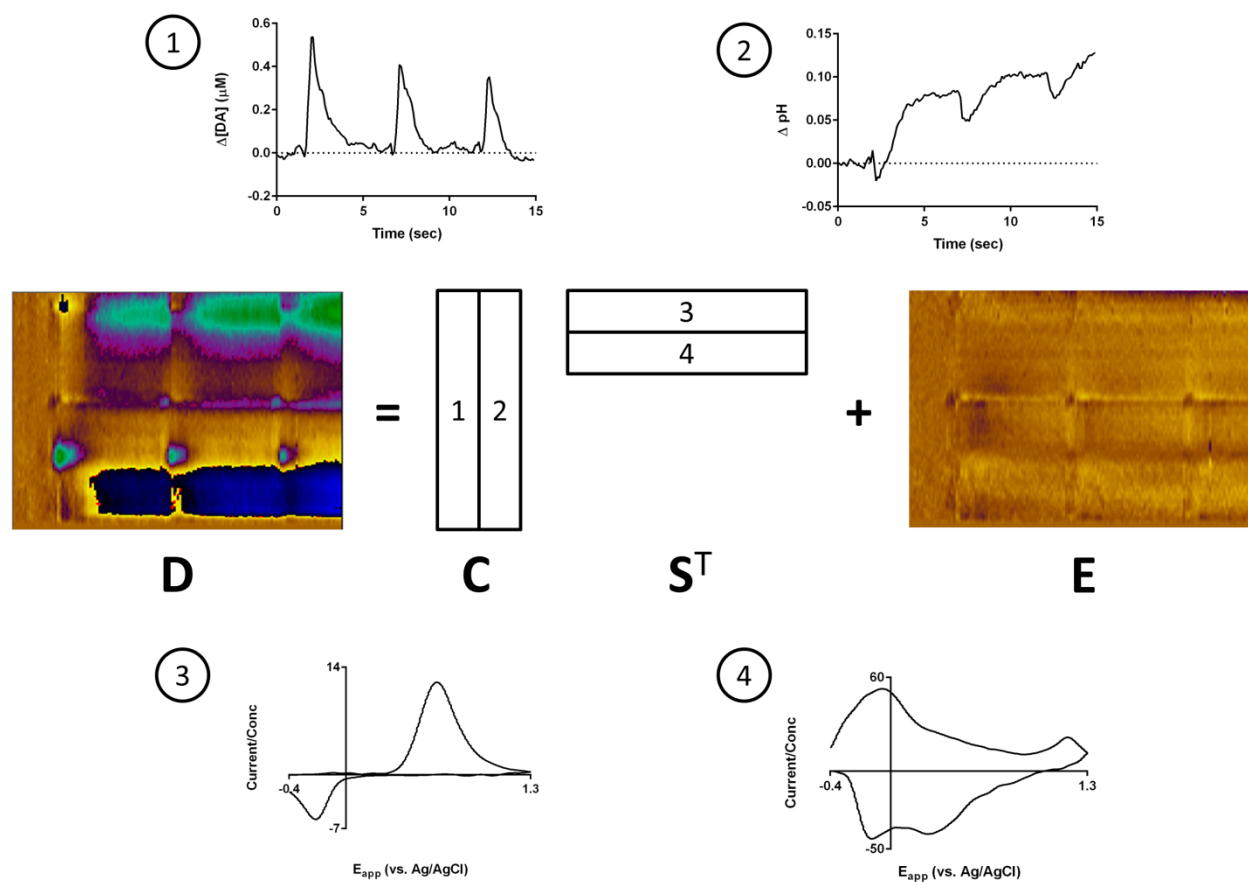
Figure 3.1. Graphical representation of the bilinear calibration model (Equation 3.1) with background-subtracted FSCV data. Above are shown the dopamine (1) and pH (2) concentration traces. Below are shown the dopamine (3) and pH (4) voltammograms.

This method has been shown to have favorable aspects compared to the Malinowski's F-test in analysis of HPLC-DAD data.(Vivo-Truyols et al., 2007) Alternatively, this can be set by the experimenter through *a priori* knowledge of the number of components or multiple fits of the data with varying number of components to yield meaningful solutions.(de Juan & Tauler, 2016; P. Tauler & Casassas, 1989; R. Tauler et al., 1991; R. Tauler, et al., 1993a; R. Tauler, et al., 1995b) For initial estimates of either the spectra or concentration values, many of the same methods may also be used. Otherwise, expected concentration or spectral profiles or even the data themselves may be used as inputs.(de Juan & Tauler, 2016; Gemperline & Cash, 2003) For this study, we explored the factor-based methods that performed well in the aforementioned LC-NMR study (Malinowski's F-test and the IND, as well as the ratio of its derivatives – ROD$_{IND}$), which have the advantage that they can be automated, and the EFA and OPA techniques, which can be used to generate initial estimates of the spectra. These are described briefly below.

With the model defined, Equation 3.1 is then solved using the alternating least squares approach. This method iterates between generating estimates of the concentration profiles or spectra, given an estimation of the spectra or concentration profile, respectively. In its unconstrained form, the following equations are used:

$$\mathbf{C}_{est} = \mathbf{D}\mathbf{S}_{est}{}^{+} \qquad \text{(Eq. 3.2)}$$

$$\mathbf{S}_{est} = \mathbf{C}_{est}{}^{+}\mathbf{D} \qquad \text{(Eq. 3.3)}$$

where the superscript + indicates the pseudoinverse of the matrix. For instance, if an initial spectral estimate is provided, Equation 3.2 is used to provide an estimate of the concentration profile, which is then used as the input for Equation 3.3. This process continues to refine the estimates of the concentration and spectral profiles until a predefined threshold of convergence is achieved or a set number of iteration cycles is reached. If constraints are to be applied, this is done either through direct alteration of the obtained estimates (de Juan & Tauler, 2016), the use of penalty functions (Gemperline & Cash, 2003), or alternative means of regression (Bro & DeJong, 1997; Bro & Sidiropoulos, 1998). Additionally, the experimental data matrix is often pretreated by factor analysis itself prior to fitting, such as PCA, as this reduces the effect of noise on the fitting results.(R. Tauler, et al., 1993b; R. Tauler, et al.,

1995b) If this is done, the reconstructed data set using only significant principal components ($\mathbf{D}^*$) is used in lieu of the original data matrix ($\mathbf{D}$) in Equations 3.2 and 3.3.

Implementation of Soft Constraints Using Penalty Functions. As mentioned before, FSCV data fails to meet the criteria for the application of many of the commonly used constraints that use prior knowledge of the properties of desired solutions or the experimental system. However, reference data may be incorporated to help define the fits through equality constraints (i.e. spectral or concentration values can be forced to equal to some reference data obtained), and the local number of components within a given window can also be defined through selectivity constraints.(Van Benthem et al., 2002) Further, these constraints need not be strictly imposed (i.e. the MCR-ALS spectra or concentration estimates need not be forced to equal the reference data), but rather enforced in a 'soft' manner, allowing deviations from the constraint values. This is done through the incorporation of weighted penalty functions into the model. Here, we use the P-ALS algorithm introduced (and described in detail) by Gemperline and Cash to realize this.(Gemperline & Cash, 2003) To illustrate this, for 'soft' equality constraints with a complete set of spectral reference data, the system of equations represented by Eq. 3.1 would be modified by the addition of the equivalent of the following:

$$w S_{ref} = w\mathbf{H} \qquad \text{(Eq. 3.4)}$$

where $\mathbf{S_{ref}}$ is the reference spectral matrix, $\mathbf{H}$ is diagonal matrix of ones, and w is a scalar weighting factor that determines the relative importance of this equation during the fitting procedure. Note that the symbol for the weighting factor here (w) is changed from that (λ) used by Gemperline and Cash to avoid confusion with its use to represent eigenvalues, which is used below and in previous work from our lab.(Keithley, et al., 2010) The power of this equation lies in its flexibility. Incomplete reference spectral data (e.g. one spectra for a multi-component system) can be used by appropriately adjusting the $\mathbf{H}$ matrix. Further, the weighting factor λ can be used to tune the how strictly this constraint is enforced. Small values of λ allow strong deviations from the reference spectra, while very large values force strict adherence of the spectral estimates to these shapes. Of note, use of the k vectors obtained from PCA

analysis of a training set as reference spectra with this P-ALS method and a high λ (approaching infinity) would produce the results obtained from PCA-ILS, highlighting the similarity between the two techniques.

Methods for Selection of the Number of Components. Here, the methods described above that were explored in this study for selection of the number of components present will be covered, with the exception of the Malinowski's F-test, which has been used and explored in detail in the context of FSCV previously.(Keithley, et al., 2010) Again, a more extensive list of methods is described in Wasim and Brereton, 2004.

Factor Indicator Function-Based Methods. The factor indicator function (IND) and the ratio of its derivatives (ROD$_{IND}$) rely on analysis of the residuals after principal component analysis of the data matrix and removal of the information described by a select number of principal components (PCs). Specifically, these make use of the residual standard deviation (RSD), which is calculated for a given PC (PC$_n$) as follows:

$$RSD_n = \sqrt{\frac{\sum_{j=n+1}^{s} \lambda_j^0}{t(s-n)}} \qquad \text{(Eq. 3.5)}$$

where λ_j^0 is the eigenvalue of the jth PC and s and t are equal to the smaller and larger of r and c, respectively. Malinowski introduced the IND to assist in determining the number of significant components, as its interpretation is more direct. The IND is calculated for PC$_n$ as follows:

$$IND_n = \frac{1}{(s-n)^2} RSD_n \qquad \text{(Eq. 3.6)}$$

Whereas a graph of the RSD as a function of n should flatten at the last significant component, the IND should reach a minimum, although this minimum is sometimes not well-defined and requires user interpretation. Alternatively, the ratio of the derivatives (ROD-IND, here referring to the second-to-third derivative ratio, as in Wasim and Brereton) of an error function like the IND can be used, as it should reach maximum at the number of significant components:

$$ROD_{IND,n} = \frac{IND(n) - IND(n+1)}{IND(n+1) - IND(n+2)} \qquad \text{(Eq. 3.7)}$$

The IND and ROD$_{IND}$ have the advantage of having clearly defined criteria for determining of the number of significant components and thus can be automated; however, it is useful to analyze their plots as a function of PC to as there can be significant ambiguity in the assignment.

Orthogonal Projection Approach. The orthogonal projection approach (OPA) does not rely on factor analysis, but rather the determination of the spectra present in the data that are the most dissimilar. This is determined in an iterative manner, comparing each spectrum to normalized reference spectra (s_{ref}), which is first set to be only the normalized mean spectrum of the data ($\bar{s}$). The dissimilarity (d_i) between the reference spectra and each data spectrum (s_i) is calculated by constructing a matrix Y_i, with s_{ref} and s_i as its rows and determining the determinant of the square matrix formed by the product of Y_i with its transpose:

$$d_i = \det(Y_i Y_i^T) \qquad \text{(Eq. 3.8)}$$

The first spectra ($s_{ref,1}$) with the highest dissimilarity as measured by d_i then replaces $\bar{s}$ as the reference spectrum in Y_i. The dissimilarities are then calculated again; however, the spectrum with the highest dissimilarity with $s_{ref,1}$ is now simply added to Y_i rather than replacing the previous spectrum. This process continues until a plot of the dissimilarity versus time (example shown in Figure 3.2A) shows no distinct peak or contains only random noise, or there is redundancy in the reference shapes.

Evolving Factor Analysis. The evolving factor analysis (EFA) approach relies on principal component analysis across the data window for the identification of the number of significant components (N$_C$) and a rough estimate of their time course, relying on the change in the rank of the data matrix with analysis of successively larger portions of the data window. This is typically done in both the forwards and backwards direction along the relevant variable (e.g. time). For example, forward EFA along the time direction begins by using PCA to calculate the eigenvalue for the first spectrum taken (S$_1$). Next, the following spectrum (S$_2$) is added to the submatrix for analysis, and PCA is performed to calculate the eigenvalues for the
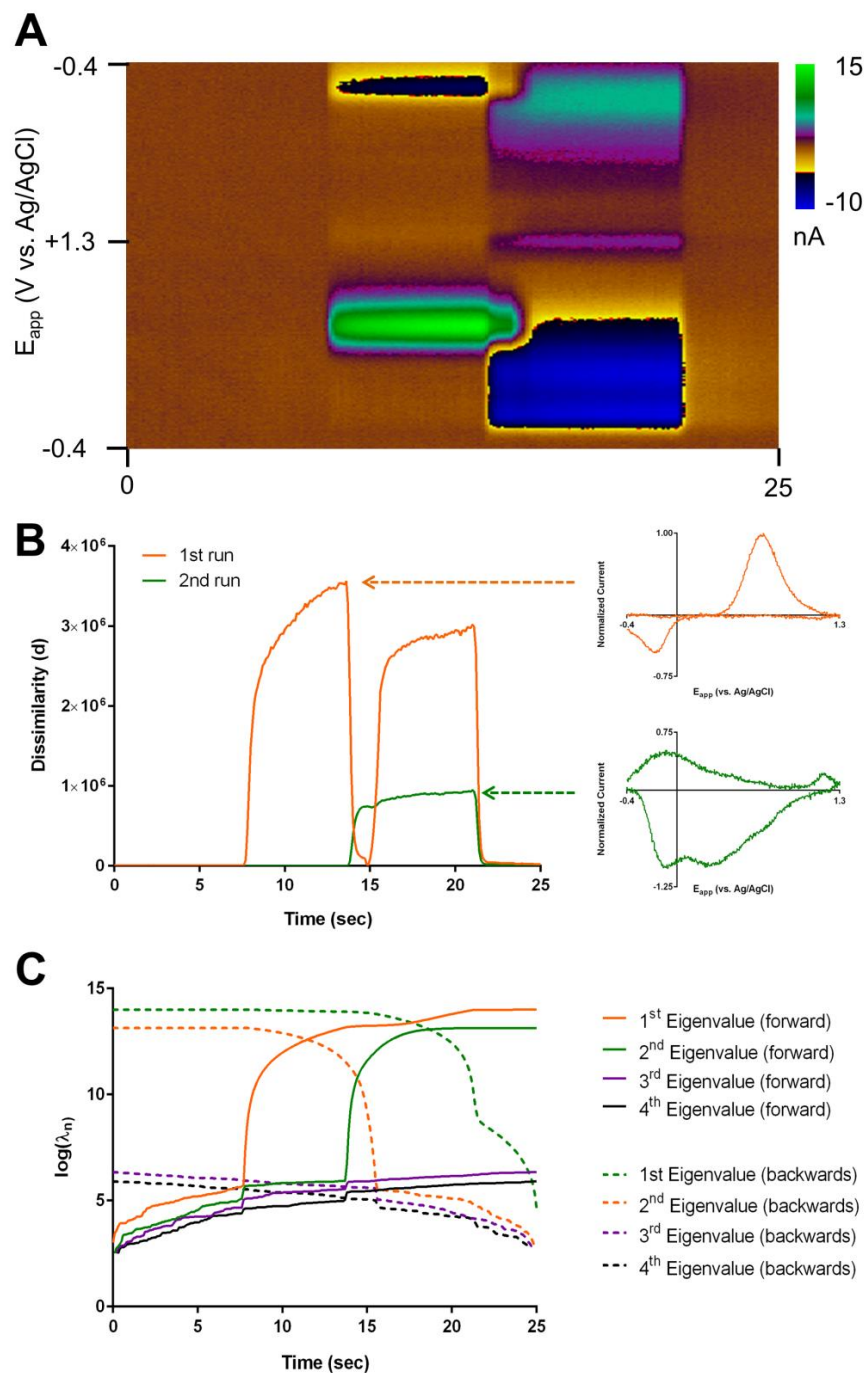
Figure 3.2. Evaluation of color plot with orthogonal projection approach (OPA) and evolving factor analysis (EFA). (A) Color plot with 8-second dopamine and pH injections, with onset separated by 6 seconds and dopamine appearing first. (B) Dissimilarity plots determined from (A) for the first (orange) and second runs (green) of OPA. The spectra shown to the right are those selected by OPA for a given run (i.e. the voltammograms at the time corresponding to the maximum dissimilarity value). (B) EFA plot of logarithm of eigenvalues shown for forward and backwards analysis. Note the colors for the first and second eigenvalues are swapped between the forward and backwards direction to aid in interpretation (i.e. the same colored lines for the forward and backwards direction indicate the appearance and disappearance of a given analyte).

submatrix defined by S_0 and S_1. This process continues, adding one spectrum at a time and calculating eigenvalues for the growing submatrix until the entire data matrix ($S_1 - S_T$) is analyzed. Backward EFA operates the same way, except the first submatrix is defined as the last spectrum taken (S_T). Spectra are added to this submatrix in regressive order (S_{T-1}, S_{T-2}, …. , S_1). For identification of the number of components, an EFA plot is constructed, typically using the logarithm of the eigenvalues plotted versus time, for both the forward and backward analysis. Analysis of this plot relies on identification of the appearance of a significant eigenvalue (i.e. above the values defined by the non-significant eigenvalues) moving along the plot in the direction the analysis was performed. In the forward direction, an increase (moving from time 1 to T) in the nth eigenvalue can be interpreted as the appearance of the nth analyte in the data window. In the backward direction, an increase (moving from time T to 1) in the nth eigenvalue can be interpreted as the disappearance of the ($N_C - n + 1$)th analyte, provided the analytes appear and disappear in successive order. An example plot is shown in Figure 3.2B.

RESULTS AND DISCUSSION

In Vitro Evaluation of Dopamine-pH Mixtures with MCR-ALS. We first sought to assess the utility and limitations of MCR-ALS for the analysis of FSCV data obtained from *in vitro* flow-injection analysis. For this, the classical FSCV system of mixtures of dopamine and pH changes was analyzed, as was the case for prior work.(Johnson, et al., 2016b; Rodeberg, et al., 2015) Note that, in the following analysis, no attempt at determining 'true' concentration values will be made, as the quantitation is not the focus here. However, this conversion would be identical to the process used in FSCV once the spectral estimates are obtained.

First, it was verified that the technique could successfully be used to isolate the signals from pure solutions. For this, unconstrained MCR-ALS was suitable for analysis of the raw data. Various initialization methods were tried (current at the dopamine oxidation potential for concentration, a spectra from the data, and an OPA-generated estimate of the dominant spectra) as well as the use of PCA for data pretreatment, and nearly identical solutions were obtained (data not shown). An example fit is shown in Figure 3.3A to FSCV data from a flow-cell analysis of a 1.0 μM dopamine bolus using this approach
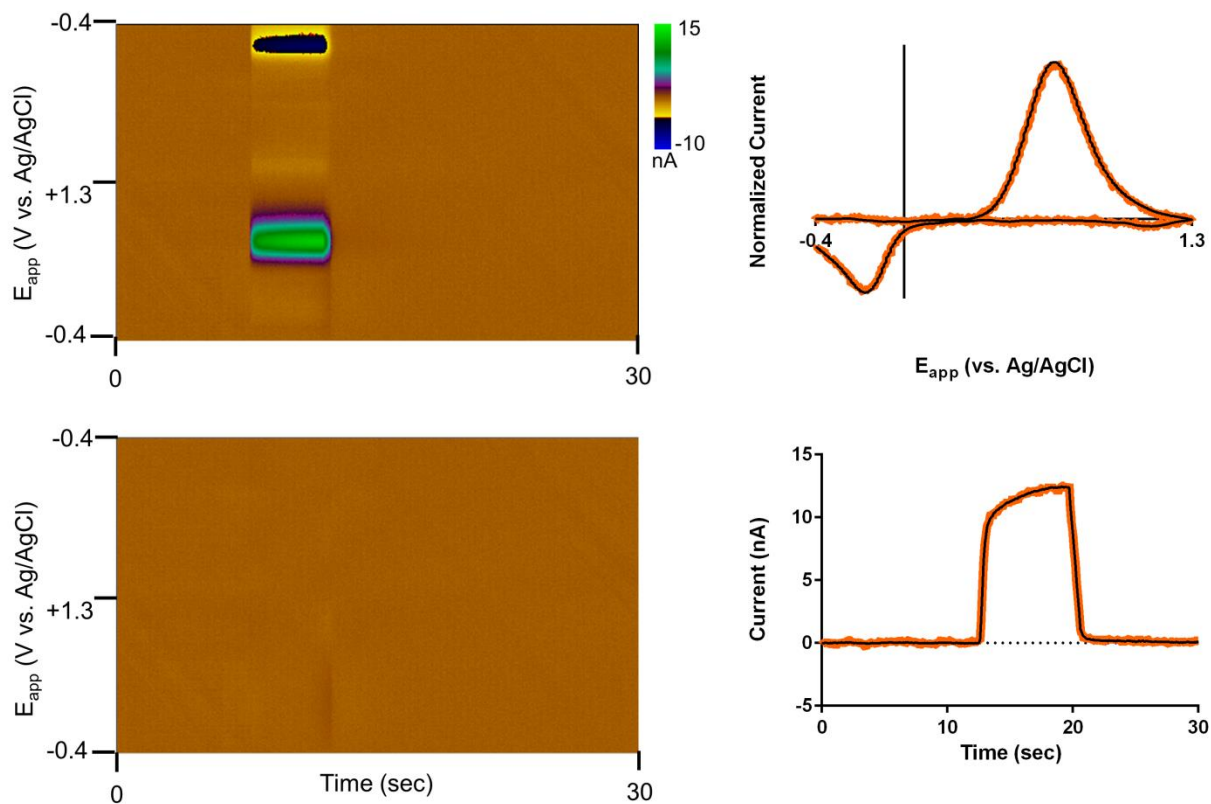
Figure 3.3. Results of unconstrained MCR-ALS analysis of FSCV data from a flow-injection analysis of a bolus of dopamine. Clockwise from top left: Color plot representation of the background-subtracted data analyzed, with time as the abscissa, the applied potential as the ordinate, and the current in false color, dopamine CV during injection (orange) and MCR-ALS estimate (black), current at the dopamine oxidation potential as a function of time (orange) and MCR-ALS estimate (black), and color plot of the residual current after MCR-ALS analysis

(initialized with the dopamine oxidation current and untreated with PCA). These estimates are shown compared to a dopamine CV and the current vs. time trace, and it can be seen that the MCR-ALS estimates are nearly identical to these references but have lower noise levels, due to the random nature of the noise present.

Next, the potential for MCR-ALS for separating DA-pH mixtures was then evaluated. As noted before, the success of MCR-ALS is anticipated to be dependent on the temporal separation of the signals. Thus, simulated mixture data was created from independent injections of dopamine and pH (DA-pH), such that the data could be added together with differing time delays between the appearances of analyte signal. First, the performance of the methods described in the Theory section for selection of the number of chemical components was evaluated (Table 3.1). Malinowski's F-test has been used in FSCV analysis in the context of rank selection in PCA-ILS; however, attempts to use this here were complicated by abnormally high rank estimates provided when large portions of the data matrix were analyzed. A similar overestimation was reported by Vivo-Truyols et al. in the analysis of HPLC-DAD data. (Vivo-Truyols, et al., 2007) Visual inspection of the principal components and the data reconstructed with principal components confirmed that these extra components consisted of random noise (data not shown). This may be due to the large number of voltammograms that carry no chemical information in the *in vitro* data or issues related to well-documented limitations and criticisms of the method (e.g. the small number of degrees of freedom used in calculation of the F-statistic and assumption of homoscedastic and uncorrelated noise).(Faber & Kowalski, 1997a, 1997b; Keithley, et al., 2010; E. R. Malinowski, 1999; Vivo-Truyols, et al., 2007) The number of predicted components could be lowered by truncation of the data matrix and increasing the confidence level; however, the results were inconsistent and always greater than 2. Thus, an alternative was sought. The ROD_{IND} was also explored; however, similar to the results reported by Vivo-Truyols, the performance was inaccurate even for the well-defined *in vitro* data and was not explored further. While not as readily automated, the orthogonal projection approach (OPA) and evolving factor analysis (EFA) approaches proved the most reliable indicator the number of components. Regardless of time separation, OPA and EFA correctly predicted two components. With regard to OPA, the most dissimilar spectra identified by in all analyses, except for the data with no separation, matched the pure DA and pH CVs present in the data. With no separation, only differently

Table 3.1. Rank estimated by Malinowski's F-Test, orthogonal projection approach, ROD function, and the EFA approach for different simulated time separations of 8-second dopamine and pH boluses.

	Analyte Separation													
	0 sec		2 sec		4 sec		6 sec		8 sec		10 sec		12 sec	
	I	T	I	T	I	T	I	T	I	T	I	T	I	T
Malinowski's F-Test (99%)	3	8	4	8	4	8	4	8	5	8	6	8	6	8
OPA	2	2	2	2	2	2	2	2	2	2	2	2	2	2
ROD	1	3	1	1	1	1	1	1	1	1	1	1	1	1
EFA	2	2	2	2	2	2	2	2	2	2	2	2	2	2

*I = analysis of data window containing injections; T = analysis of entire 50-second data window

shaped DA-pH mixture voltammograms were selected; however, the dissimilarity plots only degraded to random noise after three spectra. EFA analysis was able to correctly indicate the time of appearance and disappearance for all cases, with the exception of the data with no temporal separation. However, in that case, the technique was able to pick up subtle differences in the rate of disappearance after injection to suggest two components.

These approaches are also advantageous, as they provide information about the expected spectra (OPA) and concentration traces (OPA and EFA, the latter more reliably than the former). Since OPA provides spectra from the data itself in a straightforward and computationally inexpensive manner, this was chosen as the initialization method for the MCR-ALS fits to the mixture data. For temporal separation greater than 8 seconds (complete separation of the injections), initialization with the OPA spectral estimates and unconstrained MCR-ALS provided excellent agreement with the results expected from the individual 'pure' runs. With smaller separations, significant distortions began to appear in the solutions. For example, at separations of 2-7 seconds, the determined concentration profiles had sudden artificial changes during the periods of signal overlap, despite having very similar spectral profiles to those obtained from the pure runs. At separations of 1.5 seconds or less, the obtained spectral profiles were DA-pH mixture voltammograms. This is likely due to the rotational ambiguity in the solutions, and, thus, constraints that could provide meaningful solutions were explored.

One approach to placing constraints of the MCR-ALS solutions is the use of reference data, obtained separately from the experimental data being analyzed. We sought to explore the potential of using library reference data with 'soft' penalty functions (P-ALS) for imposing loose equality constraints to guide solutions. The library data used for this experiment was 10 DA and 10 pH CVs obtained from separate experiments using separate T-650 carbon fibers. An average was determined for each of these analyte shapes and used as the reference spectra for the two analytes. However, first, the behavior of this approach was characterized on the 'pure' runs to understand the effects of this approach and specifically of the 'weighting' parameter w of the model. MCR-ALS fits to the 'pure' runs were obtained with various values of the weighting parameter ($w = 0$ to 8), and the sum of the squares of the residual for the fits were determined. The results of this analysis are shown in Figure 3.4. For both DA and pH data
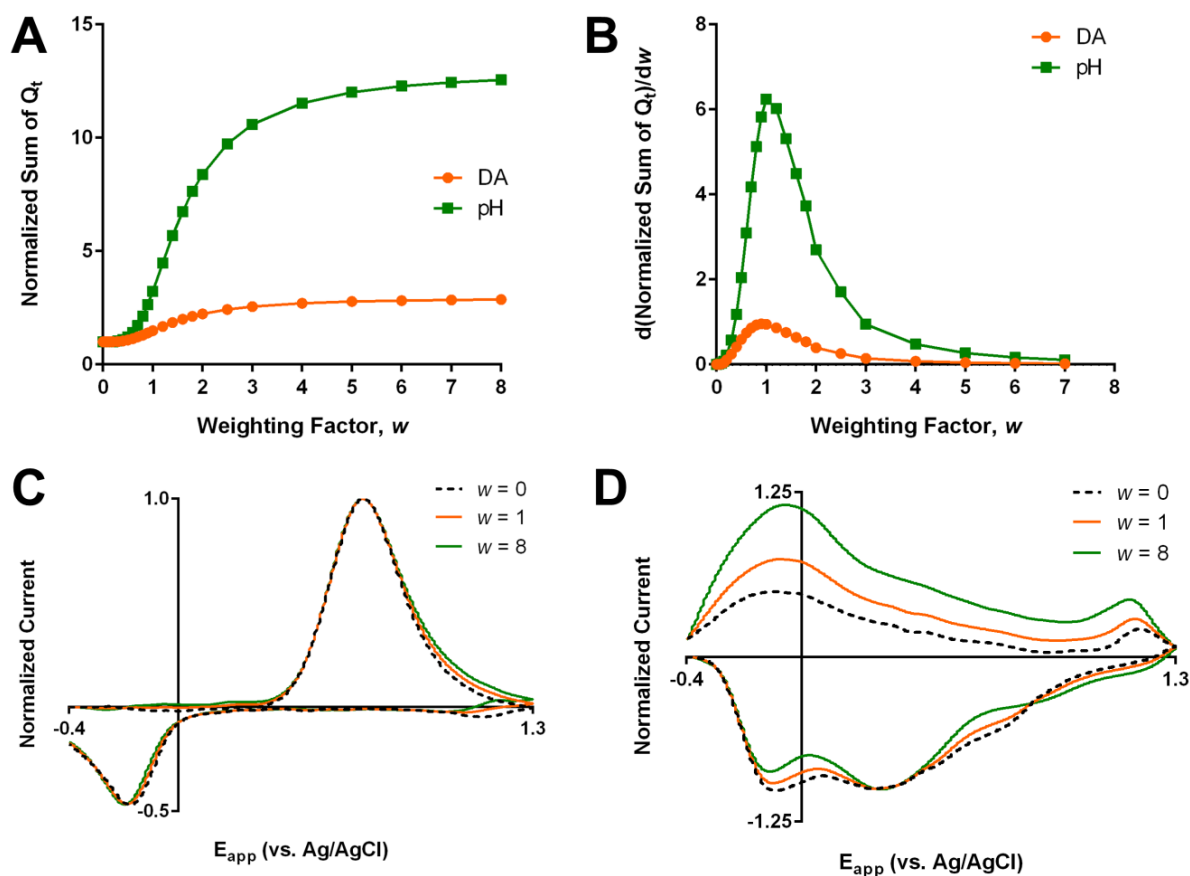
**Figure 3.4.** Effect of the weighting parameter *w* on the MCR-ALS fits to isolated injections of dopamine and pH. (A-B) Sum of the squares of the residual (A, normalized to value for *w* = 0) and its derivative plot (B) as a function of the weighting parameter *w* for the dopamine (orange) and pH (green) data. (C-D) MCR-ALS spectral estimates for dopamine (C) and pH (D) data at different values of *w*.

(Figure 3.4A), a smooth transition can be seen between two different solutions, the unconstrained ($w = 0$) and that defined entirely by the average library CV (large w). As expected, fits with large w values had higher residual values, as the average CV is unrepresentative of the data. The largest changes in the solutions occurred around w values of 1 for both data sets, as evidenced of the derivative plot of the sum of squares of the residual with w (Figure 3.4B). The use of a pH library CV for fitting also lead to considerably higher error, due to the large difference between the experimental and library pH CVs. This is expected due to the larger variability seen between pH CVs at carbon fiber electrodes as compared to DA CVs.(Keithley, et al., 2010; Rodeberg, et al., 2015) Thus, the use of DA library reference CVs is preferred to use of pH CVs. Additionally, the approach should not be used with large weighting parameters, as these introduce considerable error into the fits. However, ideally, these constraints can be initially used during the fitting procedure and lifted before the final MCR-fit is obtained.

This library P-ALS approach was then used to analyze the DA-pH mixture data that unconstrained MCR-ALS could not properly fit. During the initial fit, soft constraints (w_{pH} and $w_{DA} = 1$) were imposed on both analytes using the library CVs as reference data until convergence was achieved. Then, since the pH library is less reliable, the pH equality constraint was lifted ($w_{pH} = 0$ and $w_{DA} = 1$), and, using the previous fit as the initialization, the solution was again allowed to converge. Finally, the DA equality constrained was lifted (w_{pH} and $w_{DA} = 0$), and the final solution was obtained. The process was repeated to ensure overall convergence using this procedure. The approach proved successful in mitigating the issues seen with unconstrained MCR-ALS, as highlighted for the 1-second separation data in Figure 3.5. The unconstrained solution (Figure 3.5A) shows distortions in both the concentration and spectral profiles. After imposition of soft constraints on both analytes (Figure 3.5B), the spectral and concentration profiles significantly improve; however, the sum of squares of the residual values is over 9 times higher for this constrained fit. Removal of the pH constraint (Figure 3.5C) leads to a better fit at the cost of the spectral shapes. Finally, the removal of both constraints (Figure 3.5D) leads to improved spectral and concentration profiles with an identical residual value as that of the original unconstrained solutions.
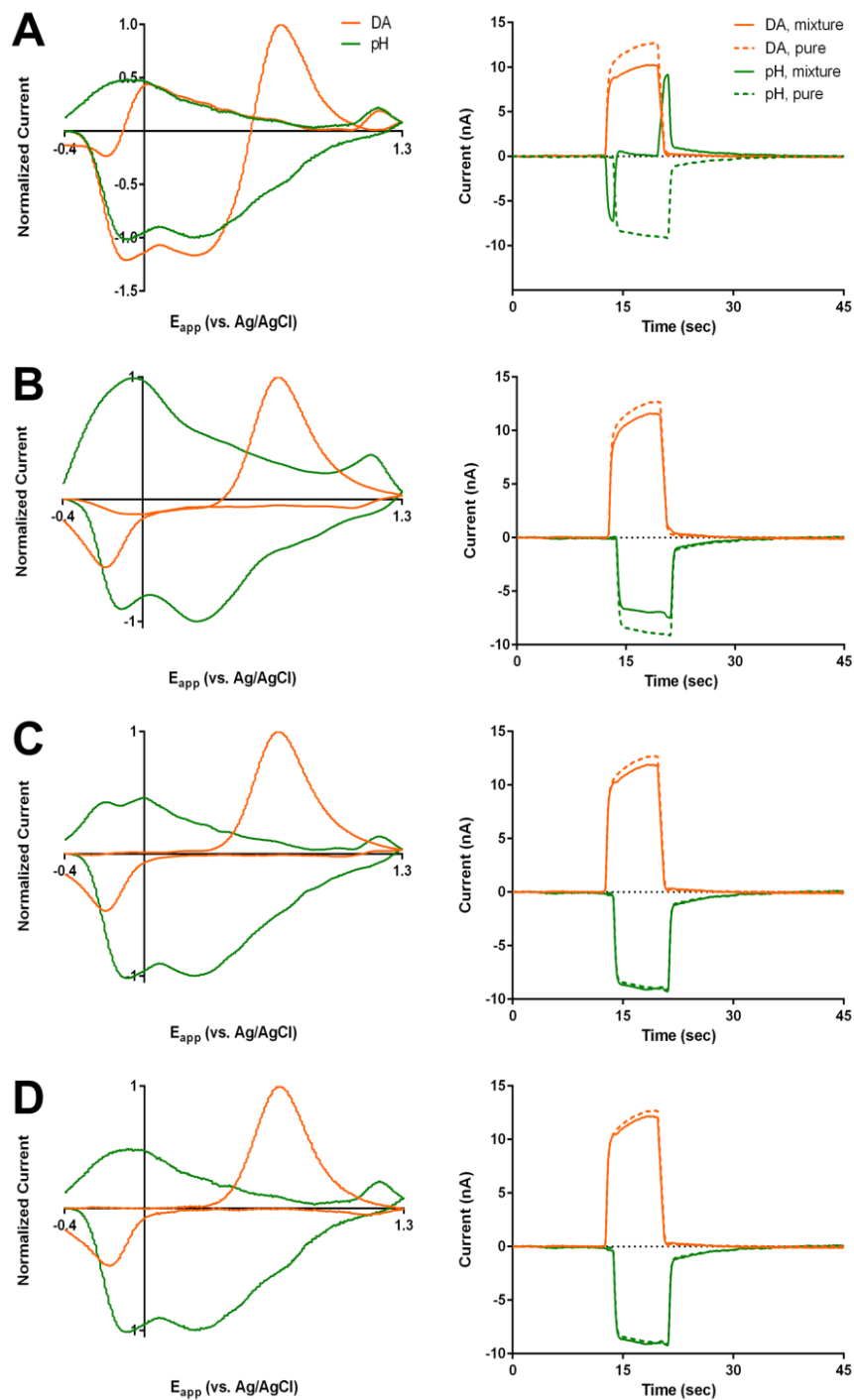
Figure 3.5. Successive fitting using P-ALS 'soft' equality constraints for analysis of simulated *in vitro* dopamine-pH mixtures (temporal separation of 1 second). (A-D) MCR-ALS spectral (left) and (concentration) estimates for the initial unconstrained model (A), the DA/pH 'soft' equality constrained model (B), the DA-only 'soft' equality constrained model (C), and the final unconstrained model after successive iterations of A-C (D). The dashed lines indicate the concentration estimates for the isolated runs for comparison.

Evaluation of In Vivo FSCV Data. The potential of MCR-ALS was then evaluated using *in vivo* FSCV data obtained during intracranial self-stimulation sessions ($n = 25$), each trial containing multiple (typically greater than 50) electrically evoked dopamine transients. These data mainly contain mainly contributions from pH and DA, but are less well defined and noisier than the *in vitro* data. However, within a given experimental run, multiple electrically evoked transients are present, opening the possibility of using multiple data sections for model definition. These data were originally analyzed using PCR models built from training data collected during the experiment, which served as a reference point for comparison of the MCR-ALS model performance in this study.

First, the advantages of using multiple transients for model definition were explored. For this, separate background-subtracted color plots were obtained from various points in a given experimental run, and these data were concatenated together to form the data matrix for MCR-ALS analysis. An example is shown in Figure 3.6, with three separate transient windows joined together (color plot shown in Figure 3.6A). The MCR-ALS spectral fits were determined (using unconstrained MCR-ALS) for increasing numbers of snippets, and the PCR *k* vectors for the analytes are shown for comparison. Analysis of only the first snippet provided a moderately estimate of the DA spectrum; however, the pH spectrum is only weakly determined and both estimates contained considerable noise (Figure 3.6B). Increasing the number of snippets (Figure 3.6C-D) provided increasingly good estimations of the underlying component spectra, with improvements in the spectral shapes (particularly for pH and the reductive wave of DA) and the noise contained in the estimates.

The most straightforward and computationally inexpensive application of MCR-ALS relies on determining a subset of the experimental data for use to define the model that will be used to analyze the entirety of the data. In our case, the spectral estimates are anticipated to remain constant throughout a given experimental session, and, thus, the spectral estimates will be determined and used to analyze the remainder of the experimental data. Selection of the training subset within the experimental data is an important consideration. Ideally, the training subset should contain all considerable contributions from all components expected throughout the experimental data. Additionally, the signals should be resolved from one another. To help determine this, the evolving factor analysis (EFA) method is particularly helpful, as it
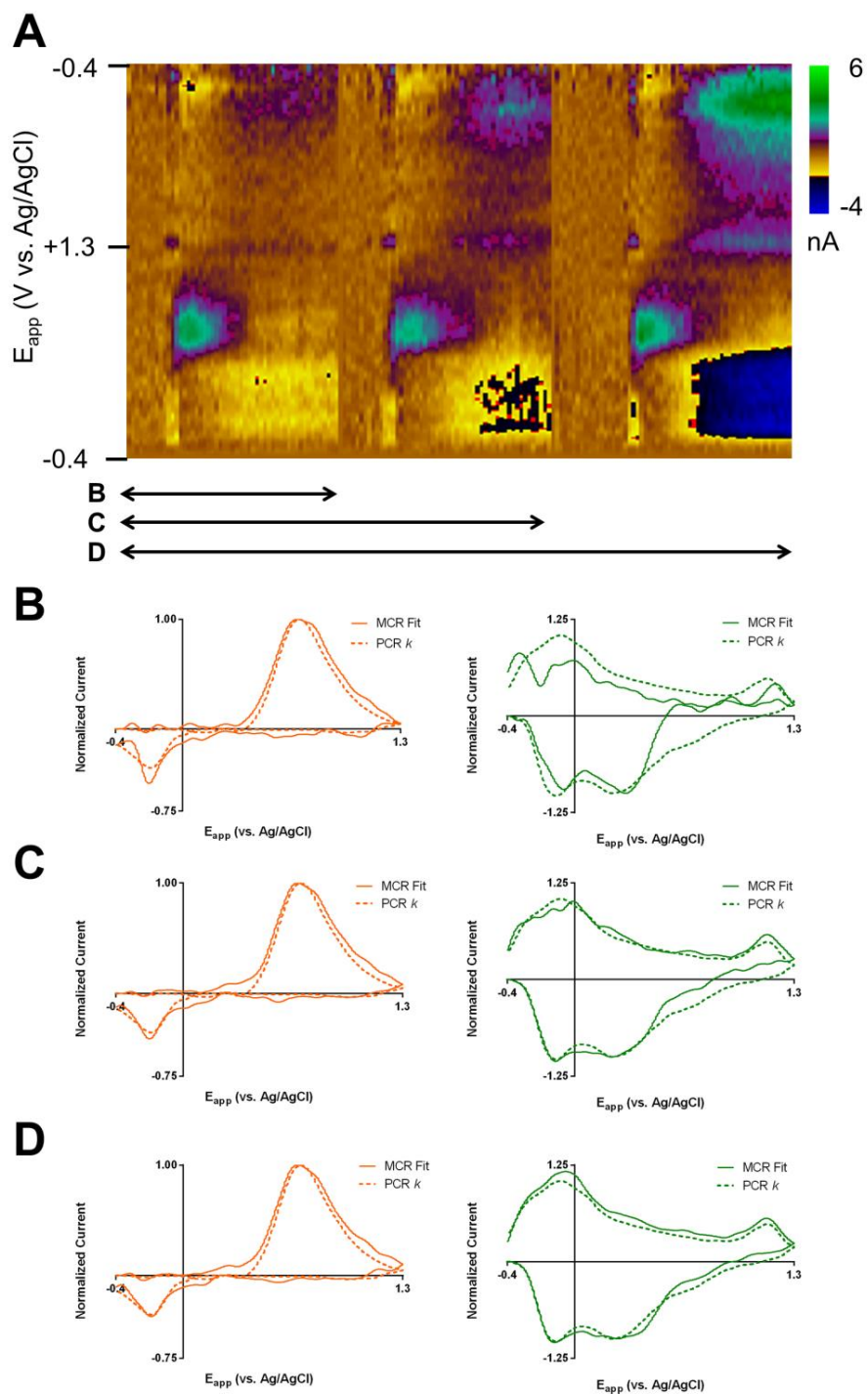
Figure 3.6. Spectral fits for MCR-ALS analysis of increasing numbers of electrically evoked dopamine transients. (A) Color plot showing three separate transients joined together for analysis, with the arrows underneath indicating the data windows analyzed for the MCR-ALS analysis. (B-D) Spectral fits (solid lines) for dopamine (left) and pH (right) for analysis of one (B), two (C), and three transients. PCR k vectors for the two analytes are shown as dashed lines for comparison.

71

can provide a good estimate of the time courses of the analytes present in a given time window. Additionally, subsets of the data that contain only one analyte can be used; however, care must be taken to ensure that all analytes contribute significantly to the total signal. Underrepresentation of a given analyte can lead to poor quality estimates of its spectral and concentration profiles, as the MCR-ALS algorithm works to capture find the profiles that minimize the residual values of the entire training submatrix. If the majority of the variance in the training submatrix is determined by a single analyte, the profiles obtained may be determined by attempts to capture this single analyte rather than all components. Further, depending on the quality of the data, constraints, like the P-ALS equality approach explored above, may need to be used, using either using single-analyte experimental CVs or a library approach using data from separate experiments. Again, the latter approach should be used with low weightings to avoid fitting the data in an unrepresentative manner.

To test the performance of the technique, each set of experimental data was analyzed to select a training submatrix. This submatrix was then used to estimate the spectral profiles of dopamine and pH that were subsequently used to analyze other experimental data in a manner analogous to PCA-ILS (or, equivalently, P-ALS with the spectral estimates weighted with high w values). The results of this approach were compared to those obtained from PCA-ILS and are presented in Table 3.2. For each fit, the correlation coefficient between the MCR-ALS and the PCA-ILS estimates, and the signal power of the difference between the MCR-ALS and PCA-ILS estimates (the lack of agreement between the two techniques, normalized to signal power of the PCA-ILS estimates), were determined for a comparison of both the shapes of these estimates and their absolute differences. Overall, there was good agreement between PCA-ILS and MCR-ALS. In general, the estimation of pH profiles differed more between the two techniques than those for DA, and there was greater variability in the performance of MCR-ALS for determining the pH profiles. This was generally due to the difficulty in finding isolated pH spectra within the data to use for model training. However, no separate training data was used in this analysis, and the collection and inclusion of even minimal amounts of reference data collected separately from the experiment could be expected to improve this performance.

Table 3.2. Summary of correlation and lack of agreement between PCA-ILS and MCR-ALS estimates of spectral and concentration profiles for *in vivo* FSCV data collected during intracranial self-stimulation trials (n = 25 rats)

	Correlation Coefficient (R^2)			Lack of Agreement[a] (%)		
	Average	Min	Max	Average	Min	Max
DA spectra	0.985	0.971	0.995	3.76	2.16	5.77
pH spectra	0.984	0.963	0.996	4.35	1.21	12.1
DA concentration	0.994	0.983	0.999	1.82	0.37	4.92
pH concentration	0.980	0.942	0.999	4.77	0.48	15.8

[a]Lack of Agreement = $100\% * \dfrac{\left[\sum_{i=0}^{N}\left(x_{i,MCR-ALS}-x_{i,PCA-ILS}\right)^2\right]}{\left[\sum_{i=0}^{N}\left(x_{i,PCA-ILS}\right)^2\right]}$

Residual Analysis. One of the primary advantages of using higher-order calibration models is the ability to rely on residual analysis for the detection of interferences that can generate errors in the model estimates. Thus, we sought to explore means of adopting the residual analysis procedure introduced by Jackson and Mudholkar, and currently used in FSCV with PCA-ILS analysis, as a first step towards establishing a means of model validation, specifically for application of a model generated from a training submatrix to the experimental data. During the training phase, significant interferences can typically be detected, through the method used to detect the number of components (e.g. EFA and/or OPA) or distortion of the fits.

Specifically, the standard residual analysis procedure relies on calculation of an experiment-specific Q_α value, a threshold for evaluating the residual values at a specific time point to determing model suitability ($Q_t > Q_\alpha$ leads to rejection of the data for analysis with that model) that is characteristic of the noise level. This relies on the use of principal component analysis, identification of the significant components, and analysis of the error eigenvalues (i.e. those associated with the non-significant principal components). In PCA-ILS analysis, this step is performed during definition of the spectral profiles through analysis of the training data. However, we sought to evaluate whether the use of the experimental data itself, when analyzed with PCA, could generate a suitable estimate. For each experimental data set, random sets of five-second windows ($n = 6$ windows/data set, 50 CVs per window, 25 data sets) were obtained for analysis. Each window was analyzed with PCA, and, using Malinowski's F-test, the rank of the submatrix was determined. This allowed for an estimation of Q_α using the eigenvalues of the non-significant components identified in this manner. The results of this analysis are presented in Table 3.3 and compared with values obtained from PCA analysis of the associated training set data. Overall, moderate agreement between the values obtained from PCA analysis of training set data and the experimental data was observed. Although there was a large spread of values for percent difference between the values obtained from the two approaches, the Q_α values obtained from the different experimental windows were consistent, with an average relative standard deviation of 17.5%. The majority of cases (60%) had lower Q_α values obtained from experimental data than from the training set data, meaning that, for this data set, the former approach would be more conservative.

74

Table 3.3. Percent difference between Q_α values determined from Malinowski's F-test analysis of independently collected training set (10 CVs x 1) and experimental data (50 CVs x 6) for 25 intracranial self-stimulation data sets and relative standard deviation of the latter.

|	*Average*	*Minimum*	*Maximum*
Percent Difference (%)	(+)10.4	(-)0.8	(+)132.9
Relative Standard Deviation	16.6	5.5	48.3
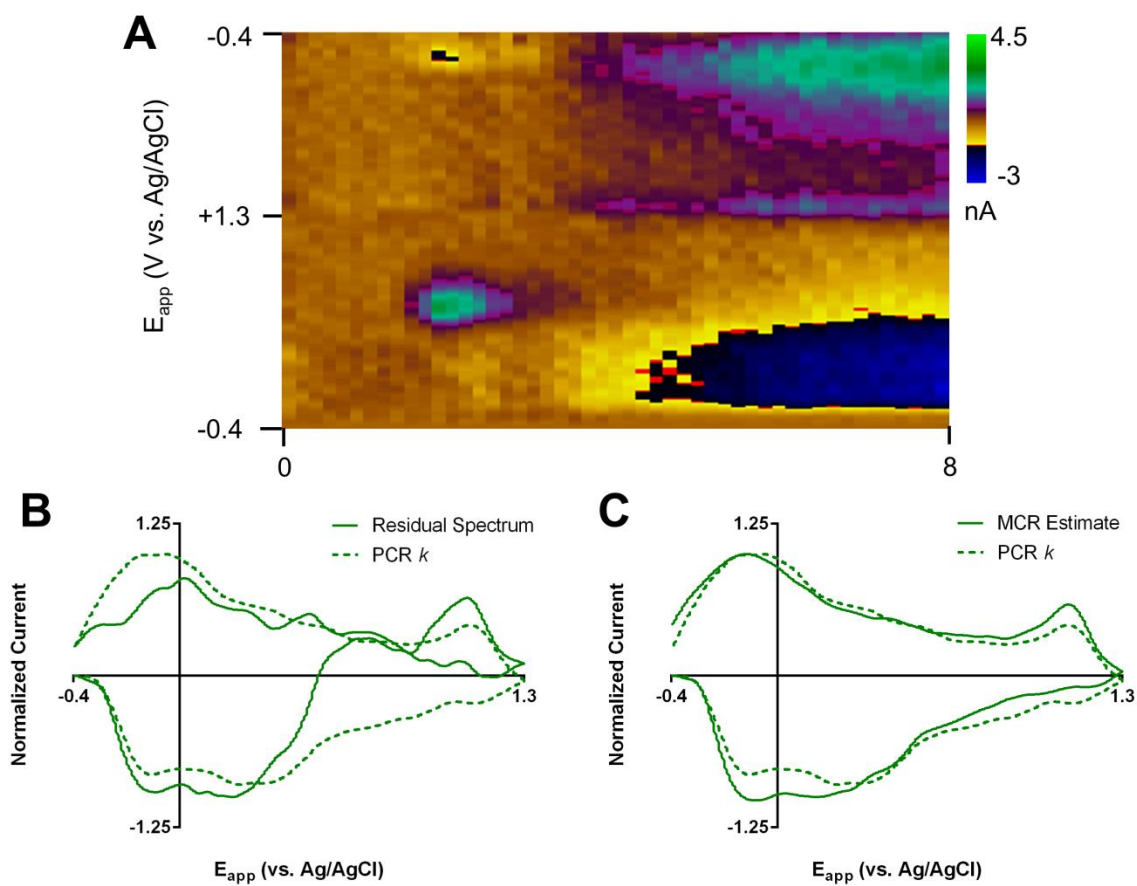
Figure 3.7. Interferent identification using MCR-ALS. (A) *In vivo* color plot containing both DA and pH signals. (B) Residual spectrum (solid line) after analysis of the data with a DA-only training set with PCA-ILS. (C) MCR-ALS spectral estimate (solid line) using a two-component model. The dashed line shows the PCR pH *k* vector.

Finally, one advantage of MCR-ALS as an exploratory technique within the context of residual analysis should be highlighted. In PCR-ALS, the number of components is defined using *a priori* knowledge of the system, and data that fails residual analysis is typically thrown out. Further, analysis of the residual plots reveals the presence of interferents; however, the residual spectrum does not necessarily provide robust information on the shape of the spectra. With MCR-ALS, should a set of data fail residual analysis, a component can be added to the model, and MCR-ALS can be performed to attempt to gather information on the nature of the interferent. This advantage is highlighted in Figure 3.7. Here, a dopamine-pH mixture (Figure 3.7A) is analyzed with both PCA-ILS (using only a dopamine training set) and MCR-ALS with two components. The PCA-ILS residual spectrum (Figure 3.7B) does have general features resembling the reference pH k vector. However, due to poor model definition and the overlapping signals between pH and dopamine, some of the current has been assigned as arising from dopamine, resulting in a deviation in the residual spectrum from a 'pure' dopamine signal. On the other hand, the MCR-ALS estimate (Figure 3.7C) gives a more robust estimate of the interferent spectra, giving greater confidence in identification of this component. This component now can be incorporated into the model to generate more accurate estimates.

CONCLUSIONS

The multivariate curve resolution-alternating least squares approach has several advantages over PCA-ILS in the analysis of FSCV data, including more flexibility in model definition, decreased experimental requirements (i.e. relaxation of the need to collect separate training data), and more robust handling of interferents. However, due to this increased freedom in model definition, considerably more caution must be employed, and the methods explored here for its deployment (OPA, EFA, and P-ALS) require more user input than the currently established PCA-ILS protocols. Regardless, in the conditions studied here, the two techniques generated highly similar spectral and concentration estimates under the conditions studied here, and MCR-ALS demonstrates considerable potential as a complementary or alternative analysis method to PCA-ILS. Indeed, with the P-ALS approach, incomplete or imperfect sets of reference data, which may generate poor PCA-ILS models, may be used to help define MCR-ALS

models that can more accurately fit the data, and, in the cases where robust reference data is available, the technique can generate identical estimates to that obtained through PCA-ILS. However, future characterization and development of the technique for FSCV, particularly in exploration of constraints that can provide robust models, will greatly help in understanding its potential and, importantly, its limitations.

REFERENCES

Booksh, K. S. (2006). Chemometric Methods in Process Analysis *Encyclopedia of Analytical Chemistry*. New York: John Wiley & Sons, Ltd.

Booksh, K. S., & Kowalski, B. R. (1994). Theory of Analytical-Chemistry. *Anal Chem, 66*(15), A782-A791.

Borgen, O. S., Davidsen, N., Zhu, M. Y., & Oyen, O. (1986). The Multivariate N-Component Resolution Problem with Minimum Assumptions. *Mikrochim Acta, 2*(1-6), 63-73.

Bortolato, S. A., & Olivieri, A. C. (2014). Chemometric processing of second-order liquid chromatographic data with UV-vis and fluorescence detection. A comparison of multivariate curve resolution and parallel factor analysis 2. *Anal Chim Acta, 842*, 11-19.

Bro, R., & DeJong, S. (1997). A fast non-negativity-constrained least squares algorithm. *J Chemometr, 11*(5), 393-401.

Bro, R., & Sidiropoulos, N. D. (1998). Least squares algorithms under unimodality and non-negativity constraints. *J Chemometr, 12*(4), 223-247.

Bucher, E. S., Brooks, K., Verber, M. D., Keithley, R. B., Owesson-White, C., Carroll, S., et al. (2013). Flexible Software Platform for Fast-Scan Cyclic Voltammetry Data Acquisition and Analysis. *Anal Chem, 85*(21), 10344-10353.

Dantas, C., Tauler, R., Miguel, M., & Ferreira, C. (2013). Exploring in vivo violacein biosynthesis by application of multivariate curve resolution on fused UV-VIS absorption, fluorescence, and liquid chromatography-mass spectrometry data. *Anal Bioanal Chem, 405*(4), 1293-1302.

de Juan, A., & Tauler, R. (2016). Multivariate Curve Resolution-Alternating Least Squares for Spectroscopic Data. In C. Ruckebusch (Ed.), *Resolving Spectral Mixtures: With Applications from Ultrafast Time-Resolved Spectroscopy to Super-Resolution Imaging* (1st ed., Vol. 30). Amsterdam: Elsevier.

Diaz-Cruz, M. S., Mendieta, J., Tauler, R., & Esteban, M. (1999). Multivariate curve resolution of cyclic voltammetric data: Application to the study of the cadmium-binding properties of glutathione. *Anal Chem, 71*(20), 4629-4636.

Esteban, M., Arino, C., Diaz-Cruz, J. M., Diaz-Cruz, M. S., & Tauler, R. (2000). Multivariate curve resolution with alternating least squares optimisation: a soft-modelling approach to metal complexation studies by voltammetric techniques. *Trac-Trend Anal Chem, 19*(1), 49-61.

Faber, K., & Kowalski, B. R. (1997a). Critical evaluation of two F-tests for selecting the number of factors in abstract factor analysis. *Anal Chim Acta, 337*(1), 57-71.

Faber, K., & Kowalski, B. R. (1997b). Modification of Malinowski's F-test for abstract factor analysis applied to the Quail Roost II data sets. *J Chemometr, 11*(1), 53-72.

Feundale, R. N., Woody, N. A., Tan, H. W., Myles, A. J., Brown, S. D., & Ferre, J. (2002). Transfer of multivariate calibration models: a review. *Chemometrics and Intelligent Laboratory Systems, 64*(2), 181-192.

Gampp, H., Maeder, M., Meyer, C. J., & Zuberbuehler, A. D. (1987). Quantification of a Known Component in an Unknown Mixture. *Anal Chim Acta, 193*, 287-293.

Gargallo, R., Tauler, R., CuestaSanchez, F., & Massart, D. L. (1996). Validation of alternating least-squares multivariate curve resolution for chromatographic resolution and quantitation. *Trac-Trend Anal Chem, 15*(7), 279-286.

Garris, P. A., Kilpatrick, M., Bunin, M. A., Michael, D., Walker, Q. D., & Wightman, R. M. (1999). Dissociation of dopamine release in the nucleus accumbens from intracranial self-stimulation. *Nature, 398*(6722), 67-69.

Gemperline, P. J. (1984). A Priori Estimates of the Elution Profiles of the Pure Components in Overlapped Liquid-Chromatography Peaks Using Target Factor-Analysis. *J Chem Inf Comp Sci, 24*(4), 206-212.

Gemperline, P. J. (1986). Target Transformation Factor-Analysis with Linear Inequality Constraints Applied to Spectroscopic Chromatographic Data. *Anal Chem, 58*(13), 2656-2663.

Gemperline, P. J., & Cash, E. (2003). Advantages of soft versus hard constraints in self-modeling curve resolution problems. Alternating least squares with penalty functions. *Anal Chem, 75*(16), 4236-4243.

Grabaric, B. S., Grabaric, Z., Tauler, R., Esteban, M., & Casassas, E. (1997). Application of multivariate curve resolution to the voltammetric data - Factor analysis ambiguities in the study of weak consecutive complexation of metal ion with ligand. *Anal Chim Acta, 341*(2-3), 105-120.

Heien, M. L. A. V., Johnson, M. A., & Wightman, R. M. (2004). Resolving neurotransmitters detected by fast-scan cyclic voltammetry. *Anal Chem, 76*(19), 5697-5704.

Heien, M. L. A. V., Khan, A. S., Ariansen, J. L., Cheer, J. F., Phillips, P. E. M., Wassum, K. M., et al. (2005). Real-time measurement of dopamine fluctuations after cocaine in the brain of behaving rats. *P Natl Acad Sci USA, 102*(29), 10023-10028.

Johnson, J. A., Rodeberg, N. T., & Wightman, R. M. (2016a). Failure of Standard Training Sets in the Analysis of Fast-Scan Cyclic Voltammetry Data. *ACS Chem Neurosci, 7*(3), 349-359.

Johnson, J. A., Rodeberg, N. T., & Wightman, R. M. (2016b). Failure of Standard Training Sets in the Analysis of Fast-Scan Cyclic Voltammetry Data. *Acs Chem Neurosci, 7*(3), 349-359.

Keithley, R. B., Carelli, R. M., & Wightman, R. M. (2010). Rank estimation and the multivariate analysis of in vivo fast-scan cyclic voltammetric data. *Anal Chem, 82*(13), 5541-5551.

Keithley, R. B., Heien, M. L., & Wightman, R. M. (2009). Multivariate concentration determination using principal component regression with residual analysis. *Trac-Trend Anal Chem, 28*(9), 1127-1136.

Keithley, R. B., & Wightman, R. M. (2011). Assessing Principal Component Regression Prediction of Neurochemicals Detected with Fast-Scan Cyclic Voltammetry. *Acs Chem Neurosci, 2*(9), 514-525.

Kramer, R. (1998). *Chemometric Techniques for Quantitative Analysis*. New York, NY: Marcel Dekker, Inc.

Lavine, B. K., & Workman, J. (2013). Chemometrics. *Anal Chem, 85*(2), 705-714.

Maeder, M. (1987). Evolving Factor-Analysis for the Resolution of Overlapping Chromatographic Peaks. *Anal Chem, 59*(3), 527-530.

Malik, A., & Tauler, R. (2016). Ambiguities in Multivariate Curve Resolution. In C. Ruckebusch (Ed.), *Resolving Spectral Mixtures: With Applications from Ultrafast Time-Resolved Spectroscopy to Super-Resolution Imaging* (1st ed., Vol. 30). Amsterdam: Elsevier.

Malinowski, E. R. (1989). Statistical F-tests for abstract factor analysis and target testing. *J Chemometr, 3*(1), 49-60.

Malinowski, E. R. (1999). Abstract factor analysis of data with multiple sources of error and a modified Faber-Kowalski F-test. *J Chemometr, 13*(2), 69-81.

Manne, R. (1995). On the Resolution Problem in Hyphenated Chromatography. *Chemometrics and Intelligent Laboratory Systems, 27*(1), 89-94.

Olivieri, A. C. (2008). Analytical advantages of multivariate data processing. One, two, three, infinity? *Anal Chem, 80*(15), 5713-5720.

Olivieri, A. C. (2014). Analytical Figures of Merit: From Univariate to Multiway Calibration. *Chem Rev, 114*(10), 5358-5378.

Pere-Trepat, E., Hildebrandt, A., Barcelo, D., Lacorte, S., & Tauler, R. (2004). Fast chromatography of complex biocide mixtures using diode array detection and multivariate curve resolution. *Chemometrics and Intelligent Laboratory Systems, 74*(2), 293-303.

Pere-Trepat, E., Lacorte, S., & Tauler, R. (2005). Solving liquid chromatography mass spectrometry coelution problems in the analysis of environmental samples by multivariate curve resolution. *J Chromatogr A, 1096*(1-2), 111-122.

Rodeberg, N. T., Johnson, J. A., Cameron, C. M., Saddoris, M. P., Carelli, R. M., & Wightman, R. M. (2015). Construction of Training Sets for Valid Calibration of in Vivo Cyclic Voltammetric Data by Principal Component Analysis. *Anal Chem, 87*(22), 11484-11491.

Rodeberg, N. T., Sandberg, S. G., Johnson, J. A., Phillips, P. E. M., & Wightman, R. M. (2017). Hitchhiker's Guide to Voltammetry: Acute and Chronic Electrodes for in Vivo Fast-Scan Cyclic Voltammetry. *Acs Chem Neurosci, 8*(2), 221-234.

Sanchez, F. C., Toft, J., vandenBogaert, B., & Massart, D. L. (1996). Orthogonal projection approach applied to peak purity assessment. *Anal Chem, 68*(1), 79-85.

Sinanian, M. M., Cook, D. W., Rutan, S. C., & Wijesinghe, D. S. (2016). Multivariate Curve Resolution-Alternating Least Squares Analysis of High-Resolution Liquid Chromatography-Mass Spectrometry Data. *Anal Chem, 88*(22), 11092-11099.

Smilde, A. K., Hoefsloot, H. C. J., Kiers, H. A. L., Bijlsma, S., & Boelens, H. F. M. (2001). Sufficient conditions for unique solutions within a certain class of curve resolution models. *J Chemometr, 15*(4), 405-411.

Tauler, P., & Casassas, E. (1989). Application of Principal Component Analysis to the Study of Multiple Equilibria Systems - Study of Copper(Ii) Salicylate Monoethanolamine, Diethanolamine and Triethanolamine Systems. *Anal Chim Acta, 223*(1), 257-268.

Tauler, R., Casassas, E., & Izquierdoridorsa, A. (1991). Self-Modeling Curve Resolution in Studies of Spectrometric Titrations of Multi-Equilibria Systems by Factor-Analysis. *Anal Chim Acta, 248*(2), 447-458.

Tauler, R., Izquierdoridorsa, A., & Casassas, E. (1993a). Simultaneous Analysis of Several Spectroscopic Titrations with Self-Modeling Curve Resolution. *Chemometrics and Intelligent Laboratory Systems, 18*(3), 293-300.

Tauler, R., Izquierdoridorsa, A., Gargallo, R., & Casassas, E. (1995a). Application of a New Multivariate Curve Resolution Procedure to the Simultaneous Analysis of Several Spectroscopic Titrations of the Copper(Ii)-Polyinosinic Acid System. *Chemometrics and Intelligent Laboratory Systems, 27*(2), 163-174.

Tauler, R., Kowalski, B., & Fleming, S. (1993b). Multivariate Curve Resolution Applied to Spectral Data from Multiple Runs of an Industrial-Process. *Anal Chem, 65*(15), 2040-2047.

Tauler, R., Smilde, A., & Kowalski, B. (1995b). Selectivity, Local Rank, 3-Way Data-Analysis and Ambiguity in Multivariate Curve Resolution. *J Chemometr, 9*(1), 31-58.

Torres, M., Diaz-Cruz, J. M., Arino, C., Grabaric, B. S., Tauler, R., & Esteban, M. (1998). Multivariate curve resolution analysis of voltammetric data obtained at different time windows: study of the system Cd2+-nitrilotriacetic acid. *Anal Chim Acta, 371*(1), 23-37.

Van Benthem, M. H., Keenan, M. R., & Haaland, D. M. (2002). Application of equality constraints on variables during alternating least squares procedures. *J Chemometr, 16*(12), 613-622.

Vivo-Truyols, G., Torres-Lapasio, J. R., Garcia-Alvarez-Coque, M. C., & Schoenmakers, P. J. (2007). Towards unsupervised analysis of second-order chromatographic data: Automated selection of number of components in multivariate curve-resolution methods. *J Chromatogr A, 1158*(1-2), 258-272.

Wang, Y. D., & Kowalski, B. R. (1992). Calibration Transfer and Measurement Stability of near-Infrared Spectrometers. *Appl Spectrosc, 46*(5), 764-771.

Wasim, M., & Brereton, R. G. (2004). Determination of the number of significant components in liquid chromatography nuclear magnetic resonance spectroscopy. *Chemometrics and Intelligent Laboratory Systems, 72*(2), 133-151.

Woody, N. A., Feudale, R. N., Myles, A. J., & Brown, S. D. (2004). Transfer of multivariate calibrations between four near-infrared spectrometers using orthogonal signal correction. *Anal Chem, 76*(9), 2595-2600.

CHAPTER 4: REMOVAL OF DIFFERENTIAL CAPACITIVE INTERFERENCES IN FAST-SCAN CYCLIC VOLTAMMETRY[2]

INTRODUCTION

Electrochemistry provides a method for the real-time *in vivo* detection of redox-active neurotransmitters. Refinement of voltammetry for this purpose has enabled evaluation of their localized concentration dynamics in awake and behaving animals.(Bucher & Wightman, 2015; Dankoski et al., 2014; Fox et al., 2016; Owesson-White et al., 2016; Phillips et al., 2003) Cyclic voltammograms allow assignment of the signals to specific neurotransmitters, and thus permit selective tracking in the complex extracellular environment. However, compared to amperometric techniques, the use of voltammetry comes at the cost of sensitivity and time resolution.(Kawagoe & Wightman, 1994) To compensate, high scan rates are used (i.e. fast-scan cyclic voltammetry, or FSCV), which, while making *in vivo* detection practical, amplify other sources of current (e.g. the capacitive charging current and surface faradaic reactions).(Baur et al., 1988) These interferences dwarf the analytical signal and are one of the primary sources of noise.

For these reasons, FSCV data analysis typically employs digital subtraction of the background, using the current measured before the neurobiological phenomena of interest.(Howell et al., 1986) This method is effective for signal isolation given background stability. However, if neurotransmitter release is accompanied by factors that affect the background, the subtracted data contain artifacts. At the scan rates typically used (e.g. hundreds of volts per second), a significant double-layer charging current exists.(Bard & Faulkner, 2001) The magnitude and shape of this charging current, and the presence of any background faradaic current, strongly depends on the electrode material and its environment. Carbon fibers are the most common electrode material used for *in vivo* voltammetry.(Zachek et al., 2008) These

---

[2] This chapter previously appeared as an article in Analytical Chemistry. The original citation is as follows: Johnson, J.A.; Hobbs, C.N..; Wightman, R.M. "Removal of Differential Capacitive Interferences in Fast-Scan Cyclic Voltammetry," *Anal Chem.* Just Accepted.

fibers are known to have a diverse array of surface functional groups, particularly oxygen-containing ones.(McCreery, 2008) These moieties are critical in determining the electrode responses seen in FSCV (i.e. capacitive behavior, electrocatalytic properties, and adsorption).(Bath et al., 2000; Heien et al., 2003; Takmakov et al., 2010b) Further, a subset is known to be electroactive, generating peaks in the background voltammograms.(Jones et al., 1994; Kawagoe et al., 1993; Runnels et al., 1999; Takmakov et al., 2010a) Interactions with the carbon surface, through either adsorption or involvement in surface reactions, may alter these responses and contribute to the background-subtracted voltammograms. Indeed, non-faradaic and faradaic currents have been seen in background-subtracted voltammograms taken during pH changes, as H^+ plays a critical role in the redox reaction of surface-bound, quinone-like species and appears to alter the double layer.(Dengler et al., 2015; Kawagoe, et al., 1993; Runnels, et al., 1999; Takmakov, et al., 2010a) Additionally, an array of non-electroactive species, including metal cations (e.g. Ca^{2+}) and organic molecules, have been shown to adsorb to carbon microelectrodes, generating signals attributable to double-layer alteration.(Bath, et al., 2000; Takmakov, et al., 2010a; Yoshimi & Weitemier, 2014) These latter signals are largely non-specific, limiting their analytical utility.

A number of methods have been explored to deal with these background currents with fast-scan voltammetric data analysis. Early attempts by Millar and colleagues relied on the use of alternative waveforms (multiple triangular cycles or sine waves) aimed at exploiting the differential response of faradaic and non-faradaic current to repeated sweep applications or voltage shifts.(Millar et al., 1992; Millar & Williams, 1990; Stamford et al., 1984) Later, Fourier domain analysis was attempted, relying on the unique spectral signatures of the non-faradaic current for its identification and removal.(Cullison & Kuhr, 1996; Long & Weber, 1992) Such approaches, while useful, typically required changes in the measurement protocol, complicating analysis of the voltammetric signal of interest. For direct analysis of multi-component FSCV data principal component regression has also been employed with incorporation of pH and background changes into the model to study dopamine concentration changes over extended time windows.(Keithley et al., 2009; Keithley & Wightman, 2011; Rodeberg et al., 2015) However, this approach requires consistency of signal shape over time and is poorly characterized for ionic interferences. More recently, Atcherley et al. have shown successful measurement of basal levels of dopamine using fast-scan controlled adsorption voltammetry, which relies on the use of previously

measured CVs in conjunction with convolution for minimization of the non-faradaic current.(Atcherley et al., 2013) Additionally, Yoshimi and Weitemier have also reported on the use of chronoamperometry to separate temporally the non-faradaic currents due to pH changes from the faradaic currents of dopamine oxidation.(Yoshimi & Weitemier, 2014)

Here, we build on this prior work to explore the origin of the background current seen at carbon-fiber microelectrodes and develop a novel method for its mitigation. First, the specific FSCV signals seen during local ion concentration changes (e.g. those of the major cations found in extracellular solutions and FSCV calibration buffers – K^+, Na^+, Ca^{2+}, and Mg^{2+}) are revisited. This information is used to build a model of the double layer that can qualitatively account for the observed CV shapes. Further, we introduce a procedure for the prediction and removal of the non-faradaic component of the background signal that does not require considerable changes to the measurement protocol. The method utilizes a similar approach as the one suggested by Yoshimi and Weitemier in which a small amplitude step is paired with each FSCV sweep. Here, this step is used to estimate the impulse response of the electrochemical cell prior to each measurement through differentiation of the step response. The impulse response estimate is then convoluted with the triangular sweep to generate a prediction of the non-faradaic charging current expected for the sweep application. Subtraction of the predicted charging current allows for removal of this component, diminishing artifacts that arise from changes in these contributions. This approach permits removal of some spurious signals, as will be shown for both *in vitro* and *in vivo* FSCV recordings.

EXPERIMENTAL SECTION

Instrumentation and Software. T-650 type, cylindrical carbon-fiber microelectrodes (Thornel, Amoco Corporation, Greenville, SC; pulled in glass capillaries and cut to 75-125 μm exposed lengths) were used in experimentation. After pulling, the seals of electrodes were dipped in epoxy (EPON Resin 828, Miller-Stephenson, Danbury, Connecticut) mixed with 14% w/w *m*-phenylenediamine (Sigma-Aldrich, St. Louis, MO) at 80°C, briefly washed with acetone, and heated at 100°C (5 hours) then 150°C (at least 12 hours).

Data was acquired with a commercial interface (PCI-6052, 16 bit, National instruments, Austin TX) with a personal home computer and analyzed using locally constructed hardware and software written in LabVIEW (TarHeel CV – an earlier version used for simplicity of programmatic modification – and the more user-friendly HDCV, National Instruments, Austin, TX).(Bucher et al., 2013) Unless otherwise noted, triangular excursions of the potential were made at a scan rate of 400 V/s and repeated at a frequency of 10 Hz. Measurements were conducted inside a grounded Faraday cage to minimize electrical noise.

Electrochemical Experiments. Flow-injection analysis experiments were performed using a syringe pump (Harvard Apparatus, Holliston, MA) operated at 0.8 mL/min using PEEK tubing (Sigma-Aldrich) connected to a pneumatically controlled six-port injection valve (Rheodyne, Rohnert Park, CA). All solutions were prepared in either PBS (137 mM NaCl, 10 mM NaH_2PO_4, 2.7 mM KCl, and 2 mM $K_2H_2PO_4$) or TRIS buffer (2.0 mM Na_2SO_4, 1.25 mM $NaH_2PO_4 \cdot H_2O$, 140 mM NaCl, 3.25 KCl, 1.2 mM $CaCl_2 \cdot 2H_2O$, 1.2 mM $MgCl_2 \cdot 6H_2O$, and 15 mM Trizma HCl), adjusted to pH 7.4 with NaOH as necessary. Dopamine solutions were bubbled under nitrogen to prevent oxidative degradation prior to use. Electrochemical conditioning of the carbon fiber was achieved through repeated voltammetric sweeps to +1.3 V vs. Ag/AgCl to increase the surface concentration of bound oxides.(Heien, et al., 2003)

For convolution-based prediction, a waveform was created with a small amplitude pulse placed prior (i.e. 1-3 ms) to the triangular sweep. After measurements were complete, the data was analyzed in locally written software in LabView. The discrete derivative of the current response to the potential pulse was used to generate an estimate of the system impulse response, which was convoluted with the waveform to yield the background current prediction that was digitally subtracted from a given recording.(Bracewell, 2000) For color plots generation, digital background subtraction was performed using these prediction-subtracted backgrounds. To estimate electrode capacitances at specific potentials, small amplitude triangular waves were used. The capacitance was determined as

$$C = \frac{i_{av}}{v} = \frac{(i_a + i_c)/2}{v} \qquad \text{(Eq. 4.1)}$$

where C is the capacitance, i_{av} is the average current amplitude at the potential, v is the scan rate, and i_a and i_c are the current amplitude on the positive and negative sweeps, respectively.

In Vivo Measurements. Male Sprague-Dawley rats from Charles River (Wilmington, MA, USA) were pair-housed on a 12/12 h light/dark cycle. Animal procedures were approved by the UNC-Chapel Hill Institutional Animal Care and Use Committee (IACUC). For anesthetized experiments, rats (300-550 g) were injected with urethane (1.5 g/kg, i.p.) and placed in a stereotaxic frame. Holes were drilled in the skull for the working and reference, with an additional three holes for the delivery of pin pricks to induce spreading depression, using coordinates (relative to bregma) from the brain atlas of Paxinos and Watson.(Paxinos & Watson, 1998) The carbon-fiber microelectrode was placed in the nucleus accumbens at coordinates relative to bregma: anterior/posterior (AP) +2.2 mm, medial/lateral (ML) +1.7 mm, and dorsal/ventral (DV) -7.0 mm. The additional holes were located at: -0.8 AP, +0.8 ML; -0.8 AP, +3.2 ML; and -2.8 AP, +1.7 ML. A Ag/AgCl reference electrode was inserted in the contralateral hemisphere. For the recording presented, a pinprick was delivered using 27-G hypodermic needles at a depth of -7.5 DV approximately 2-3 mm from the recording site.

RESULTS AND DISCUSSION

Background Current and Ionic Interferences at Carbon-Fiber Microelectrodes

Metal Cation Sensitivity and Voltammetric Signals in PBS Buffer. As shown in Figure 4.1A, the background voltammetric signal seen at carbon fiber microelectrodes in PBS (-0.8 to +0.8 V vs Ag/AgCl) deviates from that expected for application of a triangular voltage ramp to an ideal RC circuit.(Bard & Faulkner, 2001) Peaks are seen around 0.0 and -0.3 V vs. Ag/AgCl on the positive and negative sweeps, respectively, which have been attributed to the two-electron, two-proton reaction of quinone-like moieties on the surface and match the location of peaks seen during an acidic pH change (Figure 4.1B).(Kawagoe, et al., 1993) Additionally, there is a sharp asymmetry in the impedance properties of the electrode between more positive (> 0.0 V) and negative potentials (< 0.0 V). With electrochemical conditioning, this asymmetry grows, with relatively large changes seen at only at negative potentials.
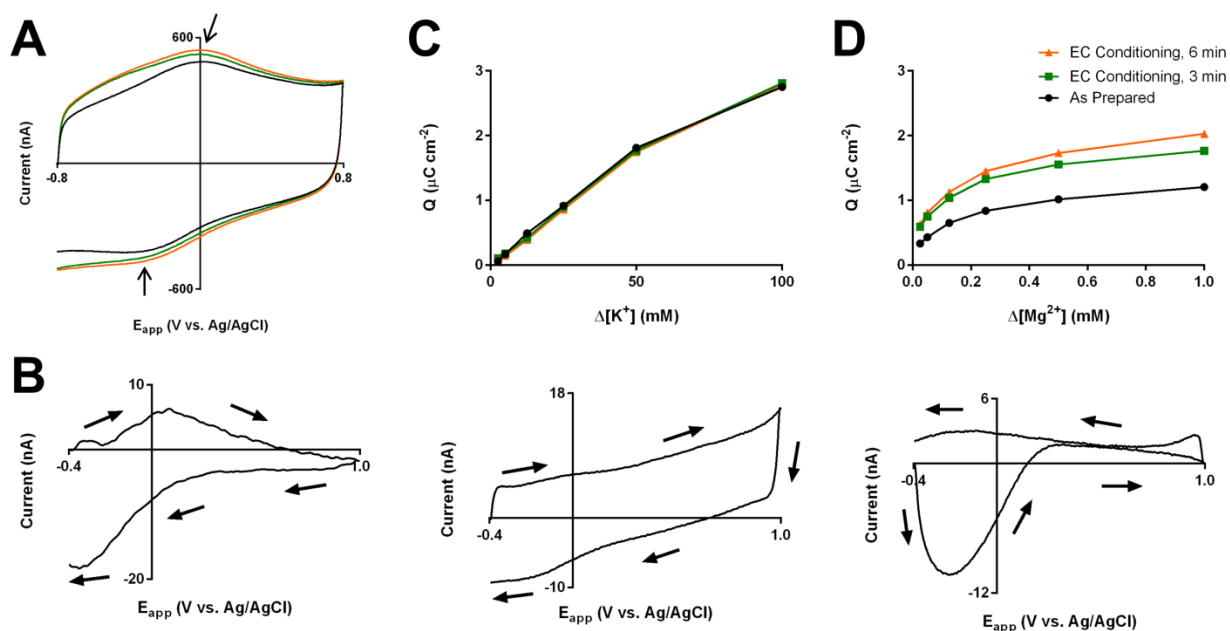
Figure 4.1. FSCV signals in the absence of analytes and during ionic concentration changes in phosphate-buffered saline. (A) Total background currents for as-prepared carbon fiber microelectrodes (black) and after electrochemical conditioning for 3 and 6 minutes (green and orange, respectively). Arrows indicate the location of the peaks referenced in the text. (B) Background-subtracted CV (-0.4-1.0 V vs Ag/AgCl, 400 V/s, 10 Hz) for acidic pH shift (-0.15 pH units from pH 7.4) (C) Adsorption curves (2.5-100 mM, top) at each conditioning time point and representative background-subtracted CV (100 mM, bottom) for potassium injections. (D) Adsorption curves (0.025-1.0 mM, top) at each oxidation time point and representative background-subtracted CV (1.0 mM, bottom) for magnesium injections.
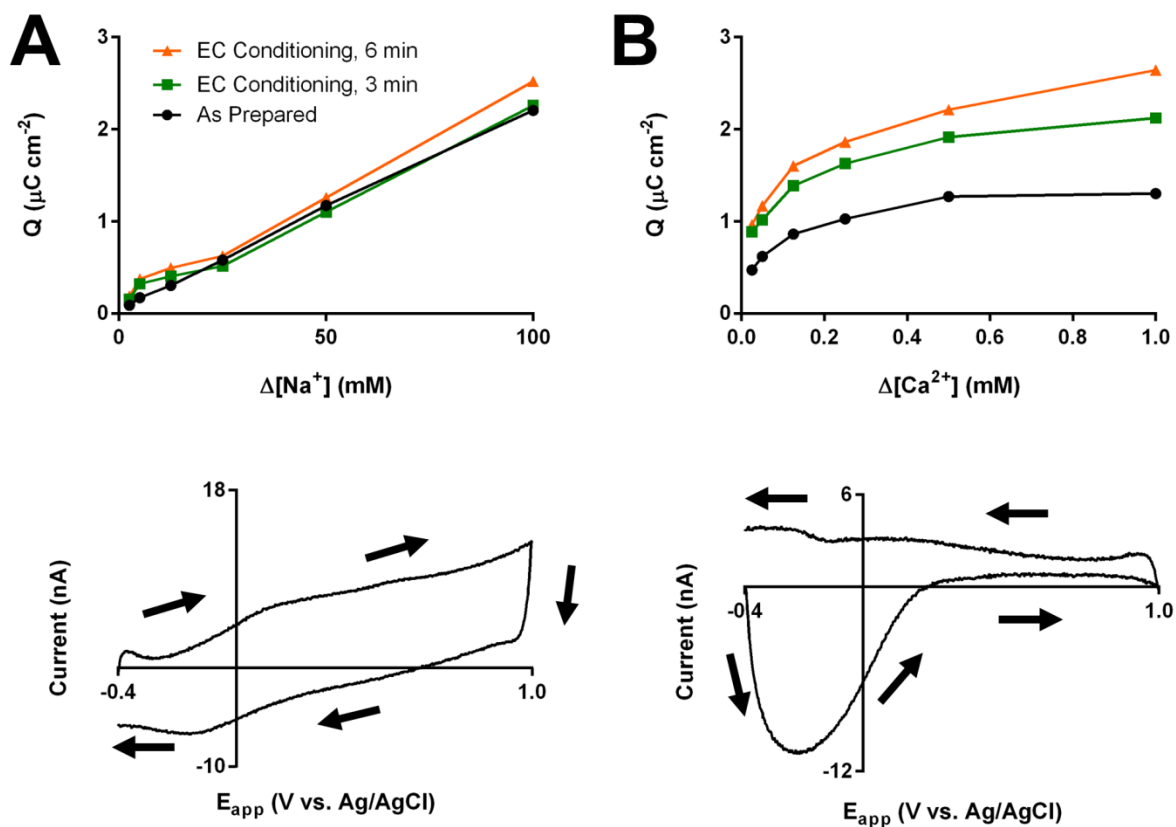
**Figure 4.2.** Background-subtracted FSCV signals for Na+ and Ca2+ concentration changes in phosphate-buffered saline. Adsorption curves (2.5-100 mM, top) for differing lengths of electrochemical conditioning (as prepared, black; 3-minute conditioning, green; 6-minute conditioning, orange) and representative background-subtracted CV (100 mM, bottom) for sodium injections (A) and calcium (B) injections.

Of interest, these changes with conditioning correspond with sensitivity changes to electrochemically inert ionic species, whose signals should originate solely from background considerations. After each conditioning interval (0, 3, and 6 minutes), background-subtracted cyclic voltammograms for concentration changes of KCl, NaCl, $MgCl_2$, and $CaCl_2$ were obtained (-0.4 to 1.0 V). In these data, a noticeable difference is seen between the responses seen with changes in pH (Figure 4.1B), other monovalent cations (Figure 4.1C and 4.2A, bottom), and divalent cations (Figure 4.1D and 4.2B, bottom). The origins of the peaks seen in the pH voltammogram have been extensively studied and are hypothesized to be primarily due to the direct participation of the hydrogen ion in the two-electron redox reaction of a quinone-like surface-confined moiety.(Dengler, et al., 2015; Karweik et al., 1985; Runnels, et al., 1999; Takmakov, et al., 2010a) The hydrogen ion's role in the surface faradaic reaction makes FSCV at carbon particularly sensitive to changes in its concentration (e.g. yielding a 4.6 μC cm^{-2} signal for a -0.15 pH shift, or $\Delta[H^+]$ = 16 nM, in Figure 4.1B). Other monovalent cations (i.e. K^+ and Na^+) gave background-subtracted signals similar to classical double-layer charging voltammograms at considerably higher concentrations (> 1 mM). Of note, an overall slope is seen in the background-subtracted voltammograms, suggesting a resistance change linked to the large ionic strength changes at the concentrations studied. Finally, divalent cations give oxidation-responsive voltammetric signals that are prevalent at negative potentials and evoked at considerably lower concentrations (μM vs mM). These signals, which give negative peaks in the background-subtracted voltammograms, indicate a decrease in capacitance, which has previously been attributed to displacement of charge in the double layer by the divalent cation.(Takmakov, et al., 2010a) Integration of the absolute current values across the entire voltammograms yield adsorption curves that are linear for non-hydrogen monovalent cations and curved for the divalent cations.

This behavior corresponds to the well-documented ion exchange capabilities of these ions. At cation exchange resins, monovalent cations are known to have weaker interactions than divalent cations (with ~1-2 fold lower selectivity coefficients), leading to the former's displacement by the latter.(Fritz & Gjerde, 2000; Haddad & Jackson, 1990; Walton, 1992) Here, injections of the divalent cations likely lead to ion exchange with the ambient monovalent cations at a surface functionality. Monovalent ion concentration changes, on the other hand, lead to minimal displacement of the ambient ions and require

much higher concentrations to produce effects. This ion exchange functionality appears to be redox-active, giving the potential-dependence in the divalent voltammograms. Given the coincidence of potentials of the decay in the divalent voltammograms and the quinone-like faradaic peak, , the working hypothesis is that the surface-bound, quinone-like species (or one with overlapping electrochemical behavior) has considerably different binding affinities for cations in the oxidized and reduced state. Indeed, quinone-containing species have been shown to have such redox-dependent metal cation affinities.(Y. J. Kim et al., 2014; Lee et al., 2006)

To develop this further, a model was developed to simulate the expected current to a voltammetric sweep, given a surface-bound species that undergoes a reversible redox reaction and holds more charge to the surface, and thus exhibits a higher capacitance, in its reduced state (Appendix 4.1). In this framework, the double layer (in the absence of electroactive compounds in solution) is treated as a network consisting of a voltage-dependent impedance element (Z_{QH}, representing the quinone-like redox reaction and having a Nerstian relation to potential) and two capacitors (all in series to R_s, the solution resistance). The first capacitor (C_{QH}^*) represents the double-layer capacitance at the quinone-like surface sites. . This area-normalized redox-coupled capacitance is assumed to be a linear function of the concentration of the reduced surface species ($C_{QH}(\Gamma_{QH}(E))$). The second capacitor (C_I) is the remaining double-layer capacitance (representing the rest of the surface), which is treated as voltage-independent. Of note, such a model can qualitatively account for the shape of the background-subtracted voltammograms seen with local concentration changes in cations, as well as the background voltammograms seen at carbon fibers .

Metal Cation Sensitivity and Voltammetric Signals in TRIS Buffer. To explore this further in a medium more closely resembling the in vivo environment, the responses to these ionic species were also investigated in TRIS buffer, which contains ambient levels of all cations studied (145 mM Na+, 3.25 mM K+, 1.2 mM Ca2+, and 1.2 mM Mg2+). Additionally, some of the electrochemically inert tris(hydroxymethyl)aminomethane (TRIS) is positively charged at the pH studied here (7.4) and has previously been shown to interfere with pH detection, suggesting some interaction with the quinone-like moiety. There is then expected to be considerable occupation of the binding sites prior to changes in local
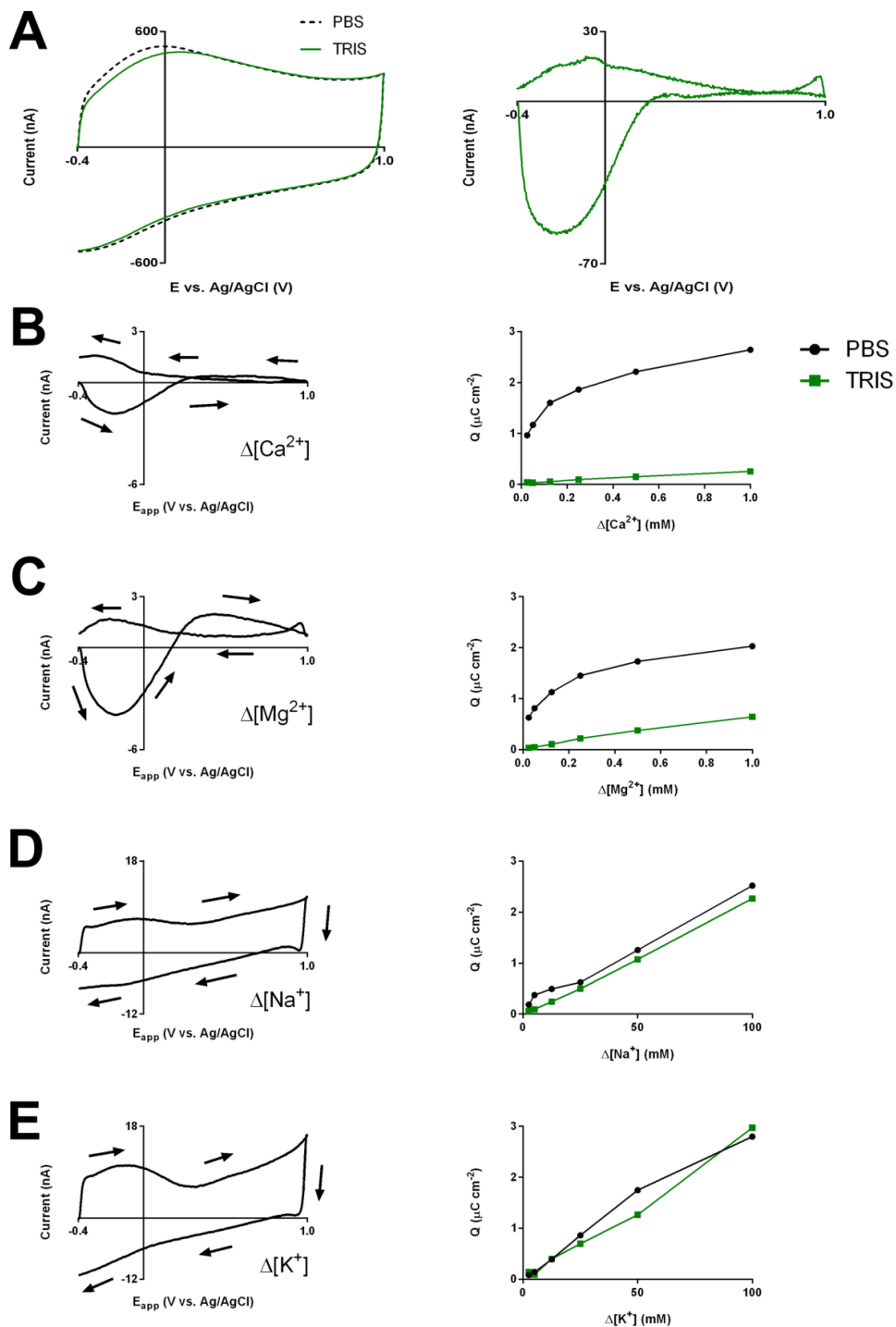
Figure 4.3. FSCV signals seen during ionic concentration changes in TRIS buffer. (A) Background CVs (left, -0.4-1.0 V vs Ag/AgCl, 400 V/s, 10 Hz) in PBS (dashed black) and after injection of TRIS buffer (green), as well as the background-subtracted CV (right, TRIS-PBS). (B-E) Representative background-subtracted CVs (left) and adsorption curves (right, obtained from integration of full CV; black – PBS, green - TRIS) for Ca^{2+} (B), Mg^{2+} (C), Na^+ (D), and K^+ (E). The PBS data is that from Figures 1 and S-1 for the 6-minute conditioning time points.

concentration of ionic species. Supporting this hypothesis, injections of TRIS buffer for an electrode in PBS (both at pH 7.4) show significant changes mainly in the negative region and give a divalent cation-like background-subtracted voltammogram (Figure 4.3A).

Representative background-subtracted voltammograms and full voltammogram adsorption curves are shown in Figure 4.3B-E. As compared to those in PBS, the divalent cation responses are considerably attenuated, as expected, given the ambient competition for the binding sites. In comparison, the monovalent cations give intermediate-type signals, with behavior consistent to that seen in PBS but with increased complexity around the quinone-governed region, which is more pronounced for K^+ than for Na^+. However, this may be due ambient additional species available for ion exchange.

Convolution-Based Prediction of Non-Faradaic Current

As discussed previously, there has been considerable work done towards the minimization of these background currents and interferences. Here, we build on these approaches to develop a novel method for removal of non-faradaic current from FSCV recordings while retaining much of the general measurement protocol. Previously, chronoamperometry was shown to allow separation of the non-faradaic current due to pH changes from the faradaic current of dopamine oxidation, and it was suggested that the alternation between chronoamperometry and FSCV during recording sessions would prove advantageous.(Yoshimi & Weitemier, 2014) We explored the hypothesis that the step response measured in chronoamperometry, which probes the impedance characteristics of the electrochemical cell, could be used to predict directly the non-faradaic current seen for the triangular sweep application. To do this, the cell was considered to be a linear system, and we predicted its response for a given excitation waveform with its impulse response (i.e. the system response to a unit impulse).(Atcherley, et al., 2013; Bracewell, 2000; Manolakis & Ingle, 2011) The output (y) for an arbitrary input signal (x) is given through convolution with the impulse response (h):

$$y(t) = h(t) * x(t) \qquad \text{(Eq. 4.2)}$$

The current during voltage steps can be used to arrive at suitable estimates of the impulse response, as
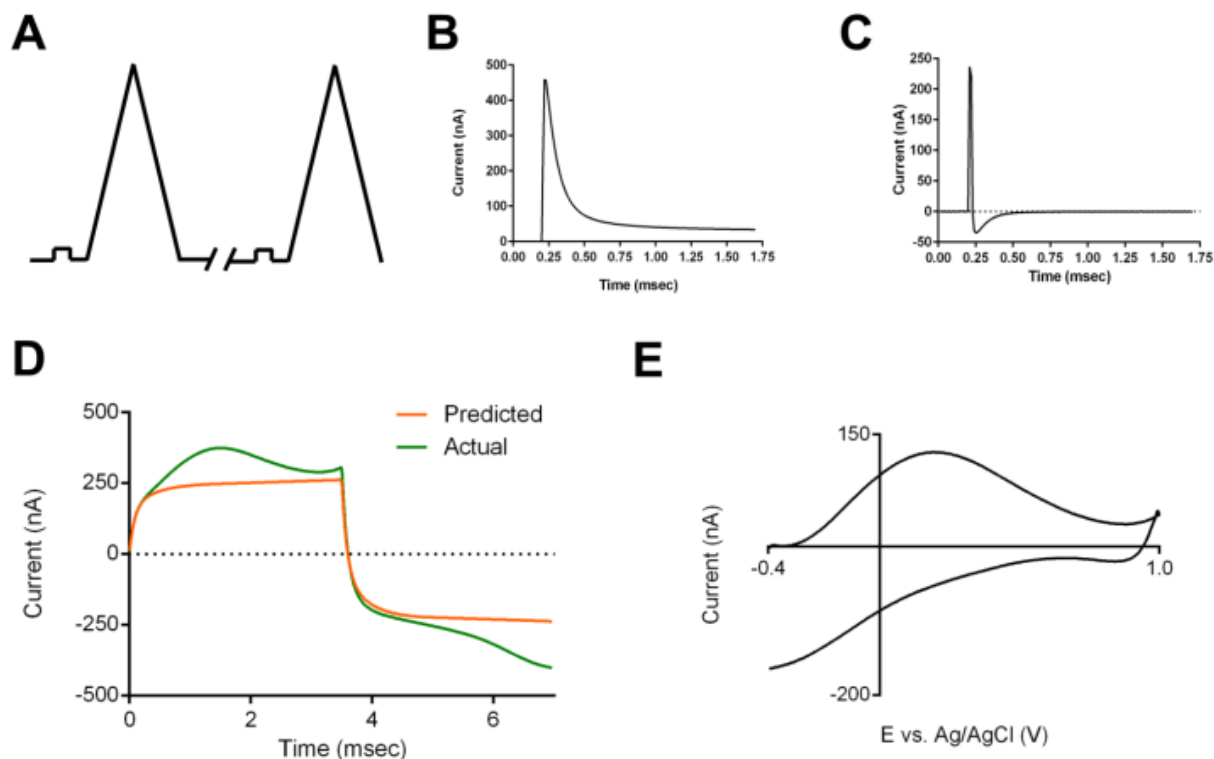
Figure 4.4. Convolution-based approach for removal of ionic artifacts. (A) Waveform used for measurements with a small-amplitude pre-pulse placed in front of every FSCV sweep. (B) Typical step response measured at carbon-fiber microelectrode. (C) Typical impulse response estimate obtained from the discrete differentiation of the step response in (B). (D) Figure showing a measured background current (green) and the corresponding prediction (orange) generated using convolution of the impulse estimate in (C) with the FSCV waveform. (E) Residual current after subtraction of the prediction for the data shown in (D).

the derivative of the current response to the step provides an estimate of the impulse function.(Chang &
Park, 2010; Kawagoe & Wightman, 1994)

This approach requires the use of a pulse immediately before every FSCV sweep to account for
changes that may occur between sweeps (Figure 4.4A). The current response (Figure 4.4B) to the step
provides information on the impedance before each measurement. Due to the small amplitude of the
potential step, the current response should be largely determined by the non-faradaic characteristics of
the electrochemical cell assuming appropriate choice of voltage range.(Bard & Faulkner, 2001) This
information is then used offline to predict the current response to the triangular FSCV sweep. Discrete
differentiation of each step response is used to estimate the cell's impulse response (Figure 4.4C), and
this is convoluted with the FSCV waveform to generate the prediction of the non-faradaic response
(Figure 4.4D). In practice, even in the absence of electroactive species, residual current remains (Figure
4.4E, approximately 20% of the total background current). Evidence of a faradaic surface species is seen
(matching background peaks previously assigned to the redox reaction of quinone-like moieties), as well
as some unexplained current at positive potentials. However, these prediction-subtracted total
voltammograms can be used with digital background subtraction to generate background-subtracted
voltammograms with attenuated non-faradaic interferences.

Convolution-Based Removal of Ionic Signals

In Vitro Separation of Ionic and Dopamine Voltammetric Signals. The convolution procedure is
appropriate for linear systems and assumes the impedance is independent of potentials. Thus, this
technique should work well for removal of currents where the main interaction is with the voltage-
independent capacitance, like for those of the monovalent cations described above. To test this
hypothesis, the flow-injection analysis of dopamine, sodium, and their mixture in TRIS buffer was
performed using a waveform with a voltage step from -0.5 to -0.4 V vs Ag/AgCl (Figure 4.5A-C). The
method, while not drastically altering the shape of the pure dopamine voltammogram (Figure 4.5A), can
successfully remove contributions to the current at the dopamine oxidation potential from an injection of
TRIS buffer spiked with 100 mM sodium (Figure 4.5B). This allows removal of the bulk of the sodium
signal in the analysis of the dopamine-sodium mixture, permitting the use of the dopamine oxidation
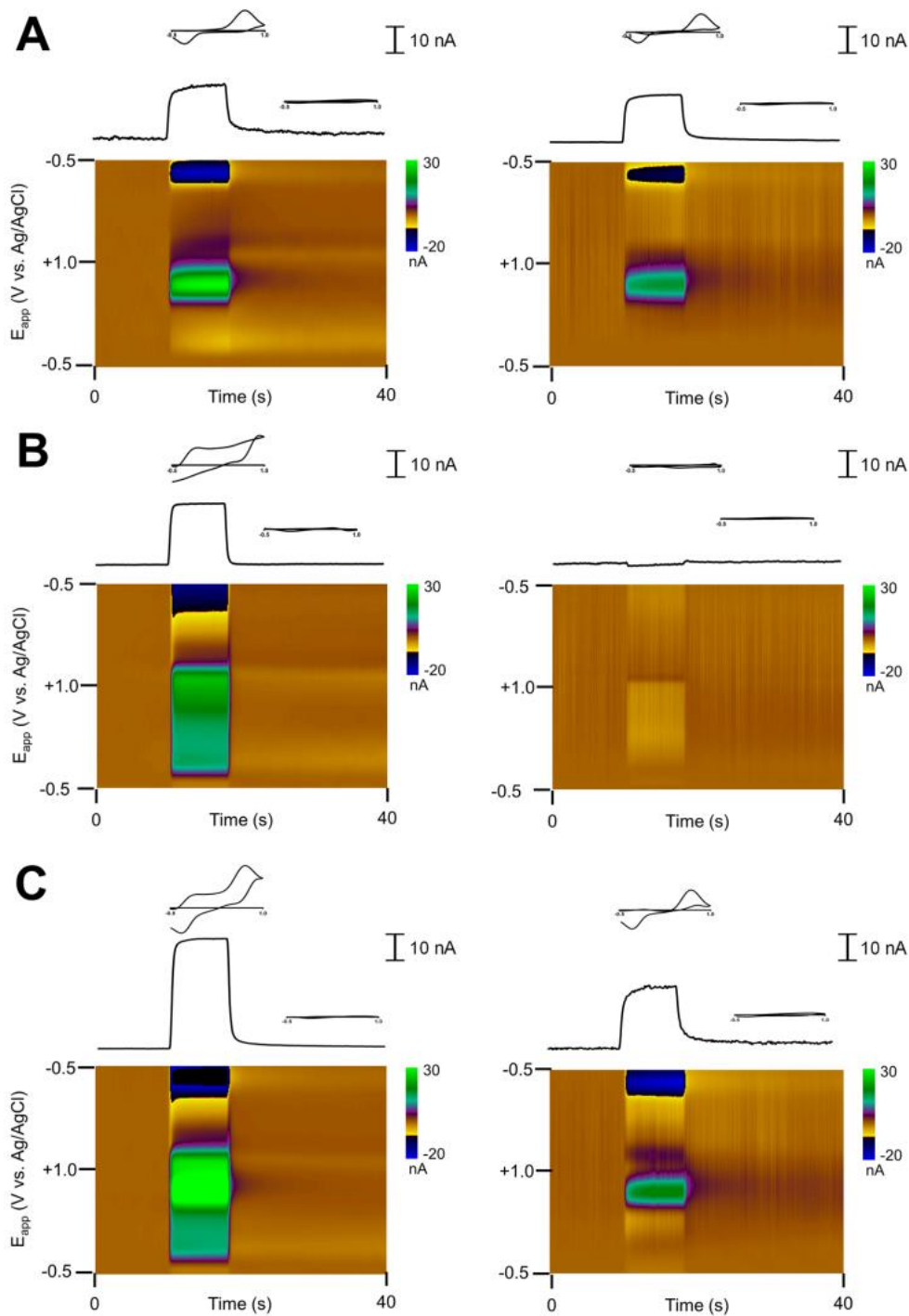
Figure 4.5. Removal of artifacts arising from Na⁺ concentration changes in TRIS buffer. Data before (left) and after (right) the convolution-based treatment for an injection of a DA (A, Δ[Na] = 1 μM) and NaCl-spiked solution (B, Δ[Na] = 100 mM) and their mixture (C), showing background-subtracted color plots (bottom) and the current-time traces at the dopamine oxidation potential (top) with cyclic voltammograms taken during and after the injection positioned above.

potential as a direct marker of dopamine concentration in a mixture of dopamine and sodium (Figure 4.5C). Note that, due to their non-linear responses, neither the quinone-like peaks nor the divalent cation signals, can be removed in this way. Further, the potentials where the quinone-like moiety redox reaction occurs should not be used for this method, as use of this information would lead to inaccurate predictions.

In Vivo Analysis of Dopamine during Spreading Depression. Spreading depression is a neurobiological phenomenon in which there is a mass depolarization of neurons, leading to a considerable shift in the ionic balance between the intracellular and extracellular spaces.(Kraig & Nicholson, 1978; Nicholson et al., 1978; Rogers et al., 2013) Millimolar changes in the concentrations of common extracellular ions (e.g. $\sim$100 mM K^+, $\sim$33 mM Na^+, and $\sim$1.5 mM Ca^{2+}), along with the concomitant release of neurotransmitters (e.g. dopamine), are expected. However, attempts to track the dopamine release using FSCV are confounded by the ionic shifts, which produce large capacitive artifacts in the obtained CVs (Figure 4.6A, -0.4 to 1.3 V), which resemble those seen for changes in the voltage-independent capacitance and local resistance.

Using the convolution-based procedure, the capacitive artifacts are removed to obtain a cleaner picture of the dopamine changes over time (Figure 4.6B). Examination of the CVs before and after correction (bottom) reveals the method successfully removes strong artifacts around the switching potential, as well as removing considerable current across the potential window. Note also that there remains a slight artifact on the negative sweep; this is attributed to differences in the impedance characteristics across the potential window. However, the artifact is considerably smaller than prior to correction. Thus, analysis of the time course of dopamine release has been considerably simplified with such an approach.

In Vitro Flow-Injection Analysis of Dopamine. As noted earlier, adsorption of organic species can also lead to capacitive artifacts. Of interest, these are seen during flow-injection experiments of dopamine, particularly at high concentration, including in recordings of dopamine during the earlier oxidation experiment (Figure 4.7). Dopamine adsorption to carbon surfaces is well characterized and has been

98
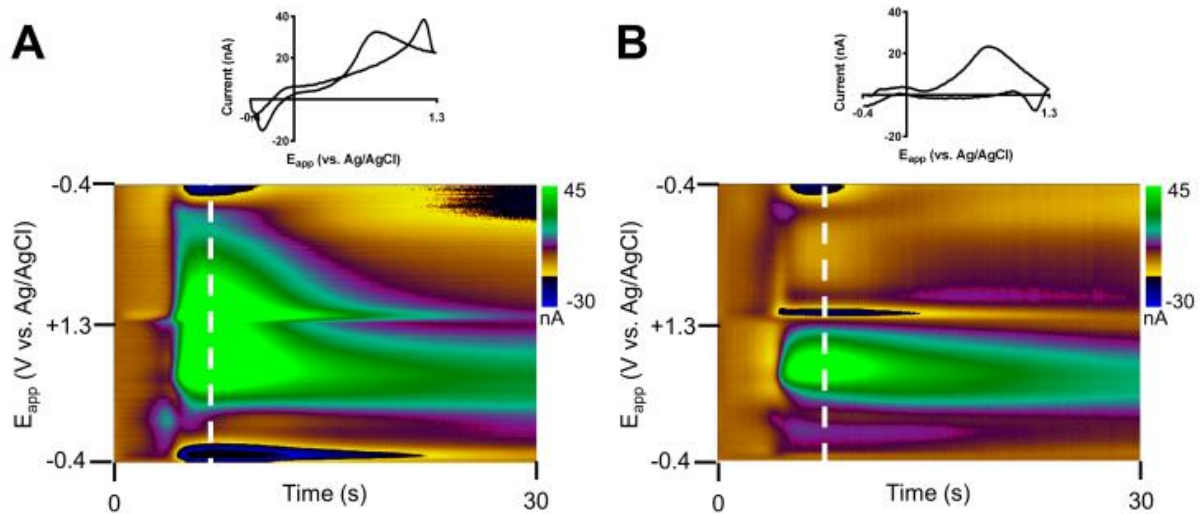
Figure 4.6. *In vivo* analysis of supraphysiological release of neurotransmitters during a spreading depression event using the convolution-based method. (A) Uncorrected background-subtracted color plot (top) and cyclic voltammogram (bottom) at 7 s into the recording. (B) Same color plot (top) and cyclic voltammogram (after) use of the convolution-based method for removal of capacitive artifacts. Note that the step portion of the waveform is not shown in the color plots. A single pinprick (-7.5 DV, 2-3 mm away from the recording site) was delivered prior to this recording.
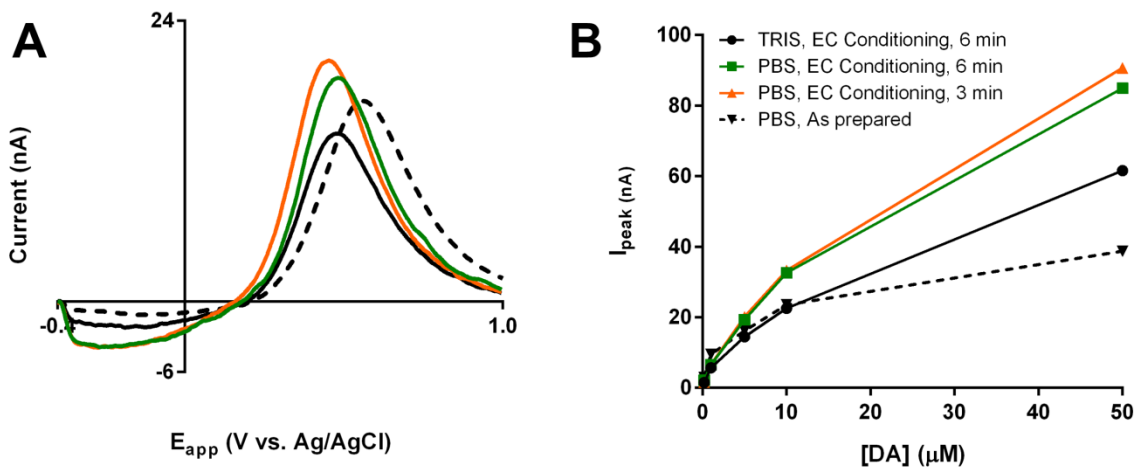
Figure 4.7. Background-subtracted FSCV signals for dopamine concentration changes in PBS and TRIS buffer. Representative background-subtracted CVs (A, 500 nM, forward sweep only) and adsorption curves (B) for dopamine injections for as-prepared (solid black) and after 3 and 6 minutes of electrochemical conditioning (green and orange, respectively) in PBS and subsequent change to TRIS buffer (dashed black).
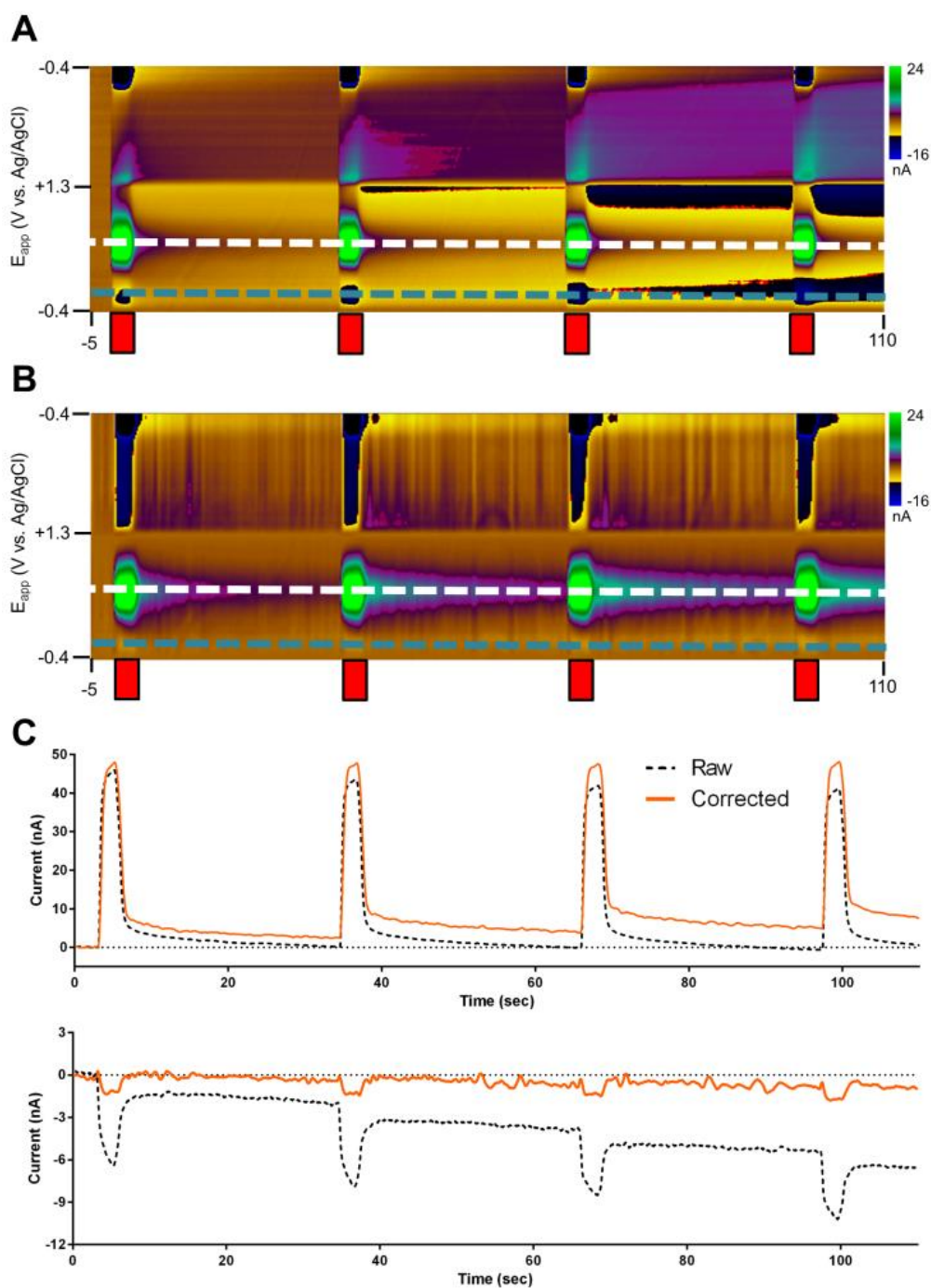
Figure 4.8. Convolution-based correction of flow-cell analysis of dopamine in PBS buffer. Dopamine (250 nM) was injected every 30 seconds (red bars). (A) Uncorrected and (B) corrected background-subtracted color plots. (C) The current at the dopamine oxidation potential (white dashed lines) and capacitive interferent potential (blue dashed lines).

shown to underlie the sensitivity of FSCV at carbon-fiber microelectrodes towards catecholamines..(Bath, et al., 2000; Heien, et al., 2003) Of note, these artifacts are more prevalent in the negative region of the potential window, suggesting these originate from interactions similar to the divalent cations shown earlier. Interestingly, it has been previously reported that the presence of calcium and magnesium decrease the sensitivity of FSCV towards dopamine.(Kume-Kick & Rice, 1998) Here, in their presence (i.e. in TRIS buffer), the absorption capacity and the intensity of the artifact are indeed decreased, suggesting that adsorption competition for the quinone-like moiety may underlie these effects.

The convolution-based technique was applied to mitigate the effects of these artifacts for an extended recording of multiple, closely spaced injections of dopamine boluses at a carbon-fiber electrode (Figure 4.8A) in PBS buffer. With a single background subtraction for this time window, distortions appear over time, both during the dopamine injections and during later measurement times. However, without correction for these contributions, the use of the dopamine peak oxidation potential as an indicator of concentration would suggest that the electrode sensitivity is decreasing over time (Figure 4.8C, top), while there is a change in the baseline dopamine current over time.

These capacitive artifacts, particularly those on the positive sweep, are removed from the data using the convolution-based procedure (Figure 4.8B). In the corrected data, the peak current during dopamine injections does not show evidence of baseline drift, and the peak current shows no significant differences between subsequent injections (Figure 4.8C, top). This is supported by analysis of the current at -0.3 V vs. Ag/AgCl on the positive sweep (Figure 4.8C, bottom), where the current is largely determined by capacitive effects.

Overall, these results suggest that the increases in dopamine concentration were leading to capacitive changes at the electrode, which is expected at the large (by physiological standards) concentrations used in the experiment (250 nM). Additionally, due to the slow desorption kinetics of dopamine and the short injection spacing, there was insufficient time for complete desorption of dopamine between injections.(Bath, et al., 2000; Venton et al., 2002) This would lead to a build-up of surface concentration and a steady drift in the capacitive characteristics throughout the recording window, an insight that would be difficult to reveal without the convolution-based approach.
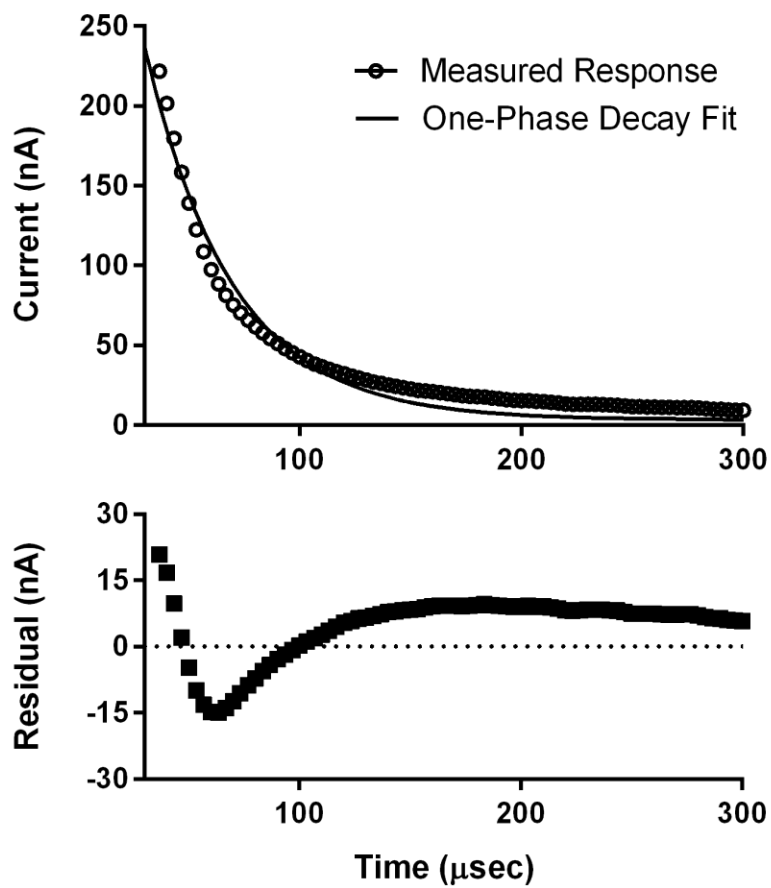
Figure 4.9. Results of one-phase exponential decay fit to current response to 40 mV voltage step at carbon-fiber microelectrode. (A) Measured response (empty circles) and exponential fit (line, RC = 39.2 μs) with residual plot (below).
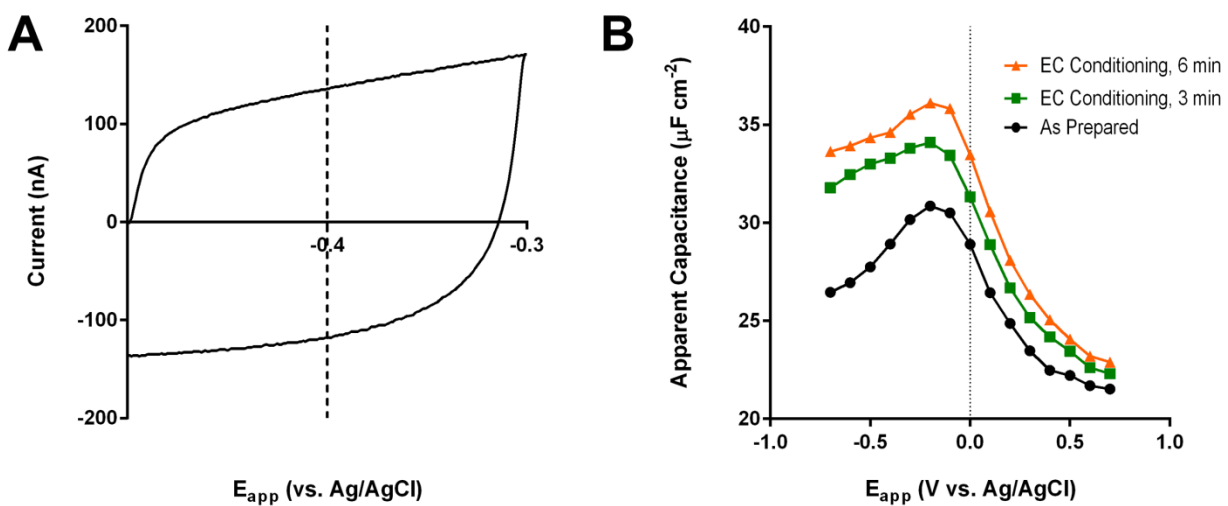
Figure 4.10. Voltage-dependent psuedocapacitance determined from small amplitude CVs. (A) Example of small amplitude (200 mV, 200 V/s) anodic CV used to determine pseudocapacitance, done by averaging the absolute values of the two current measurements at a center potential (shown by dashed line) and dividing by scan rate. (B) Pseudocapacitance measurements for as-prepared carbon fiber microelectrodes (black) and after electrochemical conditioning for 3 and 6 minutes (green and orange, respectively).

Optimization and Validation of Convolution-Based Approach

Optimization of Measurement Parameters. The idealized response to the application of a voltage step is a single-order exponential curve.(Bard & Faulkner, 2001) At carbon-fiber microelectrodes, an exponential-like decay is observed. However, it appears to be multi-order (Figure 4.9), with an extracted single-order time constant about an order of magnitude larger than that expected for a cylindrical carbon electrode in aqueous solutions (RC = 39.2 vs. 4.5 μs,).(Michael & Wightman, 1996; Wightman & Wipf, 1989) While not characterized further, this may be due to non-ideal impedance behavior (including the effects of the microstructure and internal resistance of the carbon fiber)(C.-H. Kim et al., 2003; Lambie et al., 2007) or stray impedance contributions from the instrumentation. Of note, cyclic voltammetric pseudocapacitance measurements (Figure 4.10) reveal a distribution of apparent capacitances in the range of 20-40 μF cm^{-2}, close to that reported for edge-plane carbon (although these measurements have clear Faradic contributions, likely from the quinone-like moiety), suggesting that this is not the source of the non-ideality.(McCreery, 2008) However, despite the departure from idealized responses, the convolution-based approach is nevertheless effective.

Of interest here, however, is the effect of the measurement parameters (i.e. step height and step width). The convolution theorem states that the time domain convolution is equivalent to pointwise multiplication in the frequency domain.(Manolakis & Ingle, 2011) Therefore, insight can be gained through analysis of the collected data in both the time and Fourier domains (Figure 4.11).

Concerning step height, smaller perturbations are preferred, as they probe the impedance characteristics of the electrochemical cell with minimal perturbation. However, the effect of noise needs to be considered, as the discrete derivative is a high-pass filter. This becomes important when considering that FSCV waveforms are typically low-pass filtered (most often with a cut-off frequency of 2 kHz). Such filtering distorts rapid potential changes, and higher cut-off frequencies are required (increasing noise in the data).(Keithley et al., 2011) As such, a trade-off exists – larger pulses improve signal-to-noise while perturbing the system more and requiring stronger consideration of the instrumentation used. Here, we consider the practical implications for the instrumentation (described in Reference 47) common for *in vivo* FSCV. Figure S-7 shows the current responses in PBS for applications of voltage steps between 20 and 200 mV, as well as the resulting impulse response estimations in the time and frequency domains. While
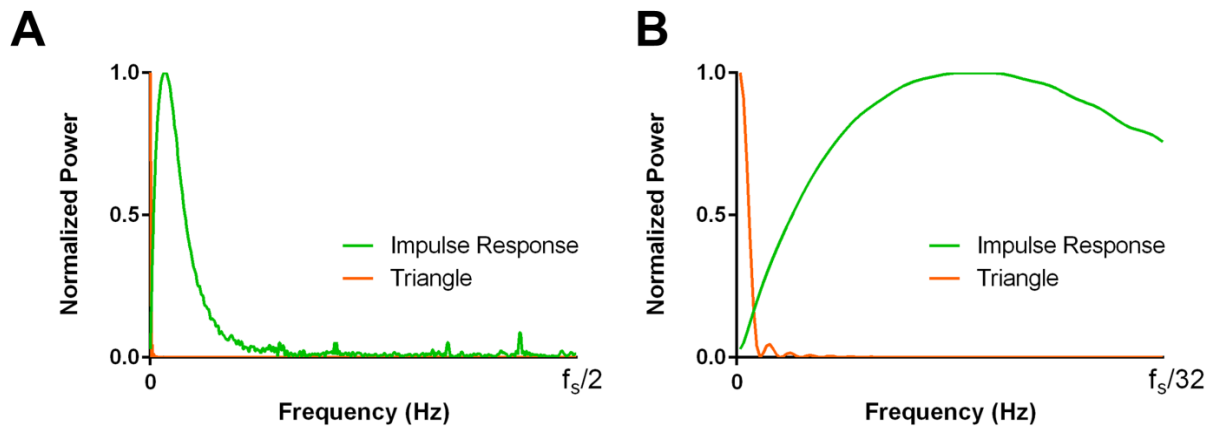
Figure 4.11. Power spectra for a triangular voltage wave and a typical impulse response estimation over the entire frequency range (A, zero to half the sampling frequency, f_s – here, 300 kHz) and in the lower frequency range (B, zero to $f_x/32$ – here, 9.375 kHz)
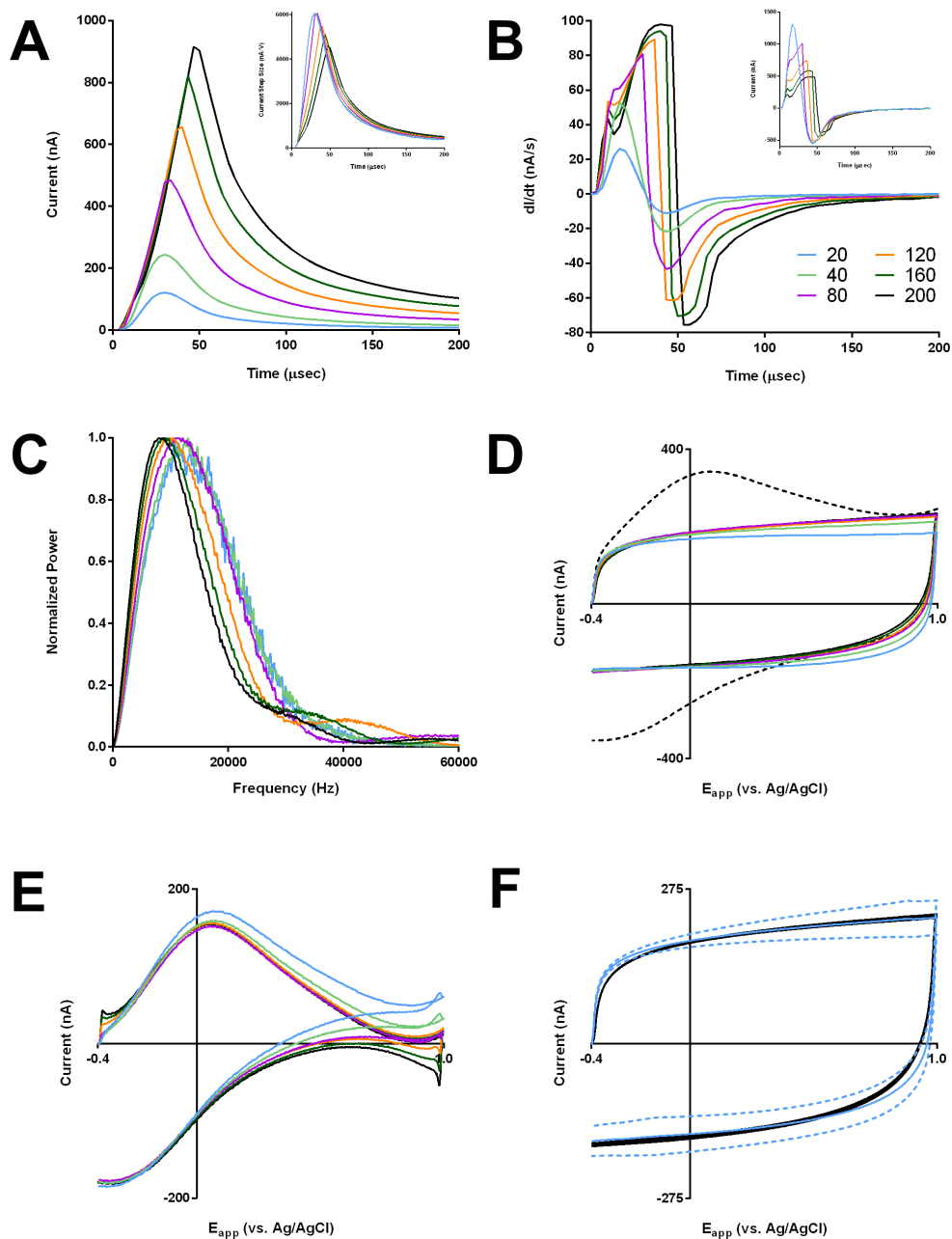
Figure 4.12. Effect of step size on prediction for different voltage step amplitudes (20-200 mV) using a low-pass voltage filter (cut-off frequency of 25 kHz) and sampling frequency of 300 kHz. (A) Current response obtained to voltage step, normalized to step height in inset. (B) Impulse response estimations from (A), normalized to step height in inset. (C) Fourier transforms of impulse response estimations from (B). (D) Predictions generated from convolution of impulse response estimations with 400 V/s triangular voltage sweep, with actual response shown as dotted line. (E) Prediction-subtracted voltammograms (actual less prediction) from (D). (F) Average prediction (solid) ± one standard deviation (dotted) estimated from a five-second recording for 20 mV (blue) and 200 mV (black) voltage pulses.

lower S/N ratios are seen for smaller step sizes, increasing step height brings a flattening of the current response and distortion of the impulse response estimates (likely due to the passive components used for current transduction in the headstage).(Takmakov et al., 2011) When used for prediction, larger pulses can result in distortion around the switching potentials of the waveform, where the high frequency impedance dominates. However, smaller pulses are inadequate for measuring the low-frequency impedance, resulting in errors that increase with potential away from the step voltage region. Analysis of the average predictions, and their variance, given by 20 and 200 mV pulses for five-second recordings (Figure 4.12) reveal nearly identical average predictions but considerably higher uncertainty for more removed potentials with smaller pulses. Use of moderate step sizes (80-120 mV), where both these issues are minimized is thus recommended.

The pulse width is determined by the frequency range about which information is needed.(Chang & Park, 2010; Jurczakowski & Lasia, 2004)   Ideally, a Heaviside step function would be used to give information on all frequencies; however, the step must be limited. For application of a step, an ideal RC circuit would decay to 99.3% over a period equal to five times the RC time constant (for reference, 5*RC = 196 and 22.5 μs for the experimental value from Figure S-4 and the theoretical value, respectively). Thus, to be conservative, the lower bound was placed at 25 time constants (here, 1 ms).

Comparison with Principal Component Regression. The current standard for resolving overlapping signals in FSCV is the use of multivariate analysis, specifically principal component regression (PCR).(Johnson et al., 2016; Keithley, et al., 2009; Rodeberg, et al., 2015) Combined with residual analysis, PCR has proven a powerful tool for dealing with chemical interferents. To compare the results of the convolution-based method here with the established PCR paradigm, separate data was recorded for the flow-injection analysis of a mixture of dopamine (200 nM) and potassium chloride (120 mM) solutions in phosphate-buffered saline. For this experiment, training sets were also built from injections of solutions of pure dopamine and pure potassium chloride at different concentrations. The data was then analyzed in three different ways. First, PCR models, constructed using either only dopamine standards (Approach 1) or dopamine and potassium chloride standards (Approach 2), were applied to the data. Next, the convolution-based method was first used to pre-treat the data, after which it was analyzed using a PCR

108
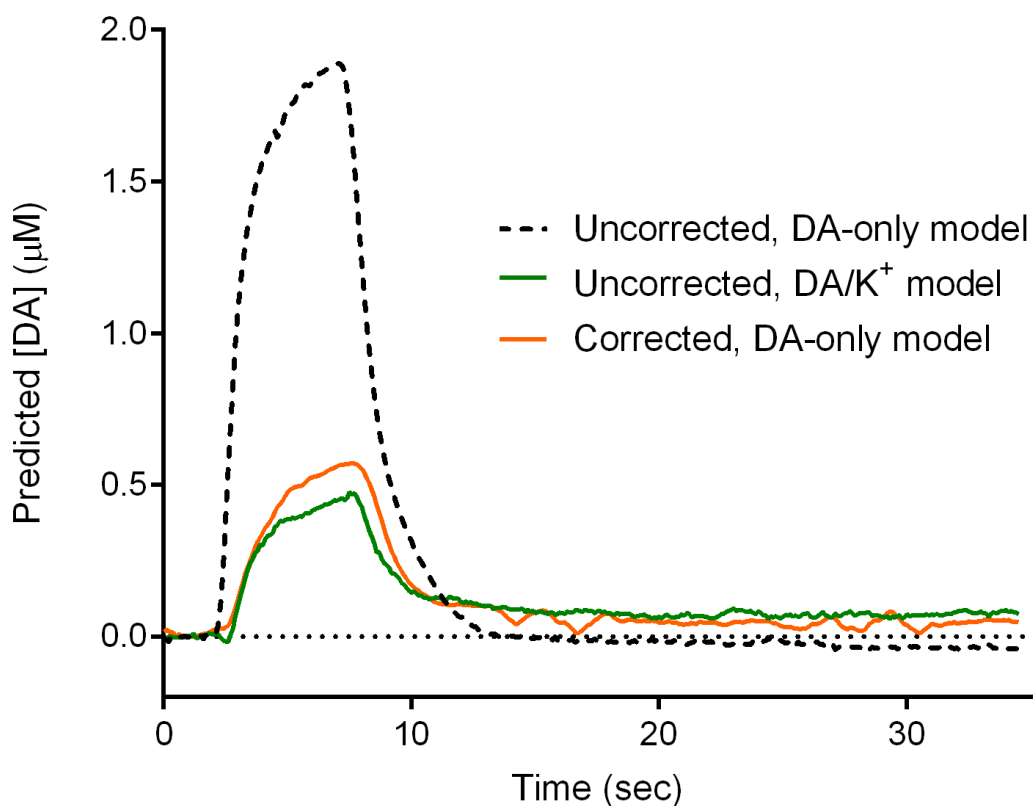
Figure 4.13. Comparison of convolution-based and PCR –only removal of ionic artifacts. The PCR predicted concentration traces for flow injection analysis of a mixture 500 nM dopamine and 120 mM potassium chloride (in PBS buffer) for the uncorrected data analyzed with a PCR model trained with only dopamine standards (dotted line) and dopamane/potassium chloride standards (green line), as well as the corrected data analyzed using PCR model containing only dopamine (orange line).

model consisting solely of the dopamine standards (Approach 3).

The current vs. time traces for the three different approaches are shown in Figure 4.13. As expected, analysis of the untreated data with a dopamine-only model (Approach 1) resulted in a considerable overestimate (about four-fold) of the dopamine concentration over time (dotted line), due to improper assignment of potassium signal to dopamine (as indicated by the failure of residual analysis, not shown). However, comparable results are obtained with the PCR-only (Approach 2, green) and convolution/PCR approach (Approach 3, orange), with only slight differences in the peak concentrations predicted and more noise seen for the latter approach.

While giving similar results, the true advantage of the convolution-based approach lies in the experimental simplicity. As noted, to build the PCR model with both analytes, multiple standards were needed for each, requiring additional experimental work. The use of the convolution-based approach required only collection of the dopamine standards and the use of the pulse during measurements. Further, *in vivo* PCR model building is considerably harder, requiring a method for eliciting the interferent responses. Currently, there are no established protocols for generating ionic changes for this purpose.

CONCLUSIONS

The data presented here suggest two main types of ionic interactions with carbon fibers exposed to moderate oxidation, which determine the shape of the voltammetric responses seen with local ion concentration changes. Using this framework, we designed a measurement protocol to remove interference with voltammetric detection of electroactive species from the voltage-independent capacitance, building on previous literature approaches. This method uses a small-amplitude pulse coupled to a voltage sweep for probing and predicting the non-faradaic behavior of the electrode. It was successfully able to remove interfering signals arising from interaction with the voltage-independent capacitance.

REFERENCES

Atcherley, C. W., Laude, N. D., Parent, K. L., & Heien, M. L. (2013). Fast-scan controlled-adsorption voltammetry for the quantification of absolute concentrations and adsorption dynamics. *Langmuir, 29*(48), 14885-14892.

Bard, A. J., & Faulkner, L. R. (2001). *Electrochemical Methods: Fundamentals and Applications* (2nd ed.). New York, NY: John Wiley & Sons, Inc.

Bath, B. D., Michael, D. J., Trafton, B. J., Joseph, J. D., Runnels, P. L., & Wightman, R. M. (2000). Subsecond adsorption and desorption of dopamine at carbon-fiber microelectrodes. *Anal Chem, 72*(24), 5994-6002.

Baur, J. E., Kristensen, E. W., May, L. J., Wiedemann, D. J., & Wightman, R. M. (1988). Fast-scan voltammetry of biogenic amines. *Anal Chem, 60*(13), 1268-1272.

Bracewell, R. N. (2000). *The Fourier transform and its applications* (3rd ed.). Boston: McGraw Hill.

Bucher, E. S., Brooks, K., Verber, M. D., Keithley, R. B., Owesson-White, C., Carroll, S., et al. (2013). Flexible Software Platform for Fast-Scan Cyclic Voltammetry Data Acquisition and Analysis. *Anal Chem, 85*(21), 10344-10353.

Bucher, E. S., & Wightman, R. M. (2015). Electrochemical Analysis of Neurotransmitters. *Annu Rev Anal Chem (Palo Alto Calif), 8*, 239-261.

Chang, B. Y., & Park, S. M. (2010). Electrochemical impedance spectroscopy. *Annu Rev Anal Chem (Palo Alto Calif), 3*, 207-229.

Cullison, J. K., & Kuhr, W. G. (1996). Cyclic voltammetry with harmonic lock-in detection: Applications to flow streams. *Electroanal, 8*(4), 314-319.

Dankoski, E. C., Agster, K. L., Fox, M. E., Moy, S. S., & Wightman, R. M. (2014). Facilitation of Serotonin Signaling by SSRIs is Attenuated by Social Isolation. *Neuropsychopharmacology, 39*(13), 2928-2937.

Dengler, A. K., Wightman, R. M., & McCarty, G. S. (2015). Microfabricated Collector-Generator Electrode Sensor for Measuring Absolute pH and Oxygen Concentrations. *Analytical Chemistry, 87*(20), 10556-10564.

Fox, M. E., Rodeberg, N. T., & Wightman, R. M. (2016). Reciprocal Catecholamine Changes during Opiate Exposure and Withdrawal. *Neuropsychopharmacology*.

Fritz, J. S., & Gjerde, D. T. (2000). *Ion Chromatography* (3rd ed.). New York: Wiley-VCH.

Haddad, P. R., & Jackson, P. E. (1990). *Ion Chromatography: Priniciples and Applications* (Vol. 46). Amsterdam: Elsevier.

Heien, M. L., Phillips, P. E., Stuber, G. D., Seipel, A. T., & Wightman, R. M. (2003). Overoxidation of carbon-fiber microelectrodes enhances dopamine adsorption and increases sensitivity. *Analyst, 128*(12), 1413-1419.

Howell, J. O., Kuhr, W. G., Ensman, R. E., & Wightman, R. M. (1986). Background Subtraction for Rapid Scan Voltammetry. *J Electroanal Chem, 209*(1), 77-90.

Johnson, J. A., Rodeberg, N. T., & Wightman, R. M. (2016). Failure of Standard Training Sets in the Analysis of Fast-Scan Cyclic Voltammetry Data. *ACS Chem Neurosci, 7*(3), 349-359.

Jones, S. R., Mickelson, G. E., Collins, L. B., Kawagoe, K. T., & Wightman, R. M. (1994). Interference by Ph and Ca2+ Ions during Measurements of Catecholamine Release in Slices of Rat Amygdala with Fast-Scan Cyclic Voltammetry. *J Neurosci Meth, 52*(1), 1-10.

Jurczakowski, R., & Lasia, A. (2004). Limitations of the potential step technique to impedance measurements using discrete time Fourier transform. *Anal Chem, 76*(17), 5033-5038.

Karweik, D. H., Hu, I. F., Weng, S., & Kuwana, T. (1985). Carbonaceous Surfaces - Modification, Characterization, and Uses for Electrocatalysis. *Acs Sym Ser, 288*, 582-595.

Kawagoe, K. T., Garris, P. A., & Wightman, R. M. (1993). Ph-Dependent Processes at Nafion(R)-Coated Carbon-Fiber Microelectrodes. *J Electroanal Chem, 359*(1-2), 193-207.

Kawagoe, K. T., & Wightman, R. M. (1994). Characterization of amperometry for in vivo measurement of dopamine dynamics in the rat brain. *Talanta, 41*(6), 865-874.

Keithley, R. B., Heien, M. L., & Wightman, R. M. (2009). Multivariate concentration determination using principal component regression with residual analysis. *Trends Analyt Chem, 28*(9), 1127-1136.

Keithley, R. B., Takmakov, P., Bucher, E. S., Belle, A. M., Owesson-White, C. A., Park, J., et al. (2011). Higher sensitivity dopamine measurements with faster-scan cyclic voltammetry. *Anal Chem, 83*(9), 3563-3571.

Keithley, R. B., & Wightman, R. M. (2011). Assessing principal component regression prediction of neurochemicals detected with fast-scan cyclic voltammetry. *ACS Chem Neurosci, 2*(9), 514-525.

Kim, C.-H., Pyun, S.-I., & Kim, J.-H. (2003). An investigation of the capacitance dispersion on the fractal carbon electrode with edge and basal orientations. *Electrochimica Acta, 48*(23), 3455-3463.

Kim, Y. J., Wu, W., Chun, S. E., Whitacre, J. F., & Bettinger, C. J. (2014). Catechol-Mediated Reversible Binding of Multivalent Cations in Eumelanin Half-Cells. *Adv Mater, 26*(38), 6572-6579.

Kraig, R. P., & Nicholson, C. (1978). Extracellular ionic variations during spreading depression. *Neuroscience, 3*(11), 1045-1059.

Kume-Kick, J., & Rice, M. E. (1998). Dependence of dopamine calibration factors on media Ca2+ and Mg2+ at carbon-fiber microelectrodes used with fast-scan cyclic voltammetry. *J Neurosci Meth, 84*(1-2), 55-62.

Lambie, B. A., Brennan, C., Olofsson, J., Orwar, O., & Weber, S. G. (2007). Experimentally determining the iR drop in solution at carbon fiber microelectrodes with current interruption and application to single-cell electroporation. *Anal Chem, 79*(10), 3771-3778.

Lee, H., Scherer, N. F., & Messersmith, P. B. (2006). Single-molecule mechanics of mussel adhesion. *P Natl Acad Sci USA, 103*(35), 12999-13003.

Long, J. T., & Weber, S. G. (1992). Voltammetry in Static and Flowing Solutions with a Large-Amplitude Sine Wave Potential. *Electroanal, 4*(4), 429-437.

Manolakis, D. G., & Ingle, V. K. (2011). *Applied digital signal processing: theory and practice*. New York: Cambridge University Press.

McCreery, R. L. (2008). Advanced carbon electrode materials for molecular electrochemistry. *Chem Rev, 108*(7), 2646-2687.

Michael, A. C., & Wightman, R. M. (1996). In P. T. Kissinger (Ed.), *Laboratory Techniques in Electroanalytical Chemistry*. New York: Marcel Dekker.

Millar, J., Oconnor, J. J., Trout, S. J., & Kruk, Z. L. (1992). Continuous Scan Cyclic Voltammetry (Cscv) - a New High-Speed Electrochemical Method for Monitoring Neuronal Dopamine Release. *J Neurosci Meth, 43*(2-3), 109-118.

Millar, J., & Williams, G. V. (1990). Fast Differential Ramp Voltammetry - a New Voltammetric Technique Designed Specifically for Use in Neuronal Tissue. *J Electroanal Chem, 282*(1-2), 33-49.

Nicholson, C., Kraig, R. P., ten Bruggencate, G., Stockle, H., & Steinberg, R. (1978). Potassium, calcium, chloride and sodium changes in extracellular space during spreading depression in cerebellum [proceedings]. *Arzneimittelforschung, 28*(5), 874-875.

Owesson-White, C., Belle, A. M., Herr, N. R., Peele, J. L., Gowrishankar, P., Carelli, R. M., et al. (2016). Cue-Evoked Dopamine Release Rapidly Modulates D2 Neurons in the Nucleus Accumbens During Motivated Behavior. *J Neurosci, 36*(22), 6011-6021.

Paxinos, G., & Watson, C. (1998). *The Rat Brain in Stereotaxic Coordinates*. San Diego, CA: Academic Press.

Phillips, P. E., Stuber, G. D., Heien, M. L., Wightman, R. M., & Carelli, R. M. (2003). Subsecond dopamine release promotes cocaine seeking. *Nature, 422*(6932), 614-618.

Rodeberg, N. T., Johnson, J. A., Cameron, C. M., Saddoris, M. P., Carelli, R. M., & Wightman, R. M. (2015). Construction of Training Sets for Valid Calibration of in Vivo Cyclic Voltammetric Data by Principal Component Analysis. *Anal Chem, 87*(22), 11484-11491.

Rogers, M. L., Feuerstein, D., Leong, C. L., Takagaki, M., Niu, X., Graf, R., et al. (2013). Continuous online microdialysis using microfluidic sensors: dynamic neurometabolic changes during spreading depolarization. *Acs Chem Neurosci, 4*(5), 799-807.

Runnels, P. L., Joseph, J. D., Logman, M. J., & Wightman, R. M. (1999). Effect of pH and surface functionalities on the cyclic voltammetric responses of carbon-fiber microelectrodes. *Anal Chem, 71*(14), 2782-2789.

Stamford, J. A., Kruk, Z. L., & Millar, J. (1984). A Double-Cycle High-Speed Voltammetric Technique Allowing Direct Measurement of Irreversibly Oxidized Species - Characterization and Application to the Temporal Measurement of Ascorbate in the Rat Central Nervous-System. *J Neurosci Meth, 10*(2), 107-118.

Takmakov, P., McKinney, C. J., Carelli, R. M., & Wightman, R. M. (2011). Instrumentation for fast-scan cyclic voltammetry combined with electrophysiology for behavioral experiments in freely moving animals. *Rev Sci Instrum, 82*(7), 074302.

Takmakov, P., Zachek, M. K., Keithley, R. B., Bucher, E. S., McCarty, G. S., & Wightman, R. M. (2010a). Characterization of Local pH Changes in Brain Using Fast-Scan Cyclic Voltammetry with Carbon Microelectrodes. *Anal Chem, 82*(23), 9892-9900.

Takmakov, P., Zachek, M. K., Keithley, R. B., Walsh, P. L., Donley, C., McCarty, G. S., et al. (2010b). Carbon microelectrodes with a renewable surface. *Anal Chem, 82*(5), 2020-2028.

Venton, B. J., Troyer, K. P., & Wightman, R. M. (2002). Response times of carbon fiber microelectrodes to dynamic changes in catecholamine concentration. *Anal Chem, 74*(3), 539-546.

Walton, H. F. (1992). Ion-Exchange Chromatography. In E. Heftmann (Ed.), *Chromatography: Fundamentals and Applications of Chromatography and Related Differential Migration Methods* (5th ed.). Amsterdam: Elsevier.

Wightman, R. M., & Wipf, D. O. (1989). Voltammetry at Ultramicroelectrodes. In A. J. Bard (Ed.), *Electroanalytical Chemistry*. New York: Marcel Dekker.

Yoshimi, K., & Weitemier, A. (2014). Temporal Differentiation of pH-Dependent Capacitive Current from Dopamine. *Anal Chem, 86*(17), 8576-8584.

Zachek, M. K., Hermans, A., Wightman, R. M., & McCarty, G. S. (2008). Electrochemical Dopamine Detection: Comparing Gold and Carbon Fiber Microelectrodes using Background Subtracted Fast Scan Cyclic Voltammetry. *J Electroanal Chem (Lausanne), 614*(1-2), 113-120.

CHAPTER 5: MEASUREMENT OF PHASIC AND BASAL DOPAMINE CHANGES USING CONVOLUTION-BASED REMOVAL OF BACKGROUND CURRENT

INTRODUCTION

Fast-scan cyclic voltammetry (FSCV) is a powerful tool for the rapid *in vivo* measurements of electroactive neurotransmitters. The rapid scan rates enable high sensitivity measurements with subsecond time resolution, while providing a selectivity for relatively low concentration neurotransmitters like dopamine as compared to ambient species like ascorbic acid and 3,4-dihydroxyphenylacetic acid (DOPAC).(Baur et al., 1988) However, a significant drawback of this approach is the large charging current generated at the electrode from rapid potential changes. This current serves as the main interferent in FSCV measurements and mandates use of digital background subtraction to remove the background and resolve the analytical faradaic current.(Howell et al., 1986) This limits the utility of FSCV to the measurement of relative changes in neurotransmitters on the time scale over which the background remains relatively stable. This issue has not prevented significant advances being made with the technique; however, this does limit the insight that can be gained into chemical neurotransmission to the phasic release of neurotransmitters. Information about absolute ambient levels of neurotransmitters, which may change with time and underlie important neurobiological phenomena, is lost in the background-subtraction step. Further, attempts to measure changes in the ambient levels are hindered by the fact that the background currents at the carbon-fiber microelectrodes typically used in measurement do not remain stable over periods longer than a few minutes.

Thus, to access this information with electrochemical measurement techniques, changes to the widely used in FSCV *in vivo* measurement protocols must be explored. Indeed, recent reports have focused on exploration of alternative means of providing more information about ambient neurotransmitter levels. One approach has been the use of multivariate data analysis, specifically principal component regression, to account for the background changes that appear in the background-subtracted data. By incorporation of the typical background change voltammograms into the model training set, the

115

contributions of this voltammogram are identified and removed from the data, allowing for more robust isolation of dopamine signals as demonstrated *in vivo* following cocaine administration. (Hermans et al., 2008) However, this approach relies on consistency of the background signal over time and assumes linear behavior across the potential window, which is violated by non-faradaic current, particularly around the switching potentials of the waveform. Alternatively, experimental modifications have been explored. In a series of reports, Heien and colleagues have introduced fast-scan controlled adsorption voltammetry (FSCAV), a technique that alters the application frequency of the voltammetric waveform to alter the adsorption behavior of analytes at the electrode surface.(Atcherley et al., 2015a; Atcherley et al., 2013) This approach relies on periods of rapid voltammetric scanning (100 Hz) alternated with quiescent periods (~10 seconds) at negative potentials to promote robust adsorptive preconcentration at the surface. Information during the early scanning period allows determination of the ambient concentrations of neurotransmitters, while the electrode is cleaned of analytes through continued scanning. The success of this technique has been demonstrated in both brain slices and in vivo experiments.(Atcherley et al., 2015b; Burrell et al., 2015) However, the main drawback of the technique lies in the quiescent period, which drastically decreases the time resolution of the measurements and, in turn, loses information about the phasic neurotransmitter release. A similar approach was reported to track relative changes of tonic dopamine levels, which relied on a novel 'Mexican hat' waveform with a holding potential of 0.0 V vs. Ag/AgCl and a similar waveform application to FSCAV to promote background stability and minimize interferences.(Oh et al., 2016) This approach permitted measurements on the order of hours following pharmological manipulation with nomifensine (a dopamine reuptake inhibitor) and α-methyl-DL-tyrosine (α-MPT, a dopamine synthesis inhibitor).

Recently, we reported on an alternative measurement protocol that relies on the use of convolution to predict and remove portions of the non-faradaic component of the FSCV background (Chapter 4). This approach relies on a small step placed immediately before each FSCV sweep to probe the capacitive state of the electrochemical system, specifically its impulse response function. Convolution with the triangular waveform provides a prediction of the non-Faradaic component of the background, which can be removed from the measurement through digital subtraction of this prediction. The success of this approach was demonstrated for the removal of a subset of ionic interferences *in vitro* and *in vivo*.

Here, we seek to explore the possibility of using this approach to access information about the basal levels of neurotransmitters. However, as noted in that report and elsewhere, the background observed at carbon-fiber microelectrodes is a mixture of non-faradaic and faradaic components. Further, it appears the redox state of a prominent electroactive surface species (a quinone-like moiety) modulates the non-faradaic current. Thus, to completely remove the background interference, the measurement protocol must be further altered to provide a means of avoiding faradaic interferences and non-idealities introduced by their presence.

Here, we describe a means of accomplishing this by modifying the holding potential of the waveform to 0.0 V vs Ag/AgCl. Negative holding potentials have been shown to promote adsorption of catecholamines, particularly on oxidized carbon fibers, and the resulting increase in analytical sensitivity has facilitated its widespread use.(Heien et al., 2003) However, both extensive oxidation of the carbon fiber and the use of negative holding potentials complicate the use of the convolution-based removal of interferences, due to the increase in the electroactive surface species concentration and the accompanying capacitive asymmetry across the potential window. Use of holding potentials higher than the redox potential of the surface species should mitigate these issues, albeit at the cost of sensitivity. However, there are other means of increasing sensitivity, namely the use of longer holding periods for analyte preconcentration and the use of the higher scan rates. The latter is explored here, as it complements the use of the convolution-based technique as will be shown.

EXPERIMENTAL SECTION

Instrumentation and Software. T-650 (PAN-, or polyacrylonitrile-, based) and P-55 (pitch-based) type, cylindrical carbon-fiber microelectrodes (Thornel, Amoco Corporation, Greenville, SC; pulled in glass capillaries and cut to 50-100 μm exposed lengths) were used. Pulled electrodes were treated with epoxy to improve electrochemical characteristics. Data was acquired in grounded Faraday cages, using a commercial interface (PCI-6052, 16 bit, National instruments, Austin TX) with a personal home computer and analyzed using locally constructed hardware and software written in LabVIEW (HDCV, National

Instruments, Austin, TX).(Bucher et al., 2013) Analog background subtractions was implemented using the design described elsewhere.(Hermans, et al., 2008)

Electrochemical Experiments. Flow-injection analysis experiments were performed using a syringe pump (Harvard Apparatus, Holliston, MA) operated at 0.8 mL/min using PEEK tubing (Sigma-Aldrich) connected to a pneumatically controlled six-port injection valve (Rheodyne, Rohnert Park, CA). All solutions were prepared in TRIS buffer (2.0 mM Na_2SO_4, 1.25 mM $NaH_2PO_4 \cdot H_2O$, 140 mM NaCl, 3.25 KCl, 1.2 mM $CaCl_2 \cdot 2H_2O$, 1.2 mM $MgCl_2 \cdot 6H_2O$, and 15 mM Trizma HCl), adjusted to pH 7.4 with NaOH as necessary. Dopamine solutions were bubbled under nitrogen to prevent oxidative degradation prior to use. The tyramine fouling experiments described follow the protocol described by Takmakov et al., with the exception that the negative potential limits were varied (-0.4 and 0.0 vs Ag/AgCl) during the recovery phase in lieu of the positive potential limits.(Takmakov et al., 2010b) Additionally, both waveforms (randomized order, n = 5 electrodes) were tested at a given electrode, followed by conditioning and re-evaluation of the sensitivity before fouling.

The convolution-based approach used here is described in Chapter 4. Briefly, a waveform with a small amplitude pulse placed immediately prior to the FSCV sweep is used, and the derivative of the current during the step (i.e. the system impulse response estimate) is convoluted with the applied waveform to generate a prediction of the non-Faradaic current.

In Vivo Measurements. Male Sprague-Dawley rats from Charles River (Wilmington, MA, USA) were pair-housed on a 12/12 h light/dark cycle. Animal procedures were approved by the UNC-Chapel Hill Institutional Animal Care and Use Committee (IACUC). For freely-moving experiments, animals were surgerized at least three days prior to testing. Isoflurane (1.5-4%) was used for anesthesia, and guide cannulas (Bioanalytical Systems, West Lafayette, IN) were implanted above the nucleus accumbens shell (AP +1.7 mm, ML +0.8 mm, DV -2.5 mm) and the contralateral hemisphere for lowering of the working and reference electrode, respectively, on testing day. Additionally, a bipolar stimulating electrode (Plastics One, Roanoke, VA) was implanted at the ipsilateral ventral tegmental area (-5.2 mm, ML +1.0 mm, DV -8.4-8.8 mm) to assist in positioning the working electrode.

RESULTS AND DISCUSSION

Effect of Negative Holding Potentials. As noted earlier, the use of negative holding potentials has become standard, due to the increased sensitivity provided by their use for catecholamines.(Heien, et al., 2003) This was assumed to result from increased electrostatic interactions with the positively charged dopamine, although interactions with the reduced quinone-like moiety may also play a role. Here, the effects of using negative holding potentials were re-evaluated, specifically with focus on their effect on the background current.

Backgrounds collected at various holding potentials are shown in Figure 5.1A. As shown in previous reports, the background considerably decreases, in both magnitude and complexity, with the use of more positive holding potentials.(Oh, et al., 2016; Takmakov et al., 2010a) Of note, during application of FSCV waveforms, the majority of the time is spent applying the holding potential (typically greater than 90%). Although this period is not typically recorded, some current is also often seen throughout this period. After the waveform returns to the holding potential after application of the sweep, the measured current decays to a steady state value, the amplitude of which increases with increasingly negative holding potentials (Figure 5.1B). To understand its origin, slow-scan cyclic voltammetry (80 mV/s) was used (Figure 5.1C). The obtained voltammogram resembles that expected for the oxygen reduction reaction at a microelectrode, a two-step redox process that generates hydrogen peroxide during the first step (i.e. at low overpotentials).(Qu et al., 2015; Sosna et al., 2007) Indeed, this reaction was suggested in the original report on the use of negative holding potentials and has been used recently to generate a microfabricated collector-generator oxygen sensor.(Dengler et al., 2015; Heien, et al., 2003) If one assumes that the majority of the current at the holding potential does indeed originate from this reaction, a simplified calculation using Faraday's law for electrolysis (n = It/Fz, z =2 and I = 5 nA for -0.4 V) and the diffusion distance (x^2 = 6Dt, D_{H2O2} = 1.8 m^2/s) suggests that the average concentration of peroxide around the electrode is above 1 μM after one holding period (~92 ms).(Vanstroebiezen et al., 1993) Further, collection of fast-scan voltammograms (400 V/s) using differing waveform application frequencies (0.5-30 Hz) suggests that this generated peroxide may be oxidized during the forward scan (Figure 5.1D). Using the 30 Hz waveform as the reference, differential CVs collected at lower frequencies have a peak that grows larger with increasing time at the holding potential (here, -0.4 V).

119
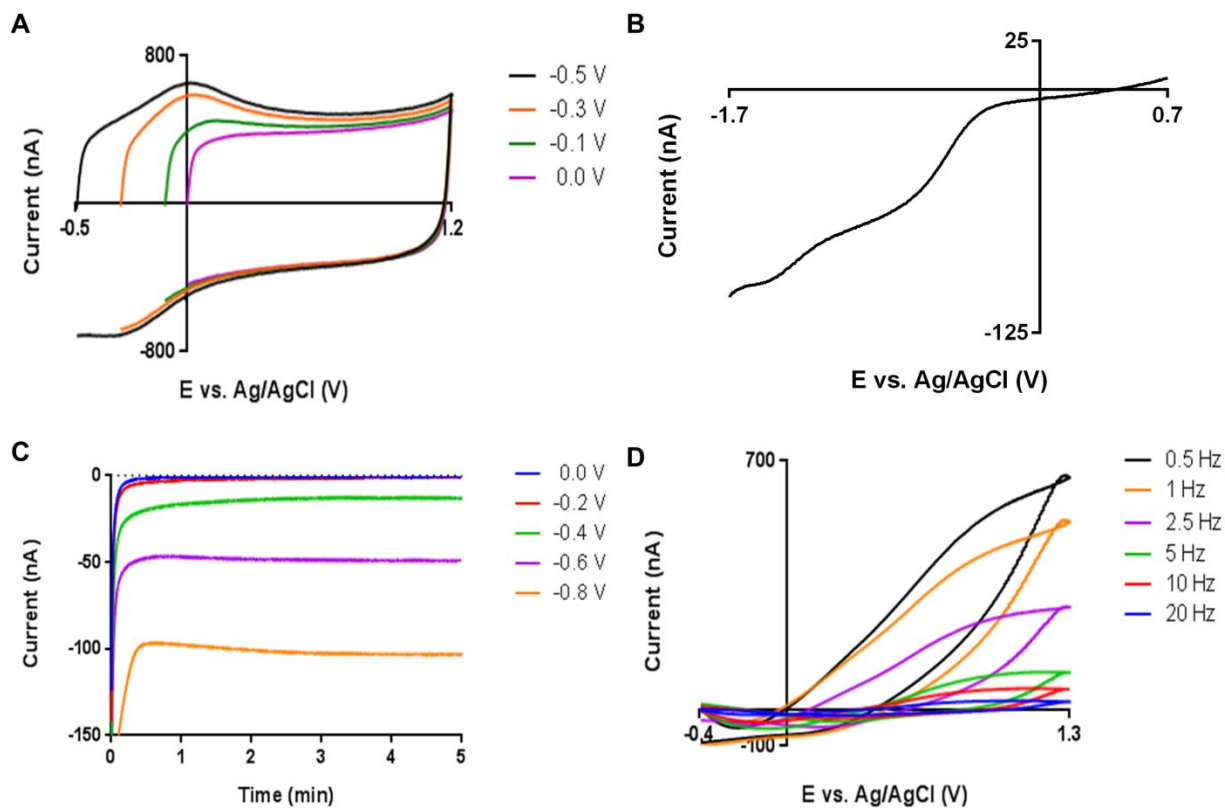
Figure 5.1. Effects of negative holding potentials. (A) Fast-scan voltammograms taken in TRIS buffer at carbon-fiber microelectrodes with different holding potentials (-0.5, -0.3, -0.1, and 0.0 V). (B) Slow scan voltammograms (80 mV/s, forward scan shown only) taken from +0.7 to -1.7 V. (C) Current observed at various negative potentials over long time scales. (D) Subtracted fast-scan voltammograms taken at various application frequencies (0.5 – 20 Hz), using the voltammograms taken at 30 Hz as the blank signal.

Further, it is known that the use of high positive potentials (> 1.0 V) in waveforms can result in etching of the carbon fiber surface, which can be advantageous for maintaining sensitivity in the heavily fouling *in vivo* environment.(Takmakov, et al., 2010b) However, the role of the negative holding potential in this process has not been characterized. To study this, a tyramine electrode fouling experiment, originally used to understand the effect of the positive potential limit, was used. In this experiment, the carbon fiber microelectrode was fouled through electro-oxidation of tyramine, which forms a film at the surface that drastically decreases the electrode capacitance and sensitivity. The success of surface renewal through waveform application was then evaluated by applying the specific waveform and subsequently testing the sensitivity (using a -0.4 to 1.0 waveform).During the surface renewal step, a positive potential limit known to promote etching (1.3 V) was used, and two different negative holding potential (-0.4 and 0.0 V) were used. Figure 5.2A shows a schematic of this experiment. Both waveforms were tested at each electrode, using a randomized order and conditioning the electrode on the full waveform (-0.4 to 1.3 V) prior to fouling. The results are summarized in Figure 5.2B. Of note, it can be seen that the sensitivity is significantly lower after use of the 0.0 V holding potential during the surface renewal phase than either prior to fouling or after treatment. This suggests that a process occurring at negative potentials promotes this etching and surface renewal process, driving the surface evolution of the electrode. While the specifics of this process are unknown, the generation of peroxide or interactions between the oxidized carbon surface and cations may underlie this phenomenon.(Dikin et al., 2007; Stankovich et al., 2006)

Convolution-Based Removal of Divalent Cation Interferences. Overall, these data suggest that some of the complexity and temporal evolution seen in the FSCV backgrounds at carbon fiber microelectrodes stem from processes occurring at negative potentials. Further, as discussed in Chapter 4, the voltammetric waves (seen around 0.0 V and -0.3 V on the forward and backward scans in Figure 5.1A, respectively) that originate from surface-bound quinone-like species introduce non-idealities and further increase this complexity. Thus, in the context of the use of the convolution-based non-faradaic current prediction approach, the use of negative holding potentials is less ideal. The use of a higher holding potential (0.0 V or greater) is anticipated to mitigate these issues, as both processes driven at the
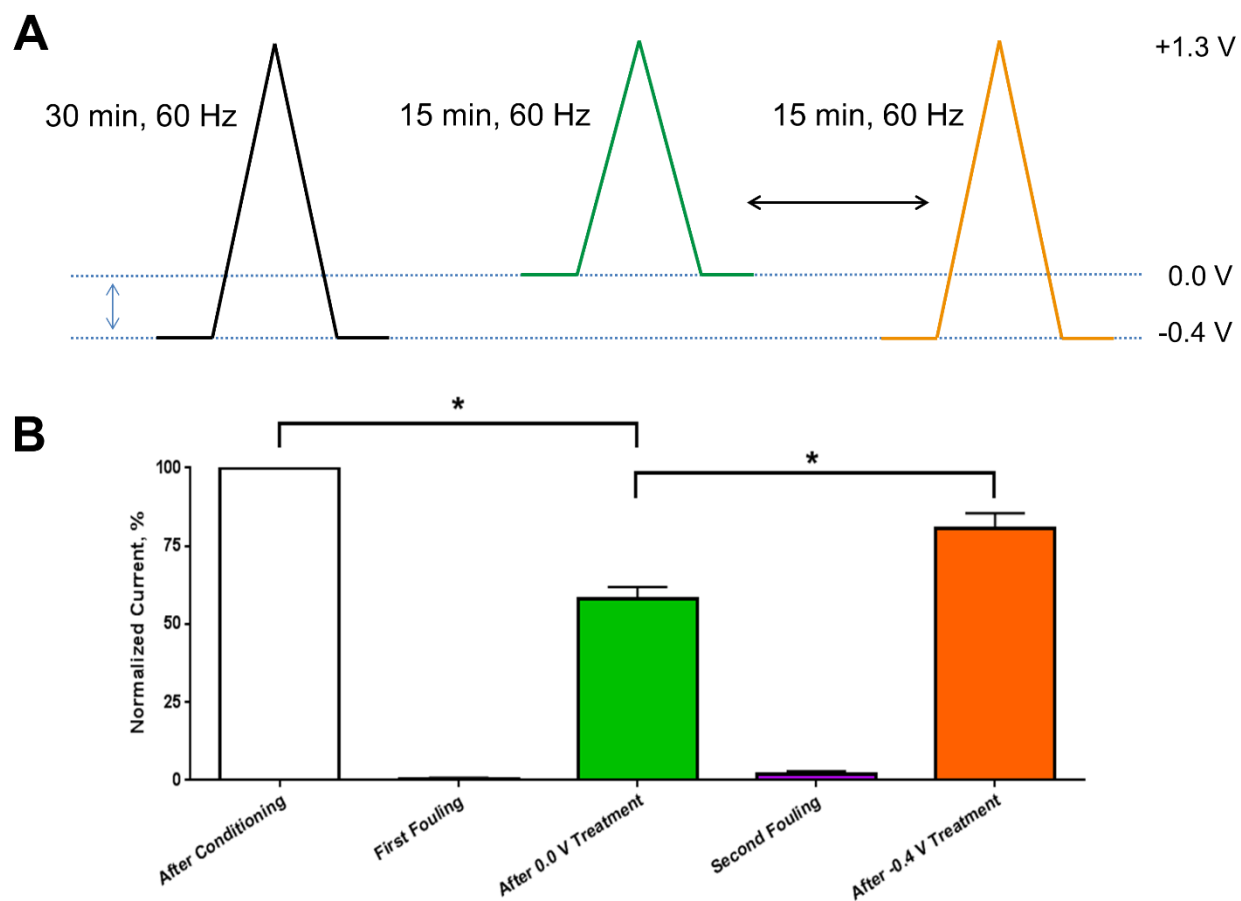
Figure 5.2. Sensitivity testing after tyramine fouling and treatment with waveforms with differing holding potentials. (A) Schematic of the experimental design. The arrow indicates that the order of waveform treatment (either 0.0 or -0.4 holding potential waveforms) was randomized. (B) Normalized peak currents observed for 1.0 µM of dopamine after each step in the experiment.
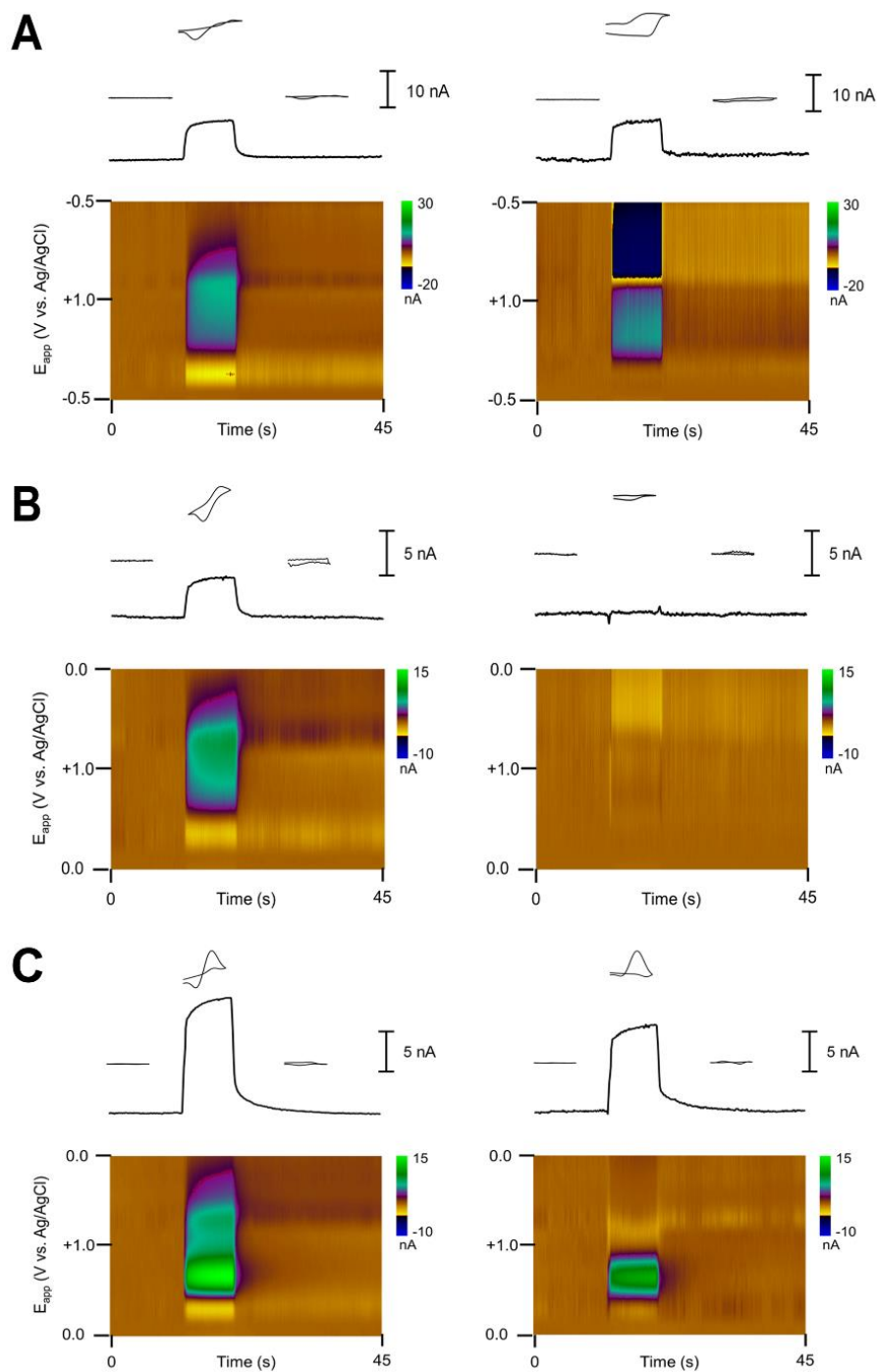
**Figure 5.3.** Removal of ionic artifacts seen during flow-injection analysis of magnesium in TRIS buffer. (A-B) Raw (left) and convolution-treated (right) background-subtracted color plots using waveforms with -0.5 V (A) and 0.0 V (B) holding potentials. (C) Raw (left) and convolution-treated (right) background-subtracted color plot during flow-injection analysis of a Mg^{2+}-dopamine mixture.

negative potentials and the surface redox reaction are avoided.

In the previous use of the convolution-based procedure, waveforms with holding potentials of -0.4 or less were used, and it was found that only a subset of ionic interference signals were able to be successfully removed (i.e. those with traditional double-layer charging voltammograms). Other ions studied (i.e. the divalent cations Mg^{2+} and Ca^{2+}) had more complex signals arising from interactions with the surface quinone-like species, introducing non-linearities that cannot be handled with the convolution method employed. The issue is highlighted in Figure 5.3A, which shows the background-subtracted signal from a $MgCl_2$-doped TRIS buffer using a waveform with a holding potential of -0.5 V. Due to the capacitive asymmetry across the potential window (i.e. the capacitance is higher at potentials more negative of the redox potential of the quinone-like moiety), use of the convolution-based method incorrectly predicts a higher signal in the positive potential region, resulting in strong artifacts in this region after treatment. However, avoidance of the region of the potential window in which the quinone-like species undergoes its redox reaction (-0.3 to 0.0 V vs Ag/AgCl) should mitigate these issues, through avoiding both the higher capacitance region and the non-linearity introduced by the change in capacitance around the quinone-like peak. Indeed, this approach (Figure 5.3B) results in a considerably smaller ionic signal that can be successfully treated with the convolution-based method, allowing for resolution of a dopamine signal from flow-injection analysis of a Mg^{2+}/dopamine mixture (Figure 5.3C).

Prediction of the Background Current. With the use of more positive holding potentials, the background should be more amenable to removal with the convolution-based method. While the technique was able to predict a significant portion of the background when using negative holding potentials, the quinone peak remained, mandating the use of background subtractions for resolution of the analytical signal. However, as shown in Figure 5.1A (using a holding potential of 0.0 V), the backgrounds observed with at higher holding potentials resemble more classical double-layer charging shapes, and the voltammetric wave associated and non-faradaic non-idealities associated with the quinone-like species largely disappears.

However, the use of alternative carbon fiber materials was first evaluated to determine if there were materials more suited for use of this technique. Traditionally, polyacrylonitrile (PAN)-based carbon fibers (referring to the carbon source) are used for FSCV measurements, although another class of fibers, pitch-based, have been explored. Of note, characterization of electrochemical properties of different types of fibers found that the type of carbon precursor (i.e. pitch and PAN) did not significantly affect the ability of the carbon fiber to detect neurotransmitters, while effects were seen from the type of waveform treatment (i.e. oxidation of the surface) and electrical conductivity of the fiber on the electrochemical kinetics.(Huffman & Venton, 2008) However, for the use of the convolution-based technique, the impedance characteristics of the fiber itself also become important considerations. In general, the PAN-type fibers tend to have lower degrees of crystallinity, higher electrical resistivity, and lower densities (due to increased pore volume in the fiber) than the PAN-type fibers.(Liu & Kumar, 2012) Thus, differences between the impedance characteristics of the types of fibers are expected. To evaluate this, the impedance characteristics of the electrodes were evaluated as a function of scan rate, and the current (I) at each measured voltage (n) were fit to the following model:

$$I(n) = vC_{fit}(n) + Z_{fit}(n) \qquad (Eq. 5.1)$$

where v is the scan rate, C_{fit} is the estimated capacitance, and Z_{fit} is the estimated impedance. Of note, this equation should largely apply at regions away from the switching potential (i.e. after the double-layer is charged). The results are shown in Figure 5.4. At both low (2.5-10 V/s, Figure 5.4A) and high (400-800 V/s, Figure 5.4B) scan rates, the P-55 pitch-based fibers (black lines) have more constant capacitive and impedance characteristics across the potential window than the T-650 PAN-based fibers (orange lines). Further, at high scan rates, the PAN-based fibers exhibit a monotonically increasing impedance on the forward sweep. This is particularly concerning in the context of the convolution-based technique, as the low-frequency characteristics of the fibers are the most difficult to estimate with a step function. While the origin of this is unclear, it is hypothesized that this may have to do with the porosity of the PAN-based fibers. It is known that porous carbons often exhibit multiple time constants due to pore effects stemming from restricted diffusion in the pores and increased local pore resistivity due to local depletion effects.(Signorelli et al., 2009) Thus, P-55 pitch-based fibers were used in the remainder of the study. To
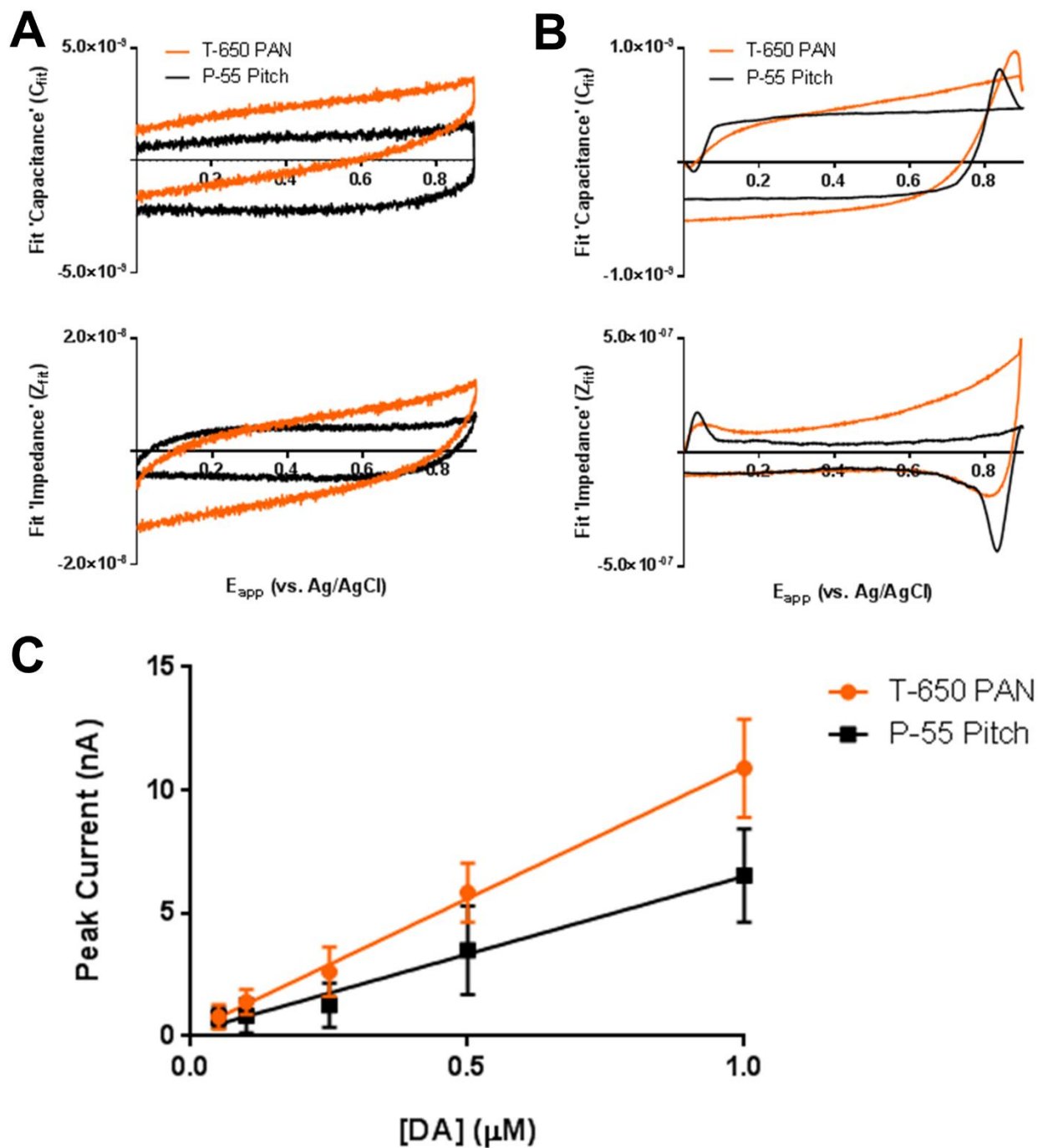
Figure 5.4. Evaluation of T-650 PAN-type and P-55 pitch-type carbon fibers. (A-B) Estimation of capacitance (top) and impedance (bottom) at each potential for both fiber types at low scan rates (2.5 – 10 V/s) and high scan rates (400 – 800 V/s). (C) Peak current observed for dopamine oxidation with a -0.4 to 1.3 V waveform at both fiber types.
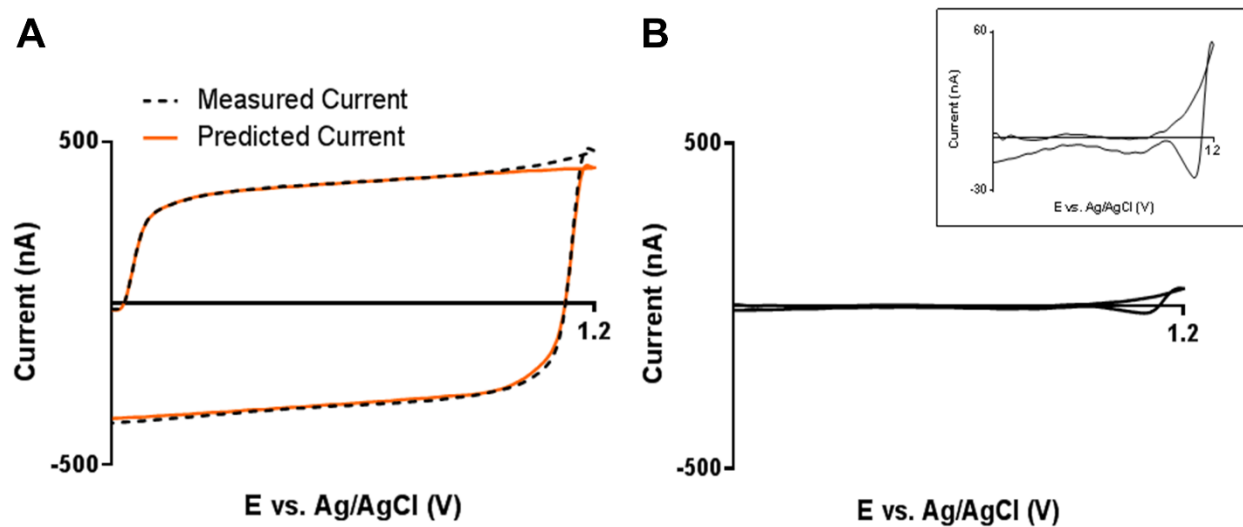
Figure 5.5. Prediction and removal of background currents using 0.0 V holding potential. (A) Measured (dashed black line) and predicted (orange line) from convolution-based method. (B) Residual current after subtraction of the prediction.

evaluate the analytical potential of these fibers, the sensitivity towards dopamine was determined and compared to the T-650 fibers (Figure 5.4C, 400 V/s, n = 5 electrodes). It can be seen that the pitch-based fibers have a significantly lower sensitivity by about 60% (-0.4 to 1.3 V waveform; T-650: 10.7 ± 0.3 nA/μM; P-55: 6.3 ± 0.3 nA/μM; P < 0.001). Of note, this lower sensitivity is in agreement with the previous comparison of these two fibers for another catecholamine, norepinephrine.(Huffman & Venton, 2008) However, with more consistent impedance characteristics, P-55 fibers, when used with the convolution-based technique, is advantageous, as the interference generated by the background current should be more easily removed.

With the P-55 fibers, the use of the convolution-based technique was evaluated for removal of the background current with a higher holding potential. The results are shown in Figure 5.5. For this data, a 100 mV step was placed 750 μs before a 400 V/s FSCV sweep in TRIS buffer at an unconditioned P-55 fiber, and five CVs were averaged and digitally low-pass filtered (Bessel 4th order low pass filter, 2 kHz cut-off). As can be seen, the agreement between the measured current and the convolution-based prediction is high (Figure 5.5A), and, after subtraction of the prediction (Figure 5.5B), only about 2.5% of the signal remains unaccounted for. In particular, the fit to the forward sweep (inset) at potentials below +0.8 V is excellent, which should permit the use of information in this region directly (i.e. without background subtraction). Above this voltage, there is a peak seen, which is likely due to oxidation reactions that may originate from surface reactions or solution species.(Heien, et al., 2003) Note that convolution artifacts are often seen around the switching potentials due to slight mismatches in time between the prediction and actual measurements.

However, as noted in the previous report, estimates generated from the convolution-based approach tend to have more noise than the raw data. This becomes a significant concern given the lower sensitivity of the P-55 fibers, the lower sensitivity expected for higher holding potentials, and the fact that ambient levels of neurotransmitters typically fall in the range of 10-100 nM. This implies that the signal arising from basal levels of neurotransmitters would be less than 1 nA, which is insufficient for robust resolution. It is known that that the sensitivity can be increased through the use of lower waveform application frequencies (which allow for longer periods of adsorption and analyte preconcentration prior to

measurement) and the use of higher scan rates.(Bath et al., 2001; Bath et al., 2000; Keithley et al., 2011) The latter approach was explored because it complements the convolution-based approach. Use of the derivative for generation of the impulse response estimate effectively serves as a high-pass filter, degrading the signal-to-noise of the low-frequency information. With higher scan rates, the signal is more strongly determined by the high frequency components and overlaps more directly with the strongest frequency region of the impulse response, as shown in the frequency power spectra in Figure 5.6A for varying scan rates.

The sensitivities of the P-55 fibers as a function of scan rate was evaluated (Figure 5.6B). Of note, the use of a higher holding potential (0.0 vs -0.4 V) decreased the sensitivity of the fibers to dopamine by approximately 25% at 400 V/s. With increases in scan rate, the sensitivity did indeed increase linearly, as is expected for adsorbed species.(Bard & Faulkner, 2001) Additionally, as expected from previous reports, the dopamine peak shifted to more positive potentials, which is attributable to the slow electron transfer kinetics of dopamine at carbon electrodes.(Baur, et al., 1988; Keithley, et al., 2011) However, the background current also increased in the same manner, mandating that analog background subtraction be used for higher scan rates due to saturation of the analog-to-digital converter. The details of this procedure are given elsewhere.(Hermans, et al., 2008) Briefly, the current is first measured and digitized, and, in subsequent runs, the current is fed to the current-to-voltage converter in the headstage to neutralize some of the measured current. For the convolution-based method, the current fed back into the headstage is also recorded and digitally added back to the measured data before convolution. However, even with this approach, the maximum scan rate attainable was approximately 4000 – 6000 V/s (depending on the impedance properties of the individual electrodes), placing a limitation on the achievable sensitivity gains. Regardless, the increase in analytical sensitivity proved sufficient to increase the signal strength such that it could be resolved against the prediction-subtracted background. An example is shown for resolution of 500 nM dopamine in TRIS buffer in a beaker (4000 V/s at 10 Hz, Figure 5.6C). The background was first measured in TRIS buffer without added dopamine to verify that the background could be removed successfully (black line). Subsequently, dopamine was added to the solution, resulting in the appearance of a signal at approximately 0.9 V (orange line), suggesting that this approach has potential for measurement of basal levels of dopamine. Importantly, the application
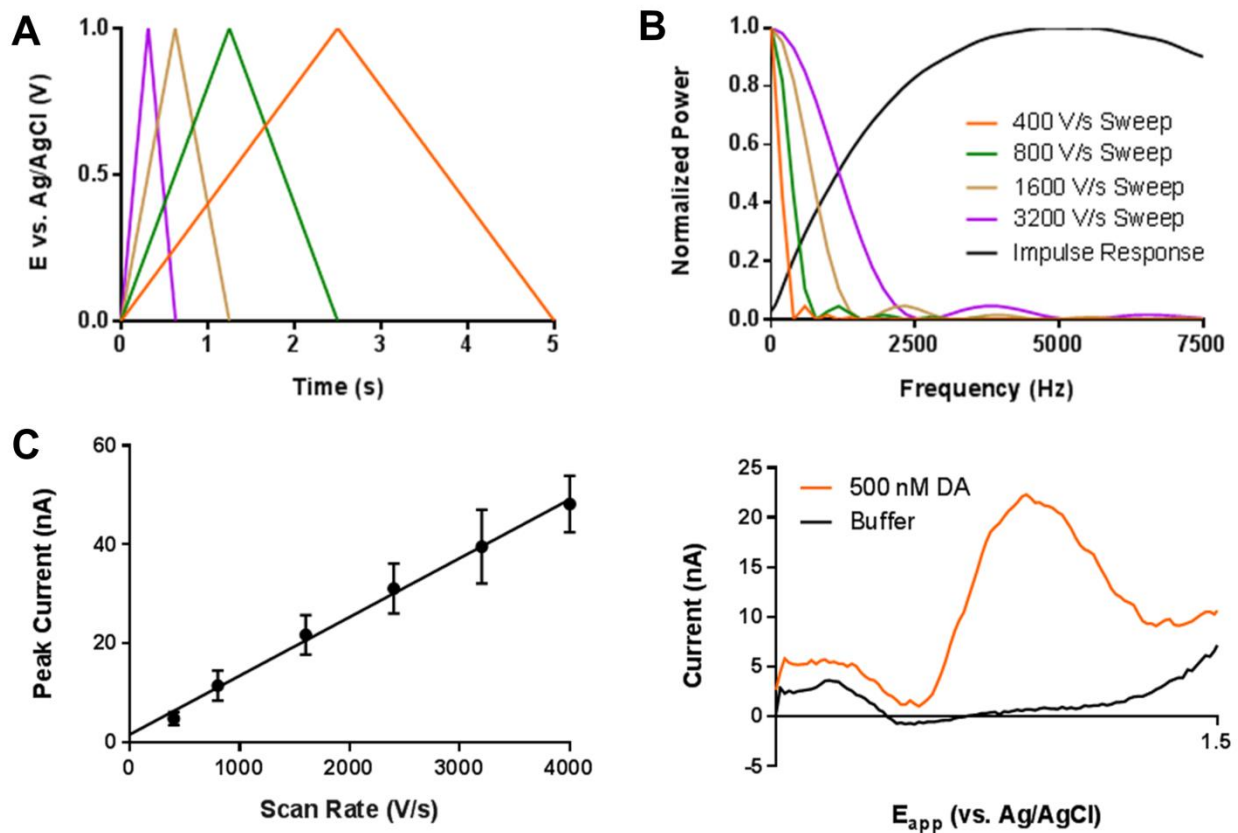
**Figure 5.6.** Use of high scan rates for detection of dopamine. (A-B) Waveforms of different scan rates shown in the time domain (A) and the frequency domain (B). A typical impulse response estimation is shown in the frequency domain for reference. (C) Peak current observed for dopamine oxidation as a function of scan rate. (D) Prediction-subtracted background currents taken in TRIS buffer (black) and after addition of 500 µM dopamine.

frequency did not have to be altered, allowing for the temporal resolution of the measurements to be maintained. Thus, this approach should allow for simultaneous access to information regarding phasic and basal dopamine levels, although measurement of absolute basal levels requires high *in vivo* sensitivity and selectivity on the oxidative sweep. Additionally, as interferences should be more amendable to convolution-based removal, it should be possible to take longer measurements than accessible with traditional FSCV protocols.

In Vivo Measurement of Phasic and Basal Changes Dopamine Levels. To test the technique *in vivo*, the changes in dopamine in the nucleus accumbens following cocaine administration were monitored in a freely moving rat. Cocaine inhibits dopamine uptake, resulting in increased extracellular concentrations.(Heien et al., 2005; Hermans, et al., 2008) For this study, a stimulating electrode was stereotaxically placed in the ventral tegmental area during surgery. On test day, voltammetric monitoring initially employed a waveform with standard voltage limits (-0.4 to +1.3 V) and a scan rate of 400 V/s (Figure 5.7A). The working electrode location was adjusted with stimulations at a constant stimulating electrode depth until a maximal dopamine signal was found. Subsequently, the waveform was switched to a 5000 V/s waveform with a holding potential of 0.1 V (Figure 5.7B). This holding potential was used to ensure the quinone peak and associated interferences would be avoided. Additionally, the waveform was modified to include a negative excursion of the reductive sweep to attempt to capture the reductive wave of dopamine, which should allow for more ready signal identification and more robust discrimination from interferences such as ascorbic acid and DOPAC. After the electrode stabilized, recording began, with administration of cocaine (30 mg/kg) intraperitoneally occurring one minute after recording had begun.

With this protocol, transients were readily identified, which did not appear approximately 10 minutes after cocaine administration and continued throughout the recording period. The technique did allow for long-term recordings, and a representative five-minute color plot showing transient signals is shown in Figure 5.7C (top, recorded 45 minutes after cocaine administration). MCR-ALS analysis permitted isolation of the dopamine signal and determination of the concentration from these data (middle, *ex vivo* sensitivity: 55 nA/μM), which was validated using residual analysis (bottom). Additionally, using the convolution-based procedure, information that appears to show changes in basal dopamine
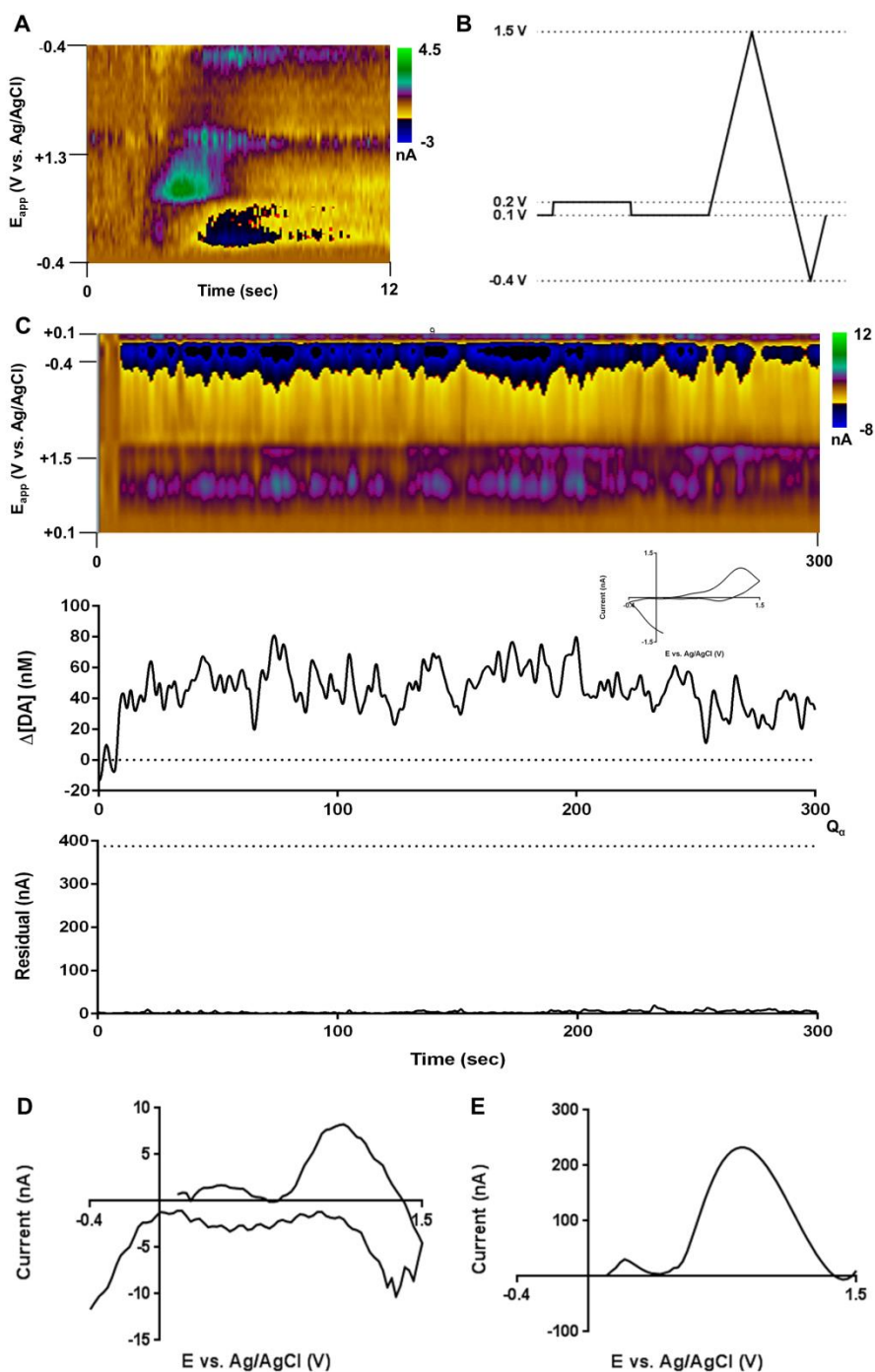
Figure 5.7. In vivo measurement of phasic and basal dopamine changes after cocaine administration. (A) Electrically stimulated release of dopamine during electrode positioning. (B) Waveform (5000 V/s) used for measurement. (C) Convolution-treated background-subtracted color plot (top, 5 minutes) showing dopamine transient signals, MCR-ALS determined dopamine concentrations and isolated DA spectra (middle), and residual values with Q_α (dotted line) for MCR-ALS model. (D) Convolution prediction- and background-subtracted (blank taken 45 minutes before) color plot showing signal around dopamine oxidation potential. (E) Ex-vivo convolution-prediction subtracted background current taken in TRIS buffer (forward sweep shown for clarity).

levels was obtained. Figure 5.7D shows a convolution-treated CV taken during the same time window as the data in Figure 5.7C, using the convolution-treated CV taken at the beginning of recording as a background (45 minutes earlier). This shows the presence of a voltammetric peak at the same oxidation potential as seen for the dopamine transients. However, attempts to access information about the absolute levels of dopamine were hindered by the unexpected appearance of a large (> 200 nA peak current) background peak at the same oxidation potential. While a similar peak has been noted previously for pH shifts in the presence of DOPAC, *ex vivo* analysis revealed the presence of this peak in TRIS buffer alone (Figure 5.7E). (Takmakov, et al., 2010a) Further, the electrode had minimal sensitivity for the common interferents DOPAC and ascorbic acid (which have slower electron kinetics than dopamine and have peak potentials more positive than dopamine at high scan rates). This suggests that this may be due to another surface redox-active functional group. Based on the current measured in this experiment, it would be expected that this peak would be a relatively small component of the background at lower scan rates (estimated peak height of about 20 nA at 400 V/s), suggesting the presence of this peak may not be obvious under these conditions. Preliminary experiments suggest this peak is introduced during oxidation of the carbon fiber and can be removed through intentional reduction through application of low anodic potentials; however, further characterization is needed to understand how to avoid its presence in the data.

Regardless, given stability in this background signal, background subtraction can still be able to be used to resolve changes in basal levels in dopamine over long periods, as the underlying species does not appear to affect the capacitance in a manner similar to that generating the quinone-like peak at more negative potentials. Based on the *ex vivo* sensitivity value, the transients detected in Figure 5.7C have peak amplitudes of approximately 50-100 nM, while the basal dopamine levels have undergone an approximately 150 nM change over the 45-minute window studied. Of note, the values for the transient amplitudes are similar to that reported previously using FSCV (~120 nM).(Heien, et al., 2005) The measured basal level is below that seen for intravenous administration for cocaine when using principal component regression for signal resolution; however, this may be due to the differing routes of administration.(Hermans, et al., 2008; Ma et al., 1999)

CONCLUSIONS

These data suggest that the use of high scan rates, holding potentials of 0.0 V vs Ag/AgCl, and alternative carbon fiber materials facilitate the use of the convolution for prediction and removal of the majority of the background current. With this background removed, information about long-term changes in and basal levels of neurotransmitters, as demonstrated here for dopamine, can be accessed without sacrificing temporal resolution, permitting simultaneous analysis of phasic dopamine changes as traditionally studied with FSCV. However, as highlighted in the *in vivo* study of dopamine following cocaine administration, measurement of absolute levels of dopamine requires careful control of the electrode state. Further study is needed to optimize the electrode pretreatment and experimental waveform limits to prevent its interference with these measurements.

REFERENCES

Atcherley, C. W., Laude, N. D., Monroe, E. B., Wood, K. M., Hashemi, P., & Heien, M. L. (2015a). Improved Calibration of Voltammetric Sensors for Studying Pharmacological Effects on Dopamine Transporter Kinetics in Vivo. *Acs Chem Neurosci, 6*(9), 1509-1516.

Atcherley, C. W., Laude, N. D., Parent, K. L., & Heien, M. L. (2013). Fast-scan controlled-adsorption voltammetry for the quantification of absolute concentrations and adsorption dynamics. *Langmuir, 29*(48), 14885-14892.

Atcherley, C. W., Wood, K. M., Parent, K. L., Hashemi, P., & Heien, M. L. (2015b). The coaction of tonic and phasic dopamine dynamics. *Chem Commun (Camb), 51*(12), 2235-2238.

Bard, A. J., & Faulkner, L. R. (2001). *Electrochemical Methods: Fundamentals and Applications* (2nd ed.). New York, NY: John Wiley & Sons, Inc.

Bath, B. D., Martin, H. B., Wightman, R. M., & Anderson, M. R. (2001). Dopamine adsorption at surface modified carbon-fiber electrodes. *Langmuir, 17*(22), 7032-7039.

Bath, B. D., Michael, D. J., Trafton, B. J., Joseph, J. D., Runnels, P. L., & Wightman, R. M. (2000). Subsecond adsorption and desorption of dopamine at carbon-fiber microelectrodes. *Anal Chem, 72*(24), 5994-6002.

Baur, J. E., Kristensen, E. W., May, L. J., Wiedemann, D. J., & Wightman, R. M. (1988). Fast-Scan Voltammetry of Biogenic-Amines. *Anal Chem, 60*(13), 1268-1272.

Bucher, E. S., Brooks, K., Verber, M. D., Keithley, R. B., Owesson-White, C., Carroll, S., et al. (2013). Flexible Software Platform for Fast-Scan Cyclic Voltammetry Data Acquisition and Analysis. *Anal Chem, 85*(21), 10344-10353.

Burrell, M. H., Atcherley, C. W., Heien, M. L., & Lipski, J. (2015). A Novel Electrochemical Approach for Prolonged Measurement of Absolute Levels of Extracellular Dopamine in Brain Slices. *Acs Chem Neurosci, 6*(11), 1802-1812.

Dengler, A. K., Wightman, R. M., & McCarty, G. S. (2015). Microfabricated Collector-Generator Electrode Sensor for Measuring Absolute pH and Oxygen Concentrations. *Anal Chem, 87*(20), 10556-10564.

Dikin, D. A., Stankovich, S., Zimney, E. J., Piner, R. D., Dommett, G. H. B., Evmenenko, G., et al. (2007). Preparation and characterization of graphene oxide paper. *Nature, 448*(7152), 457-460.

Heien, M. L. A. V., Khan, A. S., Ariansen, J. L., Cheer, J. F., Phillips, P. E. M., Wassum, K. M., et al. (2005). Real-time measurement of dopamine fluctuations after cocaine in the brain of behaving rats. *P Natl Acad Sci USA, 102*(29), 10023-10028.

Heien, M. L. A. V., Phillips, P. E. M., Stuber, G. D., Seipel, A. T., & Wightman, R. M. (2003). Overoxidation of carbon-fiber microelectrodes enhances dopamine adsorption and increases sensitivity. *Analyst, 128*(12), 1413-1419.

Hermans, A., Keithley, R. B., Kita, J. M., Sombers, L. A., & Wightman, R. M. (2008). Dopamine detection with fast-scan cyclic voltammetry used with analog background subtraction. *Anal Chem, 80*(11), 4040-4048.

Howell, J. O., Kuhr, W. G., Ensman, R. E., & Wightman, R. M. (1986). Background Subtraction for Rapid Scan Voltammetry. *J Electroanal Chem, 209*(1), 77-90.

Huffman, M. L., & Venton, B. J. (2008). Electrochemical Properties of Different Carbon-Fiber Microelectrodes Using Fast-Scan Cyclic Voltammetry. *Electroanal, 20*(22), 2422-2428.

Keithley, R. B., Takmakov, P., Bucher, E. S., Belle, A. M., Owesson-White, C. A., Park, J., et al. (2011). Higher sensitivity dopamine measurements with faster-scan cyclic voltammetry. *Anal Chem, 83*(9), 3563-3571.

Liu, Y. D., & Kumar, S. (2012). Recent Progress in Fabrication, Structure, and Properties of Carbon Fibers. *Polym Rev, 52*(3-4), 234-258.

Ma, F., Falk, J. L., & Lau, C. E. (1999). Within-subject variability in cocaine pharmacokinetics and pharmacodynamics after intraperitoneal compared with intravenous cocaine administration. *Exp Clin Psychopharm, 7*(1), 3-12.

Oh, Y., Park, C., Kim, D. H., Shin, H., Kang, Y. M., DeWaele, M., et al. (2016). Monitoring In Vivo Changes in Tonic Extracellular Dopamine Level by Charge-Balancing Multiple Waveform Fast-Scan Cyclic Voltammetry. *Anal Chem, 88*(22), 10962-10970.

Qu, D. Y., Tao, Y. Z., Guo, L. P., Xie, Z. Z., Tu, W. N., & Tang, H. L. (2015). Surface Structure Sensitive Electrocatalytic Activity of Platinum Nanofilm Decorated Gold Microelectrode for Oxygen Reduction Reaction. *Int J Electrochem Sc, 10*(4), 3363-3371.

Signorelli, R., Ku, D. C., Kassakian, J. G., & Schindall, J. E. (2009). Electrochemical Double-Layer Capacitors Using Carbon Nanotube Electrode Structures. *P Ieee, 97*(11), 1837-1847.

Sosna, M., Denuault, G., Pascal, R. W., Prien, R. D., & Mowlem, M. (2007). Development of a reliable microelectrode dissolved oxygen sensor. *Sensor Actuat B-Chem, 123*(1), 344-351.

Stankovich, S., Dikin, D. A., Dommett, G. H. B., Kohlhaas, K. M., Zimney, E. J., Stach, E. A., et al. (2006). Graphene-based composite materials. *Nature, 442*(7100), 282-286.

Takmakov, P., Zachek, M. K., Keithley, R. B., Bucher, E. S., McCarty, G. S., & Wightman, R. M. (2010a). Characterization of Local pH Changes in Brain Using Fast-Scan Cyclic Voltammetry with Carbon Microelectrodes. *Anal Chem, 82*(23), 9892-9900.

Takmakov, P., Zachek, M. K., Keithley, R. B., Walsh, P. L., Donley, C., McCarty, G. S., et al. (2010b). Carbon Microelectrodes with a Renewable Surface. *Anal Chem, 82*(5), 2020-2028.

Vanstroebiezen, S. A. M., Everaerts, F. M., Janssen, L. J. J., & Tacken, R. A. (1993). Diffusion-Coefficients of Oxygen, Hydrogen-Peroxide and Glucose in a Hydrogel. *Anal Chim Acta, 273*(1-2), 553-560.

APPENDIX 1.1: DESCRIPTION OF ERROR PROPAGATION ANALYSIS METHOD

The variance in the predicted experimental concentration value is estimated using the following formulas.

$$V(y_{pred}) = (1 + h) * SEN^{-2} * \sigma_x^2 + x_u^T V_0(\beta) x_u \qquad \text{(Eq. A1.1-1)}$$

$$h = (X_{proj})(A_{proj}A_{proj})^{-1}(X_{proj}) \qquad \text{(Eq. A1.1-2)}$$

$$X_{proj} = V_c x_u \qquad \text{(Eq. A1.1-3)}$$

$$A_{proj} = V_c A \qquad \text{(Eq. A1.1-4)}$$

$$SEN = \frac{1}{\|\beta\|} \qquad \text{(Eq. A1.1-5)}$$

$$V_0(\beta) = S_A^- A^T V_0(A) A S_A^- \qquad \text{(Eq. A1.1-6)}$$

$$S_A^- = (A_{proj}^T A_{proj})^{-1} \qquad \text{(Eq. A1.1-7)}$$

where V(y_{pred}) is the variance in the predicted y (concentration) values; h is the leverage, SEN is the multivariate sensitivity, σ_x^2 is the variance in the x values, x_u is the unknown cyclic voltammogram, X_{proj} is the score matrix for the unknown voltammogram, V_c is the prinicipal component matrix, A_{proj} is the principal component score matrix for the training set voltammograms, and β is a vector containing the regression parameters.

To use these formulas, a number of variables need to be estimated.

An estimate of the calibration factors and the electrode-to-electrode variability was taken from Rodeberg et al.(Rodeberg et al., 2015) This is for the commonly used triangular waveform at a scan rate of 400 V/s with an application frequency of 10 Hz and a T-650 carbon fiber electrode cut to 100 μm.

The next step is to determine the error in the calibration concentration estimates. To do this, an estimate for the variation in the current measurements (σ_x^2) is first needed. For a conservative estimate, the following formula is used that is based on the Q_α estimate used in residual analysis.(Keithley et al., 2009)

$$\sigma_x^2 = \frac{Q_\alpha}{N} \qquad \text{(Eq. A1.1-8)}$$

where N is the number of data points in the voltammogram. This estimate uses the information contained in the discarded PCs of the model and assumes this describes solely random, homoscedastic noise across the potential window, which is an assumption also used in the calculation of the Q_α value. Error must be then be propagated through the equation for determining the calibration concentration values:

$$C = \frac{i_{pk}}{CF}$$ (Eq. A1.1-9)

where i_{pk} is the peak current in the training voltammogram and CF is the calibration factor. The error in the concentration estimates is then calculated according to the following formula:

$$\delta C = C \sqrt{\left(\frac{\delta i_{pk}}{i_{pk}}\right)^2 + \left(\frac{\delta CF}{CF}\right)^2}$$ (Eq. A1.1-10)

These estimates are then used to construct the diagonal of the covariance matrix. However, at a single electrode, the deterministic errors in the concentration estimates, which arise from the difference between the average calibration factor used above and the actual electrode-specific calibration factor, are expected to be perfectly correlated ($r = 1$). That is, all concentrations are expected to be under- or over-estimated by the same degree. Thus, the off-diagonal terms, or the covariance between concentration errors, of the covariance matrix must also be estimated.(Farrance & Frenkel, 2012)

$$Covar(y_i, y_j) = r \sqrt{\sigma_{y_i}^2 \sigma_{y_j}^2} = \sqrt{\sigma_{y_i}^2 \sigma_{y_j}^2}$$ (Eq. A1.1-11)

With the estimates of the variance and covariance of the errors in the calibration concentrations, the covariance matrix can be constructed and the error determined using the formulas given above.

REFERENCES

Farrance, I., & Frenkel, R. (2012). Uncertainty of Measurement: A Review of the Rules for Calculating Uncertainty Components through Functional Relationships. *Clin Biochem Rev, 33*(2), 49-75.

Keithley, R. B., Heien, M. L., & Wightman, R. M. (2009). Multivariate concentration determination using principal component regression with residual analysis. *Trac-Trend Anal Chem, 28*(9), 1127-1136.

Rodeberg, N. T., Johnson, J. A., Cameron, C. M., Saddoris, M. P., Carelli, R. M., & Wightman, R. M. (2015). Construction of Training Sets for Valid Calibration of in Vivo Cyclic Voltammetric Data by Principal Component Analysis. *Anal Chem, 87*(22), 11484-11491.

APPENDIX 2.1: MATHEMATICAL DESCRIPTION OF PRINCIPAL COMPONENT ANALYSIS

Prior to PCR, a training set matrix (**A**) is constructed with dimensions of (n x m), where n is the number of data points in a spectra and m is the number of spectra. Additionally, a concentration matrix (**C**), an (l x m) array whose elements are the concentration of the lth analyte in the mth spectra, is constructed.(Kramer, 1998) Note that this definition of training set matrix is the transpose of that used in many PCR review texts.(Booksh, 2006; Wilks, 2014) Mean-centering and variance scaling are not used to prevent low amplitude, high signal-to-noise ratio spectra from having high leverage and undue influence on the regression parameters.(Heien et al., 2004; Kramer, 1998)

The goal of PCR in first-order inverse analytical calibration is to fit the following (the matrix equivalent to Eq. 2.5):

$$C = PA \tag{Eq. A2.1-1}$$

where **P** is a (l x n) matrix containing the regression coefficients. The least-squares solution to this equation is:

$$P = CA^T[AA^T]^{-1} \tag{Eq. A2.1-2}$$

However, for data where number of training spectra is less than the number of data points and there is a high degree of multicollinearity between the predictor spectral measurements, this problem is ill-posed (i.e. the term [**AA**^{T}]$^{-1}$ cannot be calculated).(Kramer, 1998; Vigneau et al., 1997) Therefore, PCR is used to reduce data dimensionality and multicollinearity between regression predictors such that an estimation of **P** can be functionally obtained.

First, singular value decomposition is performed on the training set matrix. In HDCV,(Bucher et al., 2013) the in-built SVD Matlab function is used, which relies on a form of the QR algorithm.(Watkins, 1982) Singular value decomposition factors a matrix (n x m) into three different matrices:

$$A = U\Sigma V^T \tag{Eq. A2.1-3}$$

where U is a unitary matrix containing left-singular vectors of **A** as columns (n x n), **Σ** is a matrix (m x n) with the non-negative singular values on the diagonal, and **V** is a unitary matrix (m x m) containing right-singular vectors of A as columns.(Golub & Reinsch, 1970; Hendler & Shrager, 1994) These matrices are

calculated by eigenvalue decomposition of the square matrix $\mathbf{AA}^T$. The left- and right-singular vectors are the eigenvectors of the square matrices $\mathbf{AA}^T$ and $\mathbf{A}^T\mathbf{A}$, respectively. The squares of the singular values are the eigenvalues of either.(Wilks, 2014)

The principal components are vectors defined by the first m columns (left-singular vectors) of $\mathbf{U}$, which will be referred to as the loading matrix $\mathbf{W}$ (n x m). These are mutually orthogonal vectors related to the original variables by the following:

$$PC_m = \sum_{i=1}^{n} w_{i,m} X_i \qquad \text{(Eq. A2.1-4)}$$

where PC_m is the mth principal component unit vector, $w_{i,m}$ is the loading (or weighting) of the ith variable, and X_i is the unit vector of ith original variable. The description of spectra in the principal component space is given by their scores, or projections onto the PC vectors, which is the matrix equivalent to Eq. 2.6:

$$T = W^T A \qquad \text{(Eq. A1-5)}$$

where T is the score matrix (m x m). Any given score of a spectrum on a PC is determined by the dot product of the PC's loading vector ($\mathbf{w_m} = [w_{1,m}, w_{2,m}, \dots , w_{n,m}]$) with the spectrum.

Selection of principal components relies on statistical analysis of the variance spanned by each PC, which is represented by the corresponding eigenvalue (obtained by the squares of the singular values in the $\mathbf{\Sigma}$ matrix), using Malinowski's F-test.(Keithley et al., 2010; E. R. Malinowski, 1977; Edmund R. Malinowski, 1987, 1989; E.R. Malinowski, 1990; E. R. Malinowski, 2004) Once the number of principal components to retain (i.e. the rank of the model, or r) is determined, the loading matrix is truncated to a (n x r) matrix, which will be referred to as the $\mathbf{W_r}$ matrix. Representation of this reduced model in r-dimensional principal subspace is given by substitution of the $\mathbf{W_r}$ matrix into Equation A2.1-5. The regression equation is then reformulated as:

$$C = MT \qquad \text{(Eq. A2.1-6)}$$

which is the matrix equivalent of Eq. 2.7 and has the least-squares solution of:

$$M = CT_{TS}^T \left[T_{TS}T_{TS}^T\right]^{-1} \qquad \text{(Eq. A2.1-7)}$$

In contrast to Eq. A2.1-2, this solution can be computed. The use of orthogonal vectors for principal component definition directly addresses the multicollinearity problem, while data reduction to the r-dimensional principal subspace insures the problem is well-posed. Use of Eq. A2.1-7 for experimental concentration prediction requires use of Eq. A2.1-5 for expression of experimental data ($\mathbf{A_{ex}}$) in the principal subspace. However, through combination of Eqs. A2.1-5-7, the calibration model can be stated as:

$$C = C_{TS} T_{TS}{}^{T} \left[T_{TS} T_{TS}{}^{T} \right]^{-1} W_R A \qquad \text{(Eq. A2.1-8)}$$

Comparison to Eq. 2.1 shows that the PCR model estimation of **P** is:

$$P = C_{TS} T_{TS}{}^{T} \left[T_{TS} T_{TS}{}^{T} \right]^{-1} W_R = M W_R \qquad \text{(Eq. A2.1-9)}$$

which is a fixed-value matrix after SVD calculation of **U** and rank selection.

Reconstruction of the matrix approximation ($\mathbf{A_{proj}}$) of the experimental spectra is given by:

$$A_{ex,proj} = W_R T_{ex} \qquad \text{(Eq. A2.1-10)}$$

which can be used for residual calculation through subtraction from the experimental spectra ($\mathbf{A_{ex}} - \mathbf{A_{ex,proj}}$).(Keithley et al., 2009) For the construction of model estimates of the signal from concentration, the equation of the classical formulation can be used (corresponding to Eq. 2.1)

$$A = KC \qquad \text{(Eq. A2.1-11)}$$

where **K** is the matrix pseudoinverse of **P**.(Booksh, 2006) Note that the $\mathbf{p_j}$ and $\mathbf{k_j}$ vectors are the jth rows of the **P** matrix and j^{th} columns of the **K** matrix, respectively. To obtain the $\mathbf{k_j}$ vector of any given analyte, the entire **P** matrix, containing all $\mathbf{p_j}$ vectors for the model, must be used in the calculation, and the same applies for calculation of the **P** matrix, which is necessary to obtain a any single $\mathbf{p_j}$ vector, from the **K** matrix.

REFERENCES

Booksh, K. S. (2006). Chemometric Methods in Process Analysis *Encyclopedia of Analytical Chemistry*: John Wiley & Sons, Ltd.

Bucher, E. S., Brooks, K., Verber, M. D., Keithley, R. B., Owesson-White, C., Carroll, S., et al. (2013). Flexible Software Platform for Fast-Scan Cyclic Voltammetry Data Acquisition and Analysis. *Anal Chem, 85*(21), 10344-10353.

Golub, G. H., & Reinsch, C. (1970). Singular Value Decomposition and Least Squares Solutions. *Numer Math, 14*(5), 403-&.

Heien, M. L. A. V., Johnson, M. A., & Wightman, R. M. (2004). Resolving neurotransmitters detected by fast-scan cyclic voltammetry. *Anal Chem, 76*(19), 5697-5704.

Hendler, R. W., & Shrager, R. I. (1994). Deconvolutions Based on Singular-Value Decomposition and the Pseudoinverse - a Guide for Beginners. *J Biochem Bioph Meth, 28*(1), 1-33.

Keithley, R. B., Carelli, R. M., & Wightman, R. M. (2010). Rank estimation and the multivariate analysis of in vivo fast-scan cyclic voltammetric data. *Anal Chem, 82*(13), 5541-5551.

Keithley, R. B., Heien, M. L., & Wightman, R. M. (2009). Multivariate concentration determination using principal component regression with residual analysis. *Trends Analyt Chem, 28*(9), 1127-1136.

Kramer, R. (1998). *Chemometric Techniques for Quantitative Analysis*. New York, NY: Marcel Dekker, Inc.

Malinowski, E. R. (1977). Determination of Number of Factors and Experimental Error in a Data Matrix. *Anal Chem, 49*(4), 612-617.

Malinowski, E. R. (1987). Theory of the distribution of error eigenvalues resulting from principal component analysis with applications to spectroscopic data. *J Chemometr, 1*(1), 33-40.

Malinowski, E. R. (1989). Statistical F-tests for abstract factor analysis and target testing. *J Chemometr, 3*(1), 49-60.

Malinowski, E. R. (1990). Erratum. *J Chemometr, 4*(1), 102-102.

Malinowski, E. R. (2004). Adaptation of the Vogt-Mizaikoff F-test to determine the number of principal factors responsible for a data matrix and comparison with other popular methods. *J Chemometr, 18*(9), 387-392.

Vigneau, E., Devaux, M. F., Qannari, E. M., & Robert, P. (1997). Principal component regression, ridge regression and ridge principal component regression in spectroscopy calibration. *J Chemometr, 11*(3), 239-249.

Watkins, D. S. (1982). Understanding the Qr-Algorithm. *Siam Rev, 24*(4), 427-440.

Wilks, D. (2014). *International Geophysics, 100 : Statistical Methods in the Atmospheric Sciences (2nd Edition)* (2nd ed.). Burlington, US: Academic Press.

APPENDIX 2.2: F-TEST FOR GLOBAL VS. SUBJECT-SPECIFIC MODEL COMPARISON

The F-test compares two models by comparing the residual sum of squares between models, calculating the F statistic using the following equation:(Glatting et al., 2007; Krazanowski, 2007)

$$F = \frac{\frac{(SS_{H_0} - SS_{H_1})}{SS_{H_1}}}{\frac{(DOF_{H_0} - DOF_{H_1})}{DOF_{H_1}}} \qquad \text{(Eq. A2.2-1)}$$

where SS refers to the residual sum of squares for the model, DOF refers to the degrees of freedom (DOF), and the subscripts H_0 and H_1 indicate the values for the null and alternative models, respectively. The DOF for a model is the difference between the number of data points (n_{DP}) and the number of model parameters (p_m). For the comparison of global and group-specific parameters for the regression model, the model being fitted was:

$$C_j = \sum_{i=1}^{r} m_{i,j} t_{i,j} + \epsilon \qquad \text{(Eq. A2.2-2)}$$

where C_j is the analyte concentration for a given CV in the jth training set, $t_{i,j}$ is the score on the ith PC for a given CV in the jth training set, r is the total number of PCs retained in the model, and $m_{i,j}$ is the proportionality factor between the concentration and the score on the ith PC. The null hypothesis is the global model, which has fewer parameters and assigns all training sets the same proportionality factors (m) to all training sets:

$$H_0: m_{i,1} = \cdots = m_{i,j}$$

The alternative hypothesis is the subject-specific model, with unique m values for a training set:

$$H_1: m_{i,1} \neq \cdots \neq m_{i,j}$$

The significance was evaluated by determining the associated *p* value for ($p_{H1} - p_{H0}$, $n_{DP} - p_{H1} + 1$) degrees of freedom ($\alpha = 0.05$).

REFERENCES

Glatting, G., Kletting, P., Reske, S. N., Hohl, K., & Ring, C. (2007). Choosing the optimal fit function: Comparison of the Akaike information criterion and the F-test. *Med Phys, 34*(11), 4285-4292.

Krazanowski, W. (2007). *Statistical Principles and Techniques in Scientific and Social Investigations*. Cary, NC: Oxford University Press.

APPENDIX 4.1: SIMULATION OF MODEL BACKGROUND CURRENTS

As stated in Chapter 4, we considered the double layer as a parallel network with a voltage-dependent impedance element (Z_{QH}, corresponding to the quinone-like redox reaction), a voltage-dependent capacitor (C_{QH}, the capacitance arising from species bound to the quinone-like moiety), and a voltage-independent capacitor (C_I)

To model the expected current from Z_{QH}, given a surface-bound, quinone-like species with total surface concentration of $\Gamma_{QH}*$ that undergoes a two-electron ($n = 2$), reversible reaction, we expect, from the derivation in Bard and Faulkner, Chapter 14.3.2) for adsorbed species(Bard & Faulkner, 2001), the following i-E curve for the faradaic couple to application of a voltammetric sweep:

$$i(E) = \frac{n^2 F^2}{RT} v A \Gamma_{QH}^* \frac{\left(\frac{b_O}{b_R}\right) \exp[\left(\frac{nF}{RT}\right)(E - E^O))]}{[1 + \left(\frac{b_O}{b_R}\right) \exp[\left(\frac{nF}{RT}\right)(E - E^O))]^2} \qquad \text{(Eq. A4-1.1)}$$

Since the species is surface-bound, we set the ratio (b_O/b_R) to be 1 for further use.

To model the capacitive charging current, the redox-coupled, area-normalized capacitance (C_{QH}^*, F·cm^{-2}) is assumed to be linearly dependent on the surface concentration of both species (Γ_{QH} and Γ_Q, mol·cm^{-2}) and respond immediately to their concentration:

$$C_{QH}^*(E) = C_{QH}(E) + C_Q(E) \qquad \text{(Eq. A4-1.2)}$$

$$C_{QH}^*(E) = b\Gamma_{QH}(E) + c\Gamma_Q(E) \qquad \text{(Eq. A4-1.3)}$$

$$C_{QH}^*(E) = b\Gamma_{QH}(E) + c(\Gamma_{QH}^* - \Gamma_{QH}(E)) \qquad \text{(Eq. A4-1.4)}$$

where b and c are constants (F·mol^{-1}). To simplify this further, $R_{c/b}$ (the ratio of c to b, assumed to be a constant less than 1) is introduced:

$$C^*_{QH}(E) = b[R_{c/b}\Gamma^*_{QH} + \Gamma_{QH}(E)(1 - R_{c/b})]$$ (Eq. A4-1.5)

Using the Nerst relation, this can be put in terms of the total surface concentration Γ_{QH}^*:

$$\Gamma_{QH}(E) = \frac{\Gamma^*_{QH}}{1 + \exp\left[\left(\frac{nF}{RT}\right)(E - E^O)\right]}$$ (Eq. A4-1.6)

$$C^*_{QH}(E) = b\Gamma^*_{QH}\left[R_{c/b} + \frac{1 - R_{c/b}}{1 + \exp\left[\left(\frac{nF}{RT}\right)(E - E^O)\right]}\right]$$ (Eq. A4-1.7)

Finally, there is the voltage-independent capacitance (C_I), giving a total electrode capacitance (C_{tot}) of:

$$C_T(E) = C_I + C^*_{QH}(E)$$ (Eq. A4-1.8)

With this, the i-E curve for the capacitive charging current for application of triangular sweep is expected to be:

$$i = v * C_T(E) * \left[1 - \exp\left[\frac{-t}{R_S C_T(E)}\right]\right]$$ (Eq. 4-1.9)

where R_s is the solution resistance. Here, it is noted that this equation is applicable for time-independent capacitances; that is:

$$\frac{d(C_T E)}{t} = C_T(E)\left(\frac{dE}{dt}\right) + E\left(\frac{dC_T(E)}{dt}\right)$$ (Eq. A4-1.10)

While some contribution from the latter term is anticipated, we expect that term to be considerably smaller than the former at the high scan rates (dE/dt = 400) and moderate applied potentials (-0.8-0.8 V) in the this work. Thus, it is ignored. For ease of analysis, we consider the region around the faradaic couple and assume this to be far from the switching potentials, simplifying Equation A4-1.9 to:

$$i(E) = vC_I + vC^*_R(E)$$ (Eq. A4-1.11)

$$i(E) = vC_I + v\Gamma_{QH}^* b \left[R_{c/b} + \frac{1 - R_{c/b}}{1 + \exp\left[\left(\frac{nF}{RT}\right)(E - E^O)\right]} \right] \qquad \text{(Eq. A4-1.12)}$$

We introduce $i_{QH,max}^*$ indicate the maximum redox-associated charging current (seen at very negative

potentials where $\Gamma_{QH}^* = \Gamma_{QH} = \Gamma_{QH,max}$, since $r_{b/c}$ is assumed to be less than 1) as well as the constant i_{CI}:

$$i_{CI} = vC_I \qquad \text{(Eq. A4-1.13)}$$

$$i_{QH,max}^* = vb\Gamma_{QH}^* \qquad \text{(Eq. A4-1.14)}$$

$$i(E) = i_{CI} + i_{QH,max}^* \left[R_{c/b} + \frac{(1 - R_{c/b})}{1 + \exp\left[\left(\frac{nF}{RT}\right)(E - E^O)\right]} \right] \qquad \text{(Eq. A4-1.15)}$$

For the study of ionic changes, which are expected to affect primarily the capacitance values, the

Faradaic current serves as a useful point of comparison. The equation of the peak current expected for

the Faradaic couple ($i_{p,F}$) is also normalized the Faradaic currents:

$$i_{p,F} = \frac{1}{4}\left(\frac{n^2 F^2}{RT} * vA\Gamma_R^*\right) \qquad \text{(Eq. A4-1.16)}$$

$$\frac{i(E)}{i_{p,F}} = 4\frac{\exp[\left(\frac{nF}{RT}\right)(E - E^O))]}{[1 + \exp[\left(\frac{nF}{RT}\right)(E - E^O))]^2} \qquad \text{(Eq. A4-1.17)}$$

The total expected potential-dependent current (i_T, normalized to $i_{p,F}$) is then simply the summation of

these two contributions at a given values of three constants - I_C ($i_{CI}/i_{p,F}$), I_{QH} ($i_{QH,max}^*/i_{p,F}$), and $R_{c/b}$:

$$\frac{i_T(E)}{i_{p,F}} = I_C + I_{QH}\left[R_{c/b} + \frac{(1 - R_{c/b})}{1 + \exp\left[\left(\frac{nF}{RT}\right)(E - E^O)\right]} \right] + 4\left[\frac{\exp[\left(\frac{nF}{RT}\right)(E - E^O))]}{[1 + \exp[\left(\frac{nF}{RT}\right)(E - E^O))]^2}\right] \qquad \text{(Eq. A4-1.18)}$$

For values of $I_C = 1$, $I_{QH} = 2$, and $R_{b/c} = 0.5$, this gives the current-potential curves shown in Figure A4.1-1.
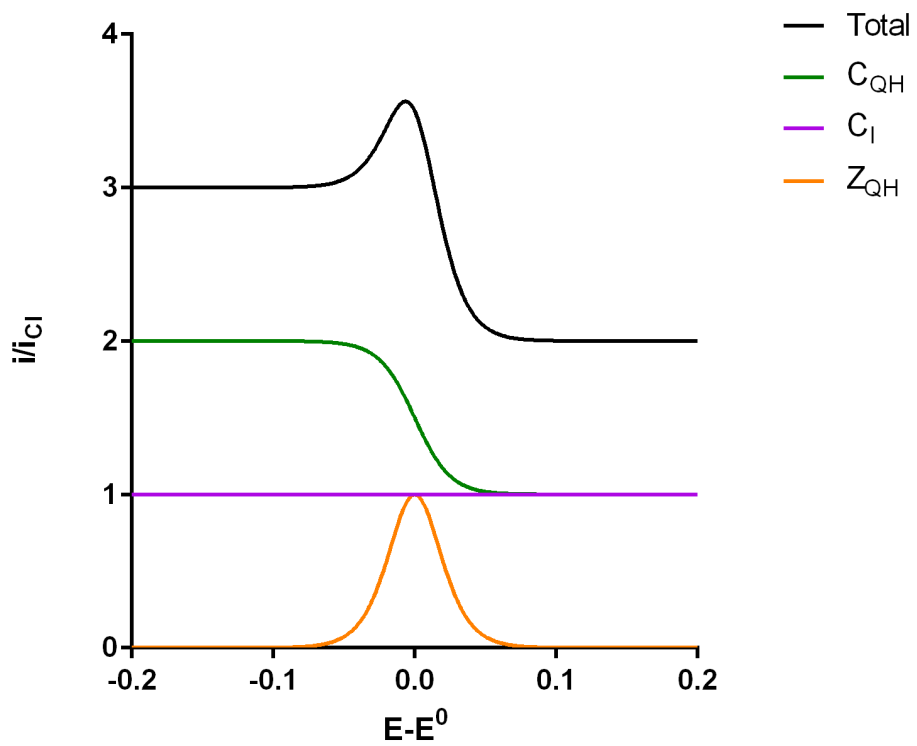
Figure A4-1.1. Model-simulated voltammetric currents for the components of the carbon-fiber double layer.

REFERENCES

Bard, A. J., & Faulkner, L. R. (2001). *Electrochemical Methods: Fundamentals and Applications* (2nd ed.). New York, NY: John Wiley & Sons, Inc.